11. SITE 655: GORTANI RIDGE, WESTERN VAVILOV BASIN[1]

Shipboard Scientific Party[2]

HOLE 655A

Date occupied: 8 February 1986

Date departed: 11 February 1986

Time on hole: 2 days, 2 hr

Position: 40°10.33′N 12°27.92′E

Water depth (sea level, corrected m, echo-sounding): 3290

Water depth (rig floor, corrected m, echo-sounding): 3301

Bottom felt (m, drill pipe length from rig floor): 3330.8

Total depth (m): 3421.2

Penetration (m): 90.4

Number of cores: 12

Total length of cored section (m): 90.4

Total core recovered (m): 77.4

Core recovery (%): 85.6

Deepest sedimentary unit cored:
Depth sub-bottom (m): 73.5
Nature: nannofossil ooze
Age: lower Pliocene
Measured vertical sound velocity (km/s): 1.6

Igneous or metamorphic basement:
Depth sub-bottom (m): 79.9
Nature: basalt
Velocity range (km/s): 4.4

HOLE 655B

Date occupied: 11 February 1986

Date departed: 13 February 1986

Time on hole: 2 days, 12 hr

Position: 40°11.32′N 12°27.93′E

Water depth (sea level, corrected m, echo-sounding): 3290

Water depth (rig floor, corrected m, echo-sounding): 3301

Bottom felt (m, drill pipe length from rig floor): 3330.8

Total depth (m): 3526.9

Penetration (m): 196.1

Number of cores: 12

Total length of cored section (m): 114.9

Total core recovered (m): 49.4

Core recovery (%): 43

Deepest sedimentary unit cored: none

Igneous or metamorphic basement:
Depth sub-bottom (m): 81.2
Nature: basalt
Velocity range (km/s): 4.4–5.2

Principal results: Site 655 was located near the crest of a north-trending ridge which lies near the inferred contact between oceanic and continental crust at the western rim of the Vavilov Basin (Fig. 1).

One sedimentary unit was recovered between the seafloor and 79.9 mbsf (Figs. 2 and 3). Basaltic basement was recovered between 79.9 mbsf and 196.1 mbsf.

Sedimentary unit: Cores 107-655-1H to 655A-9X; 0–79.9 mbsf; age: late Pliocene (MPl4) to Quaternary. The dominant sedimentary lithology is a marly nannofossil ooze, with occasional volcaniclastic layers and detrital sand layers. Six sapropels and/or sapropelic layers occur in the Pleistocene sequence. The Pliocene/Pleistocene boundary occurs at 22.3 mbsf, with no lithologic expression. The lower 6 m overlying basement exhibit a downsection color change from pale yellow to brown.

Basement unit: Cores 107-655A-9X to 107-655A-12X plus 107-655B-1R to 107-655B-12R; depth: 79.9–196.1 mbsf; age: inferred 3.4–3.6 m.y. The basement at Site 655 is made of basalt, with little obvious vertical variability in modal composition or structure. The basalt is generally aphanitic, but with occasional phenocrysts (as large as 2–3 mm) of plagioclase. Chilled glass margins were observed throughout the basalt unit, spaced an average of 2 m apart. The entire basalt section is reversely magnetized, with an inclination of 50°–60°; the intensity of natural remanent magnetization is high (3×10^{-2} to 10^{-3} G/cm^3).

Sediment within the basalt: Throughout the basalt unit, but particularly in the upper 30 m, veins and fractures were filled with indurated limestones. Planktonic foraminifers of biozone MPl4 and nannofossils of biozone NN15 are present in these carbonates.

---

[1] Kastens, K. A., Mascle, J., Auroux, C., et al., 1987. *Proc. Init. Repts. (Pt. A), ODP*, 107.

[2] Kim A. Kastens (Co-Chief Scientist), Lamont-Doherty Geological Observatory, Palisades, NY 10964; Jean Mascle (Co-Chief Scientist), Laboratoire de Géodynamique Sous-Marine, Université Pierre et Marie Curie, BP 48, 06230 Villefranche-sur-Mer, France; Christian Auroux, Staff Scientist, Ocean Drilling Program, Texas A&M University, College Station, TX 77843; Enrico Bonatti, Lamont-Doherty Geological Observatory, Palisades, NY 10964; Cristina Broglia, Lamont-Doherty Geological Observatory, Palisades, NY 10964; James Channell, Department of Geology, 1112 Turlington Hall, University of Florida, Gainesville, FL 32611; Pietro Curzi, Istituto di Geologia Marina, Via Zamboni, 65, 40127 Bologna, Italy; Kay-Christian Emeis, Ocean Drilling Program, Texas A&M University, College Station, TX 77843; Georgette Glaçon, Laboratoire de Stratigraphie et de Paleoécologie, Centre Saint-Charles, Université de Provence, 3, Place Victor Hugo, 13331 Marseille Cedex, France; Shiro Hasegawa, Institute of Geology, Faculty of Science, Tohoku University, Aobayama, Sendai, 980, Japan; Werner Hieke, Lehrstuhl für Allgemeine, Angewandte und Ingenieur-Geologie, Abt. Sedimentforschung und Meeregeologie, Technische Universität München, Lichtenbergstrasse 4, D-8046 Garching, Federal Republic of Germany; Floyd McCoy, Lamont-Doherty Geological Observatory, Palisades, NY 10964; Judith McKenzie, Department of Geology, University of Florida, 1112 Turlington Hall, Gainesville, FL 32611; Georges Mascle, Institut Dolomieu, Université Scientifique et Médicale de Grenoble, 15 Rue Maurice Gignoux, 38031 Grenoble Cedex, France; James Mendelson, Earth Resources Laboratory E34-366, Department of Earth, Atmospheric and Planetary Sciences, Massachusetts Institute of Technology, 42 Carleton Street, Cambridge, MA 02142; Carla Müller, Geol. Paläont. Institut, Universität Frankfurt/Main, 32–34 Senckenberg-Anlage, D-6000 Frankfurt/Main 1, Federal Republic of Germany (current address: 1 Rue Martignon, 92500 Rueil-Malmaison, France); Jean-Pierre Réhault, Laboratoire de Géodynamique Sous-Marine, Université Pierre et Marie Curie, BP 48, 06230 Villefranche-sur-Mer, France; Alastair Robertson, U.S. Geological Survey, 345 Middlefield Road, Menlo Park, CA 94025 (current address: Department of Geology, Grant Istitute, University of Edinburgh, Edinburgh, EH9 3JW, United Kingdom); Renzo Sartori, Istituto di Geologia Marina, Via Zamboni, 65, 40127 Bologna, Italy; Rodolfo Sprovieri, Instituto di Geologia, Corso Tukory, 131, Palermo, Italy; Masayuki Torii, Department of Geology and Mineralogy, Faculty of Science, Kyoto University, Kyoto, 606, Japan.

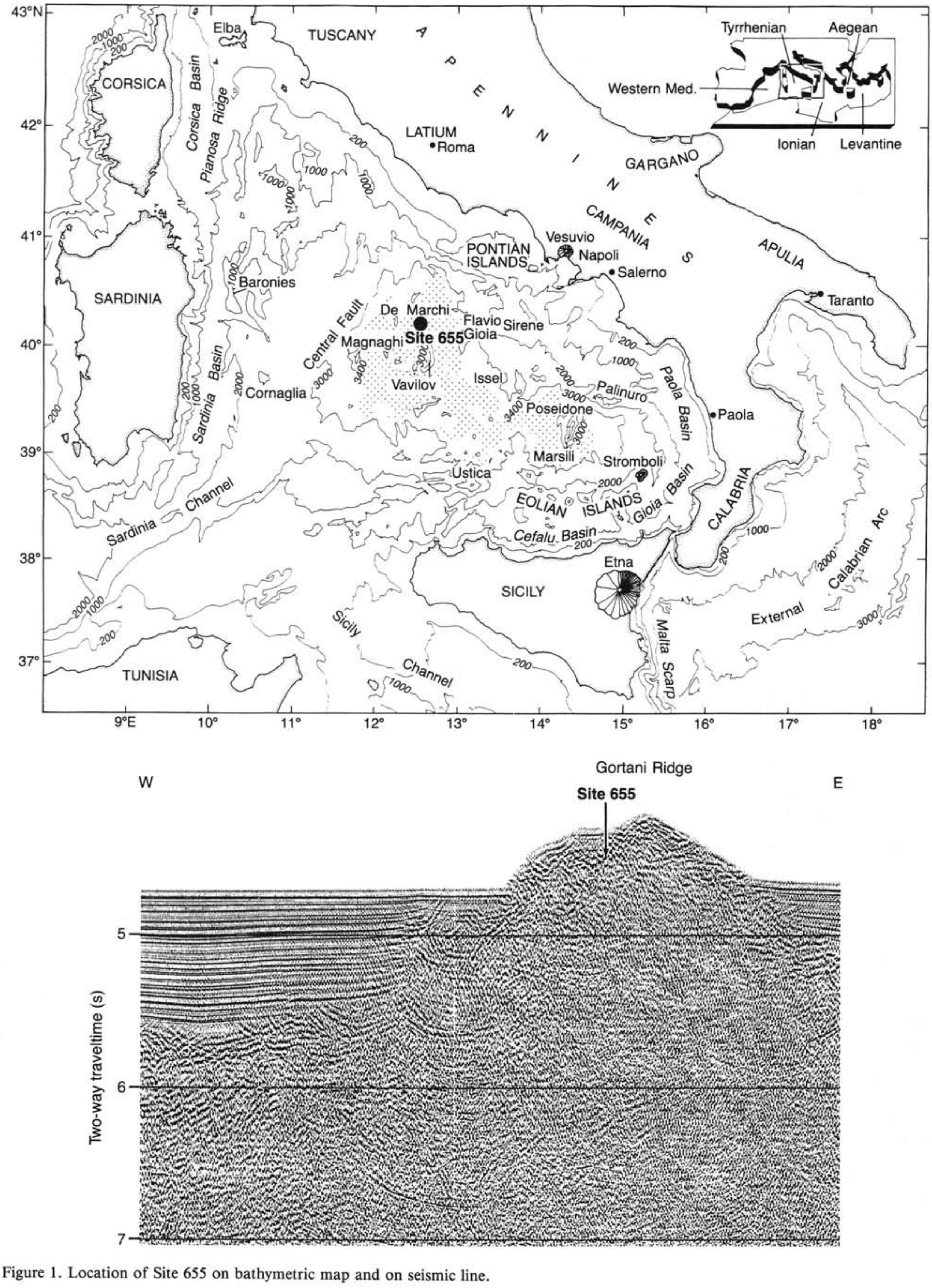

Figure 1. Location of Site 655 on bathymetric map and on seismic line.

Three heat flow measurements in Hole 655A yielded a mean heat flow value of approximately 2 HFU (heat flow units). One logging run was completed in Hole 655B with a DIL-LSS-GR-CALI combination.

BACKGROUND AND OBJECTIVES

Regional Setting and Previous Work

The sequence of events which occurs as the continental-stretching phase of basin formation ends, and injection of true oceanic basement begins, is not clear. It has been postulated that at the end of the rifting phase of basin formation but prior to the injection of basaltic crust, the upper mantle may rise very close to and possibly penetrate through the earth's surface. This hypothesis was inspired by the observation of serpentinized peridotite near the inferred ocean/continent transition in the Red Sea (Bonatti et al., 1981) and the Atlantic margin off Galicia, Spain (Boillot et al., 1980). The problem was most recently addressed by ODP Leg 103 (Site 637) (Boillot et al., 1985), which sampled serpentinized peridotite in a north-trending, sublinear, narrow (about 10 km wide and 60 km long) ridge at the base of the continental slope off Spain.

Site 655 is located on a north-trending bathymetric ridge which lies along the transition between inferred oceanic and continental lithosphere, in a position tectonically analogous to the peridotite ridge off Galicia (Fig. 4). This ridge, the Gortani Ridge, is about 5 km wide and 40 km long (Fig. 5; Moussat et al., 1985). Its height varies along strike; at Site 655 it has about 350 m of relief above the bathyal plain. A similar north-trending narrow ridge is observed on the eastern rim of Vavilov Basin in a position roughly symmetrical to Gortani Ridge. Seismic refraction experiments (Steinmetz et al., 1983; Recq et al., 1984) suggest that the Moho under Site 655 is about 6 km below the seafloor. Unlike the Galicia margin ridge drilled at Site 637, however, Gortani Ridge is associated with a positive magnetic anomaly of 170 γ.

On seismic line ST12 (Figs. 6 and 7), the Gortani Ridge appears as a narrow acoustic basement ridge rising above the well-layered acoustic reflectors filling the Vavilov Basin bathyal plain. Unprocessed seismic profiles show the ridge as a highly diffractive basement high. However, a seismic velocity analysis on top of the ridge suggests that it is covered by more than 100 m of poorly stratified uncompacted sediments characterized by an interval velocity of 1.65 km/s. The seismic velocity within the basement is 5.24 km/sec. The sediments east and west of the ridge have clearly been ponded against the ridge; there is no evidence of sediments bowed up as might be associated with recent uplift, e.g., a diapir. The seafloor east of the ridge is slightly shallower than that west of the ridge (3475 m vs. 3515 m), suggesting that the ridge has served as a dam for turbidity currents originating from the Italian margin.

Objectives

Site 655 was not viewed as a first-priority target by either the Mediterranean Working Group or most members of the shipboard party. However, the site did offer the potential for a number of significant results for a relatively small investment of shiptime.

The major objective at Site 655 was to identify the nature of the basement of the ridge and thus to test the hypothesis that the ridge is an upper mantle protrusion which rose to the earth's surface at the end of the rifting phase of basin formation. If Leg 107 could document peridotite near the oceanic/continental boundary, the hypothesis that upper mantle material rose to the surface through the thinned continental crust would be bolstered. If, on the other hand, the ridge turned out to be basalt, geochemical analysis of such samples derived from within a few kilometers of the ocean/continent transition would provide a valuable comparison with the basalts from the western edge of Marsili Basin (Site 650), with basalts from the axis of Vavilov Basin (Site 651), and with basalts from other ocean and back-arc basins.

As we reached the last week of the cruise, we still had not fully achieved our first-priority goal of obtaining a high quality-magnetic stratigraphy for the Pliocene-Quaternary which could be used to calibrate biostratigraphies and isotope stratigraphies. Site 650 had a good magnetostratigraphy, but only down through the Pleistocene. At Sites 651, 652, and 654, the upper part of the sediment column was disturbed by rotary drilling. At Site 653, which had been targeted specifically for high-resolution stratigraphic studies, the natural remanent magnetization of the upper sediment column was too weak to identify geomagnetic reversals by shipboard measurements. We therefore decided to try coring Hole 655A as an APC/XCB hole to try to get good recovery with minimal sediment disturbance in the presumably pelagic and/or hemipelagic sedimentary cap.

Site Selection

Gortani Ridge appears on site survey lines ST04, ST05, ST12, ST01, and ST08. A position on line ST12 was selected (Figs. 6 and 7). The site was originally located at the edge of the bathyal plain on the western flank of the ridge, because it was not obvious that there was enough sediment to spud in on top of the ridge. However, interval velocity analyses received just prior to departure from Malaga showed more than 100 m of sediment on top of the ridge. In light of these new data, the site was relocated on the crest of the ridge to avoid the Vavilov Basin coarse clastics which had caused hole stability problems at Site 651, to minimize the amount of overburden to be penetrated before reaching the basement target, and to recover a pelagic rather than a turbiditic sequence.

OPERATIONS

Strategy

As conceived prior to the cruise, Site 655 had been strictly a basement objective, and as such was planned for rotary drilling. However, as the final week of the cruise approached, one of the first-priority goals of the cruise had not yet been fully accomplished: to acquire a near-complete, little-disturbed, pelagic, Pliocene-Quaternary sequence which could be used to establish comparative bio-, magneto- and isotope-stratigraphies. Therefore we chose to begin coring at Hole 655A with the APC/XCB combination in hopes of recovering a useable Pliocene-Quaternary pelagic section before entering basement. With luck, the XCB would penetrate far enough to identify the nature of basement. If not, a second hole would be rotary cored into basement, washing down through the overlying sedimentary section.

Heat flow measurements were planned with the Von Herzen probe while piston coring. Since the total penetration was expected to be considerably less than 400 m, logging was optional. The final decision about whether to log or not would be made at the end of the coring program, and would depend on whether the penetration achieved and the thickness of the sediment cover were such that the basement/sediment contact could be logged, and on the amount of time remaining in the cruise.

The site approach was straightforward. Since the target was on top of a north-trending ridge, we planned to approach the site on a west to east track, slow the ship as we reached the base of the ridge, and drop the beacon when the echo-sounder showed the ridgetop. No seismic gear would be streamed.

Site Approach

During the latter part of the transit from Site 654 and throughout the site approach, the ship was navigated using the Global Positioning System (GPS). Loran C was monitored but appeared unstable. At 2200 on 8 February, the ship changed course to

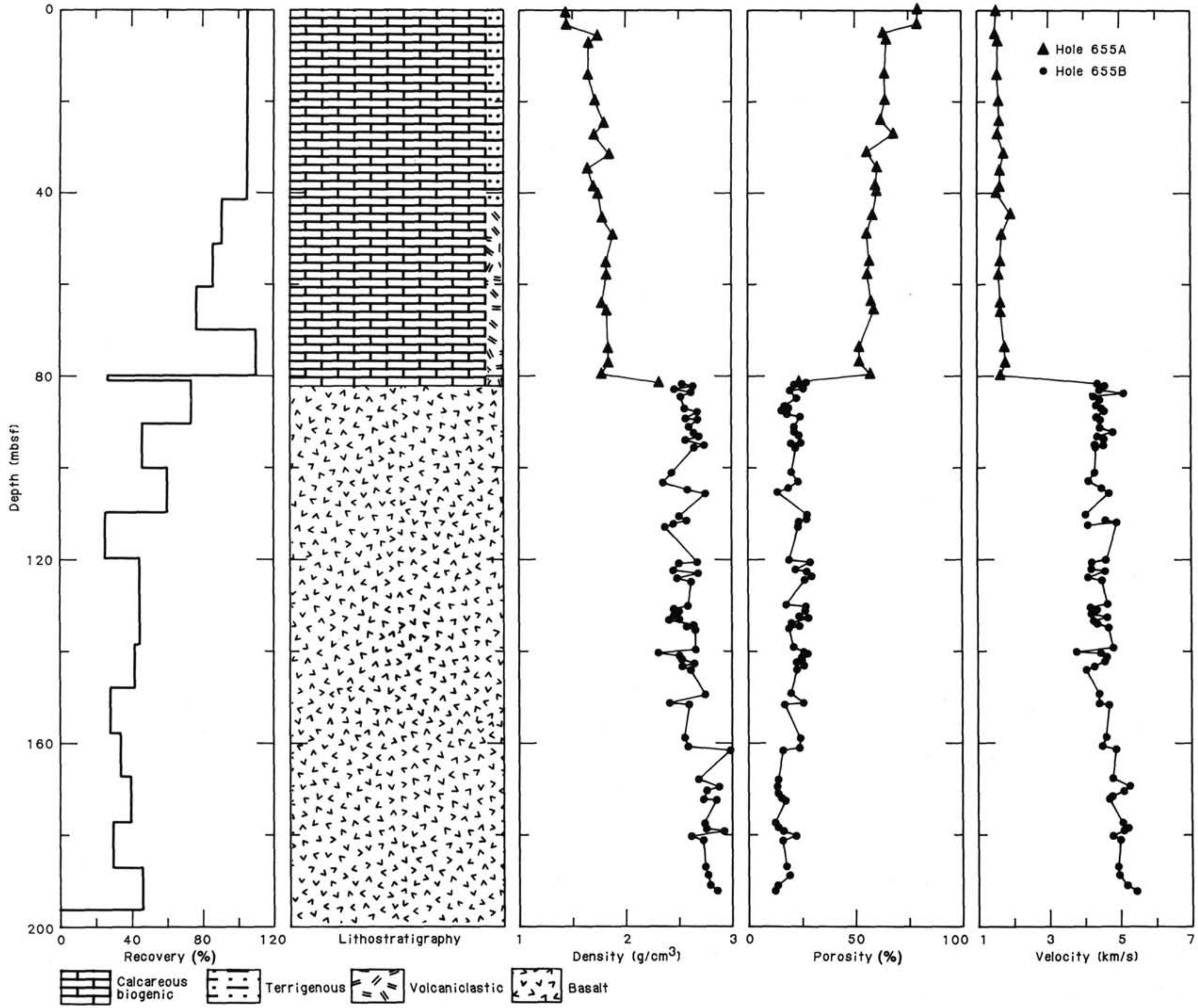
Depth (mbsf)
0
40
80
120
160
200
0 40 80 120
Recovery (%)
Lithostratigraphy
1 2 3
Density (g/cm3)
0 50 100
Porosity (%)
1 3 5 7
Velocity (km/s)
Hole 655A
Hole 655B
Calcareous biogenic
Terrigenous
Volcaniclastic
Basalt

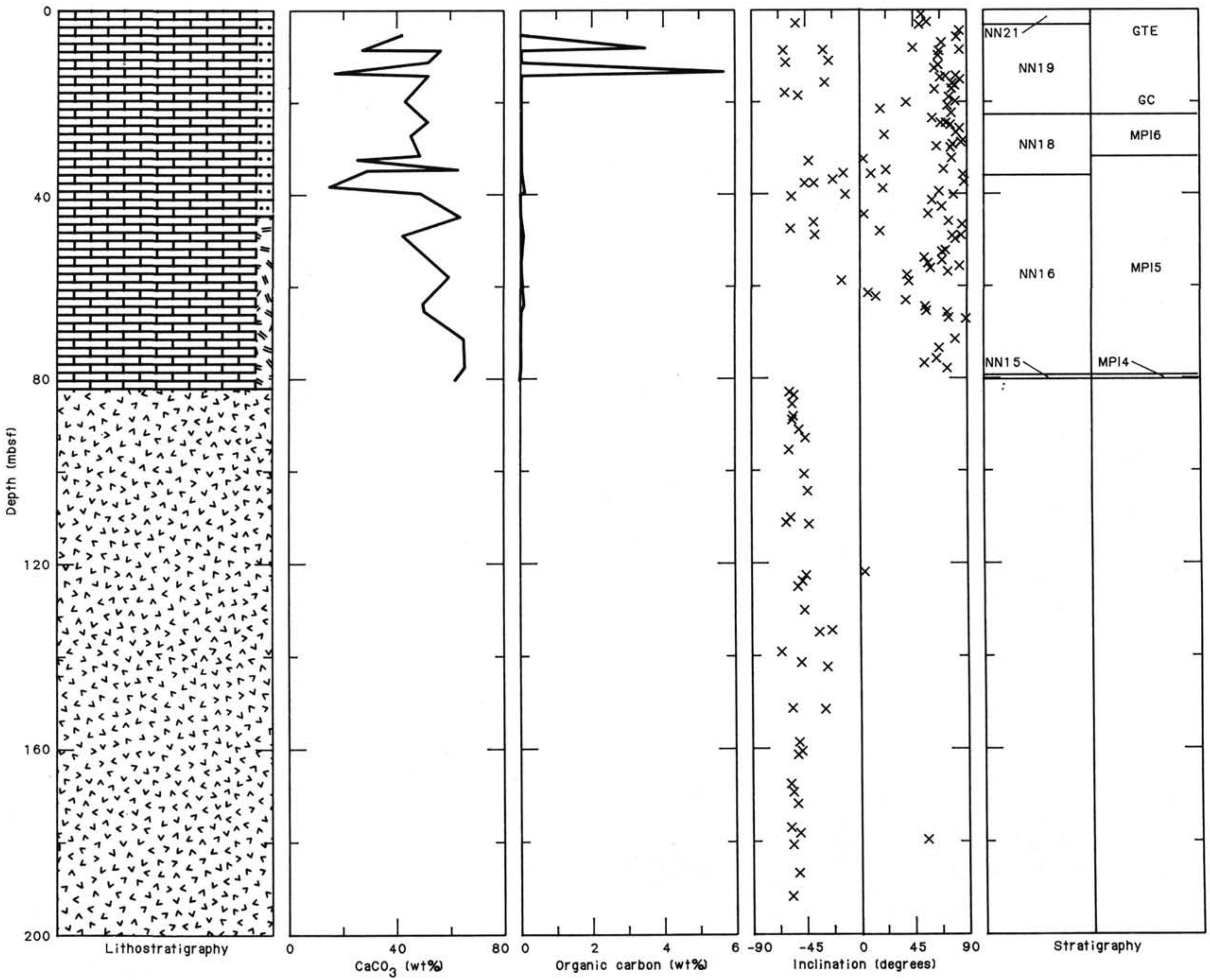

Figure 2. Summary of measurements made at Site 655.

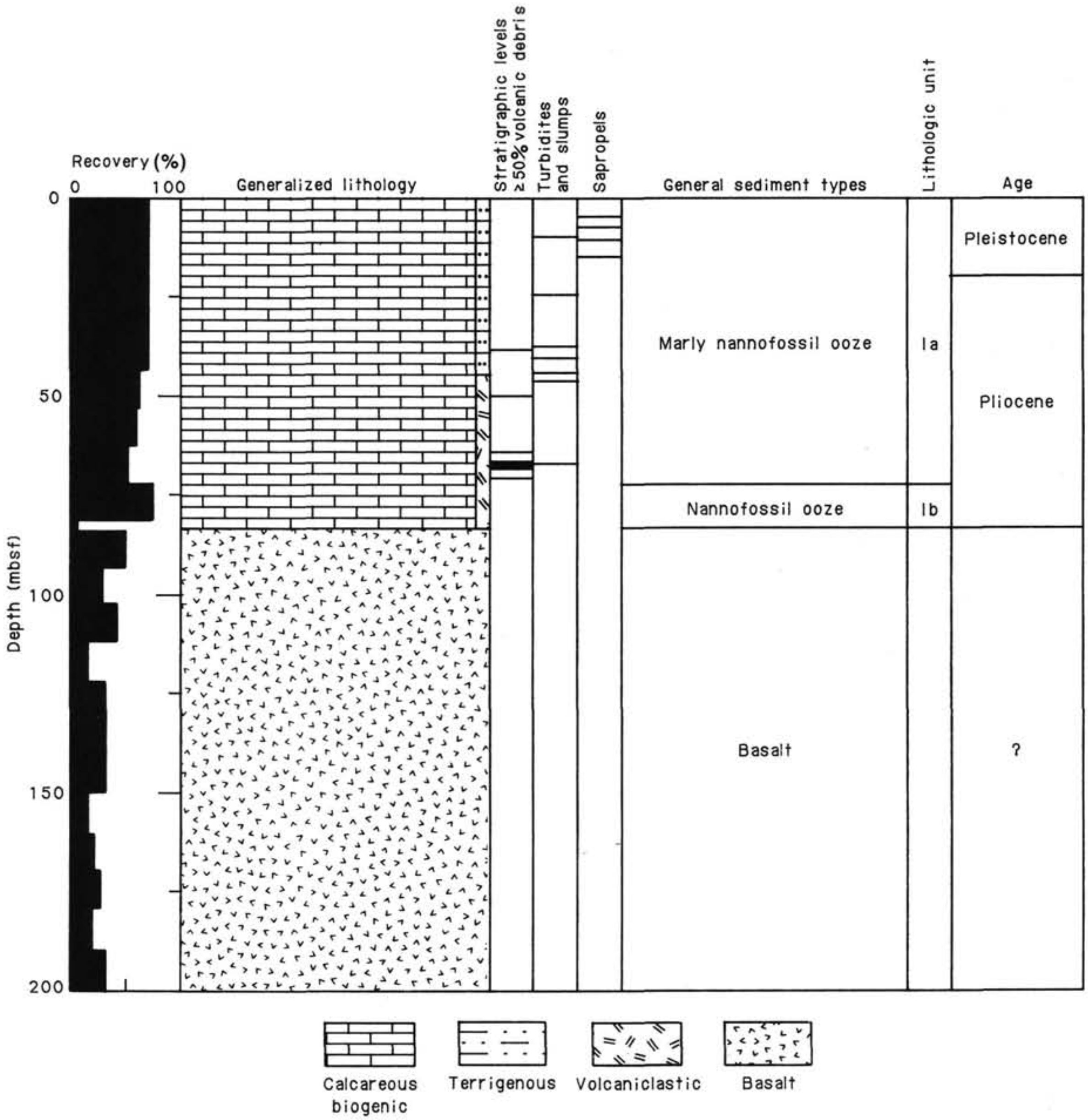

Figure 3. Composite lithologic column of Site 655.

093° to follow the track of site survey line ST12. Because the sea was fairly rough, both the 3.5-kHz and the 12-kHz echo-sounder records were very noisy at full speed (12 kt), so at 2226 the ship was slowed to 6 kt to improve the record quality.

At 2318 the side echo from the western flank of the target ridge came into view, and the ship's speed was further reduced to 3 kt. The echo-sounders were closely monitored as the ship slipped slowly over the flank of the ridge, and the beacon was dropped at 2340 when the strongest of the several hyperbolic bottom returns flattened off and began to deepen very slightly. After the beacon was dropped, another hyperbolic bottom return rose to a depth approximately 55 m shallower than the spot where the beacon was dropped. However, this second, shallower peak was a relatively weak return, and comparison with a seabeam map of the ridge (J.-P. Rehault, pers. comm., 1986) suggests that the second peak was probably a side echo from a higher part of the ridge south of the beacon position.

The echo-sounder line was continued eastward until the bathyal plain east of the ridge came into view. At 0011 on 9 February, the ship reversed course to return to beacon to begin dynamic positioning.

The ship's GPS position at the time of the beacon drop was 40°10.318′N, 12°27.915′E; the Loran C position using X and Z slaves was 40°11.04′N, 12°29.33′E. An average of transit satellites and GPS fixes received while on station gave the following positions: 655A: 40°10.33′N, 12°27.90′E; 655B: 40°10.32′N, 12°27.93′E. The Loran position at 655A was 40°10.21′N, 12° 27.75′E, using the X and Y slaves. Loran time delays were: Z, 52374.7; X, 13165.4.

Hole 655A

The APC/XCB hole was spudded with a good mud-line core at 1115 on 9 February. Oriented piston coring continued for eight cores, until indications of liner overload forced a switch to

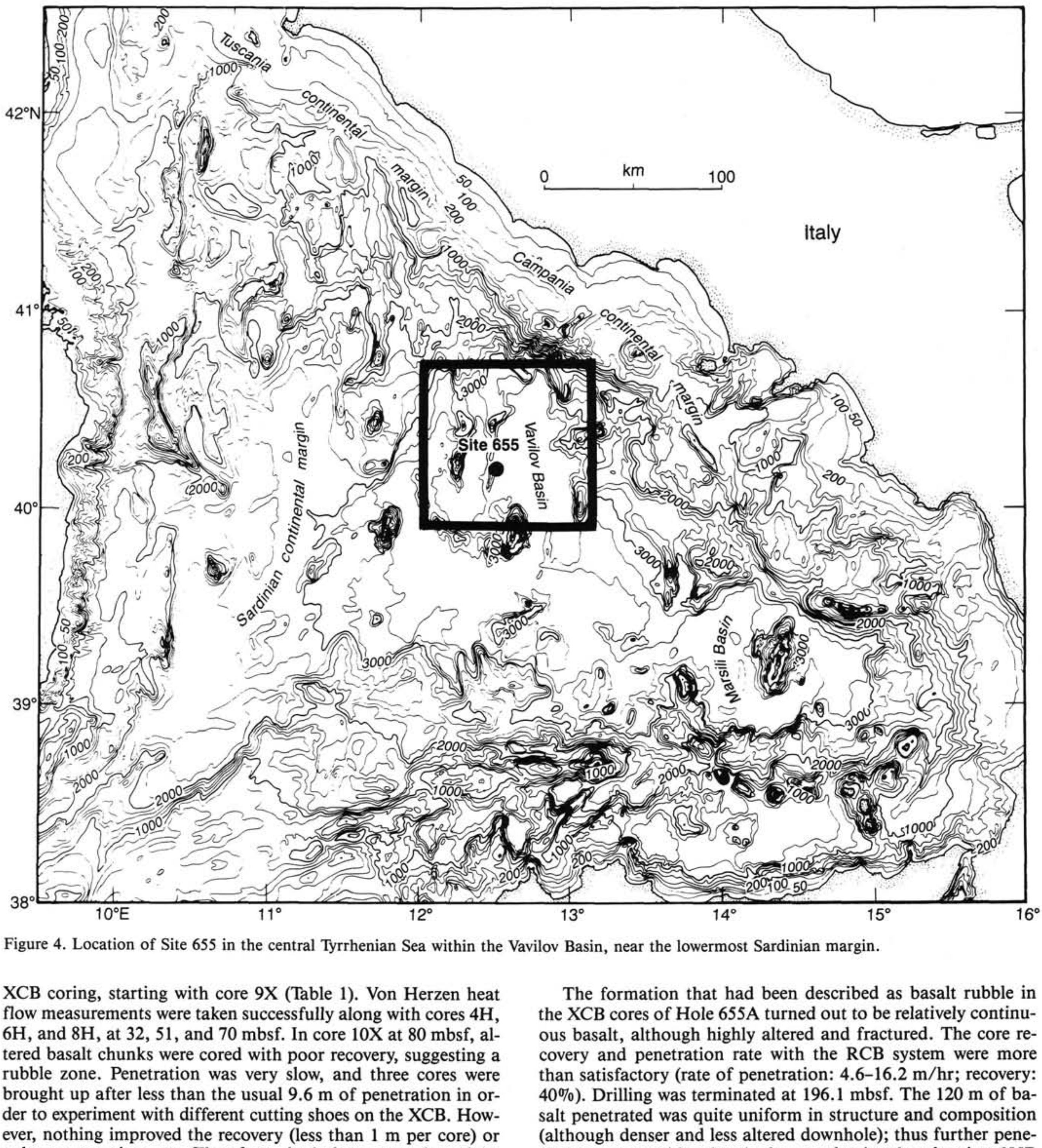

Figure 4. Location of Site 655 in the central Tyrrhenian Sea within the Vavilov Basin, near the lowermost Sardinian margin.

XCB coring, starting with core 9X (Table 1). Von Herzen heat flow measurements were taken successfully along with cores 4H, 6H, and 8H, at 32, 51, and 70 mbsf. In core 10X at 80 mbsf, altered basalt chunks were cored with poor recovery, suggesting a rubble zone. Penetration was very slow, and three cores were brought up after less than the usual 9.6 m of penetration in order to experiment with different cutting shoes on the XCB. However, nothing improved the recovery (less than 1 m per core) or paltry penetration rate. Therefore, the hole was terminated (at 90.4 mbsf) to leave time to rotary-drill a second hole.

Hole 655B

The ship was offset 15 m (50 ft) to the west while the pipe was pulled to the surface and the bottom-hole assembly was changed for RCB coring. The pipe was run back to bottom with a center bit in place and the hole was drilled to 81.2 mbsf before RCB coring resumed.

The formation that had been described as basalt rubble in the XCB cores of Hole 655A turned out to be relatively continuous basalt, although highly altered and fractured. The core recovery and penetration rate with the RCB system were more than satisfactory (rate of penetration: 4.6–16.2 m/hr; recovery: 40%). Drilling was terminated at 196.1 mbsf. The 120 m of basalt penetrated was quite uniform in structure and composition (although denser and less altered downhole); thus further penetration was considered to be less productive than logging 655B and coring one additional site before heading into port.

The hydraulic bit release was activated with some difficulty. The pipe was then pulled up to 3418 m (87.8 mbsf) and the logging equipment was rigged up. The first suite of logs consisted of dual induction log (DIL), long spacing sonic tool (LSS), gamma ray (GR), and caliper (CALI). The hole was logged from total depth up to 70 mbsf; the logged interval includes the sediment/basalt contact plus 115 m of basalt. A second logging run with the borehole televiewer (BHTV) was aborted when the cable head

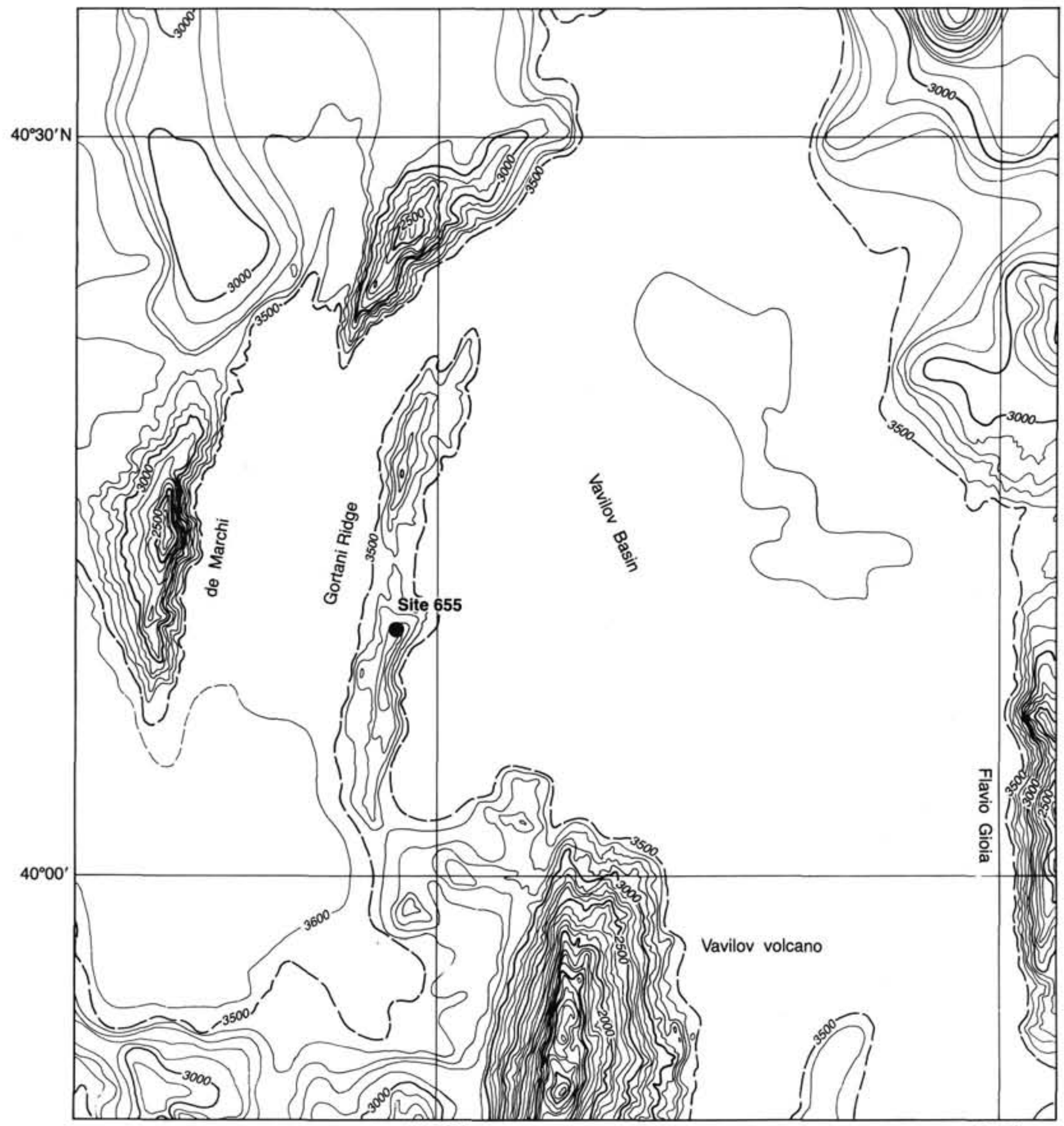

Figure 5. Sea-beam map of the Gortani Ridge and other basement features within the Vavilov Basin.

on the tool flooded as the tool was being lowered through the pipe. The BHTV was recovered and the logging equipment was rigged down. The vessel got underway for Site 656 (TYR 4) at 1355 on 13 February.

LITHOSTRATIGRAPHY

Lithologic Description

The 79.9-m thick sedimentary sequence of Hole 655A is basically very homogeneous in comparison with other Leg 107 sites; consequently only one lithologic unit is defined. This single unit has been divided into two subunits in order to emphasize the altered sediments in contact with the underlying basalts.

The sediments are mainly nannofossil oozes very similar to analogous sediments found in the previous sites. The single sedimentary unit of Site 655 is correlatable with nannofossil-ooze-dominated units of other sites: Unit I of Holes 653A and B, Unit I of Site 654, and also with Units I and II of Sites 650, 651, and 652 where nannofossil oozes represent the background sediments. The equivalent of Unit I of Sites 650, 651, and 652 (characterized by a low percent of $CaCO_3$) corresponds to the uppermost one or two cores at Site 655.

Subunit Ia (0–73.5 mbsf, Cores 107-655A-1H to 107-655A-9X-3, 30 cm). Age: Quaternary-Pliocene.

The dominant lithology is a marly nannofossil ooze to nannofossil ooze with abundant foraminifers. The $CaCO_3$ percentage ranges from 42% to 66% with an average value of 54%. Values greater than 60% were found beginning at 31.9 mbsf (Core 107-655A-5H), remaining high for the remainder of the sequence. The boundary between Pleistocene and Pliocene, situated between Cores 107-655A-3H and -4H (see "Biostratigraphy" section, this chapter), is not marked by a lithologic change. In Core 107-655A-1H, thin (0.5–3 cm) detrital sand (quartz, feldspar, lithoclasts) layers and biogenic calcareous sands rich in pteropods shells occur. One <1-mm iron/manganese-rich crust is found within marly nannofossil ooze at interval 107-655A-2H-3, 63 cm (6.7 mbsf).

Six sapropels or sapropelic layers, identified by their distinctive color, sedimentary structures, and percentage organic-carbon data, occur within the Pleistocene sediments of interval 107-

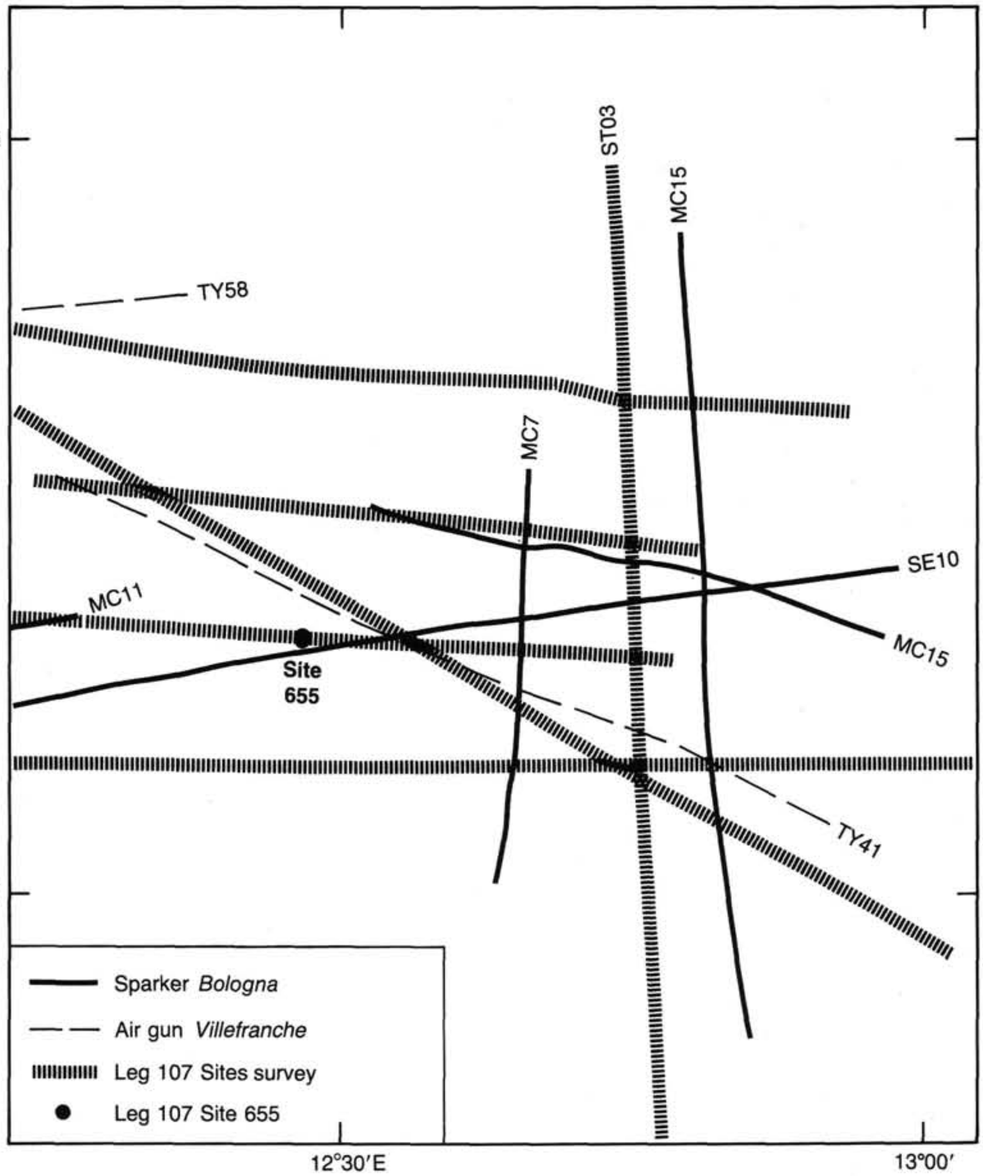

Figure 6. Track lines of recent seismic lines available in the vicinity of Site 655.

655A-2H-4, 59–70 cm (8.2 mbsf) (maximum percentage C_{org} = 5.30%), 2H-6, 85–95 cm (11.45 mbsf), and interval 107-655A-3H-1, 52–72 cm (13.3 mbsf) (maximum percentage C_{org} = 5.30%), 3H-1, 145 cm (14.15 mbsf), 3H-4, 63-78 cm (17.85 mbsf) (maximum percentage C_{org} = 3.60%), and 3H-5, 10 cm (18.8 mbsf, see discussion below).

An important characteristic of the Pliocene sediments is the frequent occurrence of banded pinkish to reddish intervals (Table 2), which could indicate variable oxygen contents in the sediments. These intervals begin to occur with Core 107-655A-4H (below 25.5 mbsf) and continue downsection to Core 107-655A-8H (below 70.2 mbsf).

Volcaniclastic layers are present throughout most of the sequence (Table 3). Normal graded bedding indicates probable deposition as turbidites. In Core 107-655A-5H, a 75-cm-thick ash layer, rich in black heavy minerals (mainly pyroxenes), shows parallel laminations within the normally graded sequence.

Subunit Ib (73.5–79.9 mbsf, Core 107-655A-9X-3, 30 cm to CC). Age: Pliocene.

The sediments are foraminifer-rich nannofossil oozes as in Subunit Ia, but a downhole progressive change in color from pale yellow to brown was noted as the underlying basalts were approached. Numerous black specks presumed to be iron sulfide are present and increase in number toward the base of the core. The last 25 cm before the basalts are strong brown in color. The last 5 cm contain an indurated, dark brown dolostone. The basalt at the sediment contact is vesicular.

Sapropels and Sapropelic Layers

Of the six sapropels or sapropelic layers identified in Cores 107-655A-2H and -3H, two are particularly illustrative of what might be considered well-developed sapropels from the Tyrrhenian Sea. The first of these (interval 107-655A-2H-4, 59–70 cm) was recovered undisturbed and basically retains its distinctive sedimentary features (Fig. 8). Features of this excellent example will be described in order of deposition from base to top. The sediments underlying the sapropel are gray, moderately to strongly bioturbated, marly nannofossil oozes with abundant foramini-

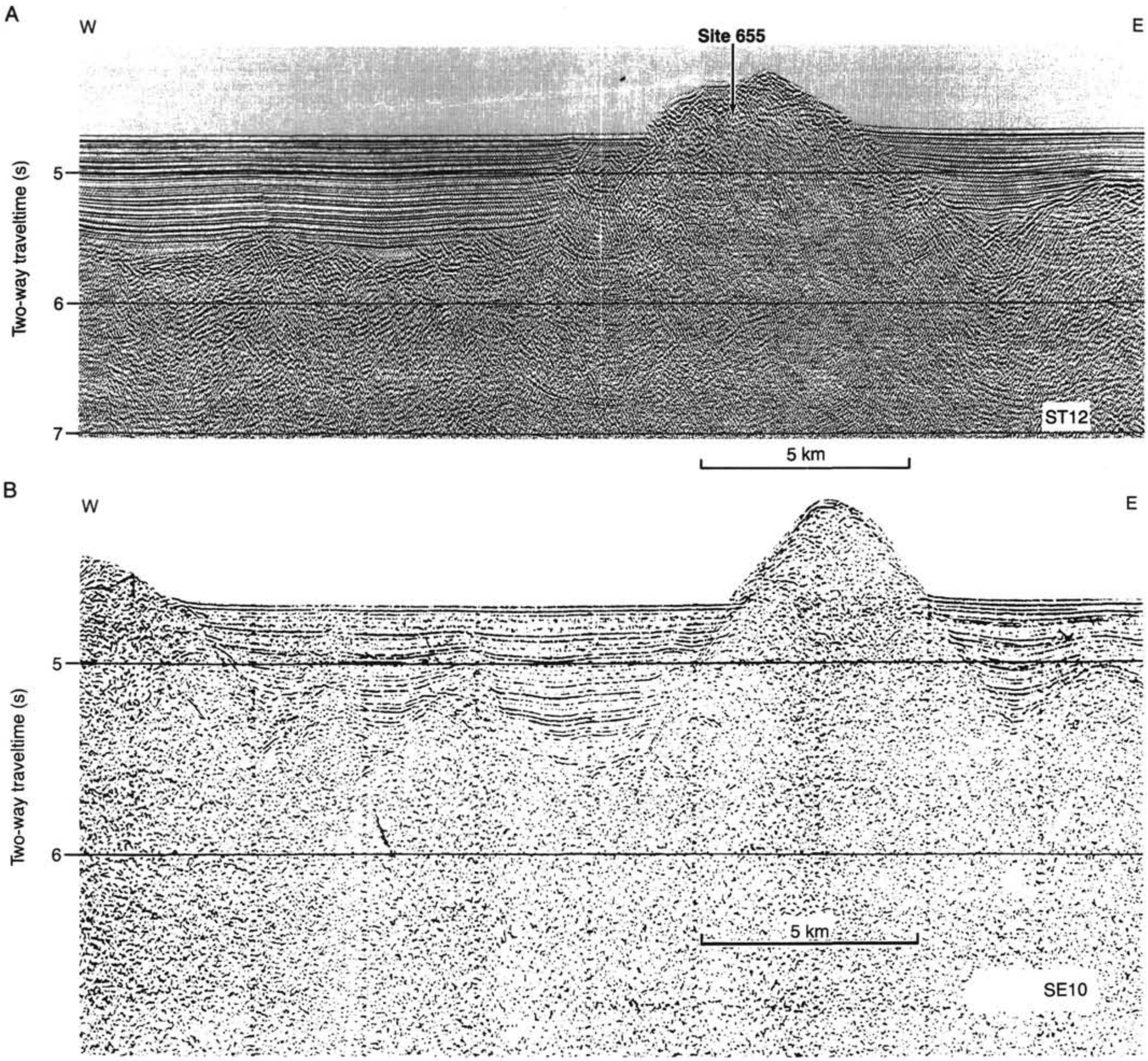

Figure 7. A. Multichannel seismic line ST12 (site survey line; LGSM, *Villefranche*) and location of Site 655 (location in Fig. 6). B. Sparker line (from I.G.M. *Bologna*) in the vicinity of Site 655 (location in Fig. 6).

fers (107-655A-2H-4, 70–146 cm). Directly beneath the sapropel (70–75 cm), the number of black, iron-sulfide-rich specks increases; the outlines of the bioturbation are defined by darker colors than the matrix, producing a modified wavy appearance. From 67–70 cm, the sediment is dark olive in color and contains very abundant foraminifers. The color then grades upward into a black, laminated interval (64.5–67 cm). A smear slide from 67 cm shows the presence of 4% micronodules in these black sediments. The black sediments contain a maximum of 5.30% organic carbon. Upsection, the sediment becomes greenish gray (59–64.5 cm) and is devoid of visible foraminifers. This latter color interval can be further divided into an underlying laminated zone (61.5–64.5 cm), which shows only faint indications of burrowing, followed by a distinct darker contact (61.5 cm) to an overlying bioturbated zone (59–61.5 cm). The amount of bioturbation appears to increase gradually upward with the burrows being particularly small (few millimeters wide) and well-defined by a lighter colored material. At 58–59 cm, a diagenetic front is marked by olive-colored sediments which have a sharp basal contact slightly cut by the fine bioturbation. Above 59 cm larger burrows appear, and above 58 cm the color grades once again to gray. Geochemical data for the carbonate and organic carbon content of samples taken at 0.5-cm-intervals throughout this sapropel are tabulated in "Geochemistry" section, this chapter.

The second of the well-developed sapropels (interval 107-655A-3H-1, 52–72 cm) was moderately disturbed during drilling, but sedimentary characteristics similar to those described above remain quite evident (Fig. 9). Closely spaced samples were collected through the sapropelic interval for the determination of carbonate and organic carbon contents. These data are graphed alongside the core photograph in Figure 9 and can be found tab-

Table 1. Coring summary table for Holes 655A and 655B.

Core no.	Date (Feb. 1986)	Time	Sub-bottom depths (m)	Cored (m)	Recovered (m)	Recovery (%)
Hole 655A						
1H	9	1130	0.0-3.1	3.1	3.1	100.7
2H	9	1300	3.1-12.7	9.6	9.8	101.7
3H	9	1415	12.7-22.3	9.6	9.8	102.2
4H	9	1600	22.3-31.9	9.6	9.8	101.8
5H	9	1730	31.9-41.5	9.6	9.8	102.3
6H	9	1915	41.5-51.1	9.6	8.5	88.8
7H	9	2145	51.1-60.6	9.5	8.1	85.2
8H	10	0030	60.6-70.2	9.6	7.2	74.8
9X	10	0300	70.7-79.9	9.1	9.8	107.7
10X	10	0630	79.9-86.4	6.5	0.6	8.9
11X	10	0815	86.4-89.4	3.0	0.2	7.7
12X	10	1015	89.4-90.4	1.0	0.7	70.0
Hole 655B						
1R	11	1745	81.2-90.8	9.6	6.9	72.1
2R	11	2045	90.8-100.4	9.6	4.2	43.2
3R	12	0015	100.4-110.0	9.6	6.1	63.7
4R	12	0215	110.0-119.5	9.5	2.3	23.9
5R	12	0445	119.5-129.1	9.6	4.5	46.4
6R	12	0645	129.1-138.8	9.7	4.4	44.9
7R	12	0845	138.8-148.3	9.5	4.0	42.5
8R	12	1115	148.3-157.9	9.6	2.5	26.5
9R	12	1345	157.9-167.5	9.6	3.2	33.3
10R	12	1615	167.5-177.1	9.6	3.9	40.4
11R	12	1900	177.1-186.8	9.7	2.9	30.3
12R	12	2300	186.8-196.1	9.3	4.5	48.1

Table 2. Banded red color intervals.

Core number	Section	Depth interval (mbsf)
Core 107-655A-4H	3	25.5-26.8
	5, 6, 7	28.3-31.7
-5H	1	32.5-33.4
-6H	1, 2, 3	42.1-47.3
	4	47.6-48.6
-8H	1	61.3-61.7
	2	62.2-62.7

Table 3. Volcaniclastic ash-bearing layers.

Core number	Section	Depth of top (mbsf)	Thickness (cm)
Core 107-655A-1H	1	0.55	3
	2	2.36	2
-2H	7	12.20	4
-3H	5	19.00	2
-4H	4	27.30	3
-5H	5	37.90	75
	6	40.85	2
-6H	4	46.38	1
-8H	4	66.10	8
	5	66.80	8

ulated in "Geochemistry" section, this chapter. It is interesting to note that the percent carbonate decreases upward gradually through the dark sapropelic interval, reaching a minimum in the upper black laminated zone at 63 cm. The percent organic carbon begins to increase steadily from the base of the dark sapropelic zone reaching a maximum of 5.69% at 1.5 cm below the carbonate minimum (64.5 cm). The percent organic carbon returns to near background values (<0.3%) just above the darkest interval at 59 cm, while the percentage carbonate continues to gradually increase to near pre-sapropelic values just above the upper limits of the diagenetic front (50.5 cm). The increased organic carbon contents are definitely confined and obviously related to changes in input or preservation characteristics restricted to within the darkest sediments. Further definition of the nature and origin of these distinctive sapropels awaits the results of shore-based studies.

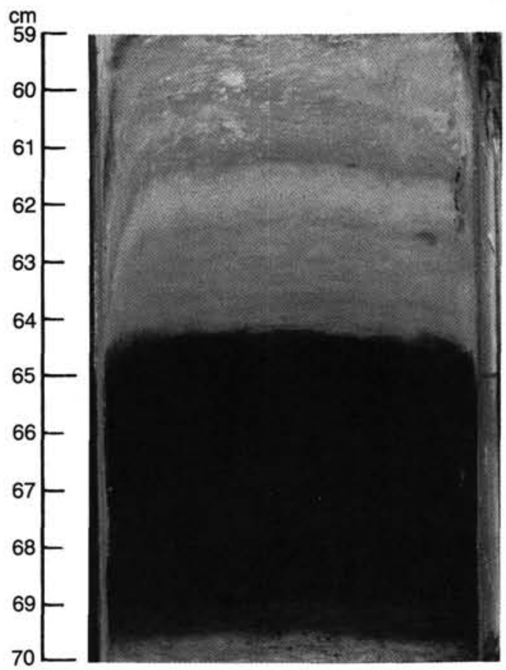

Figure 8. Probable sapropel layer (Core 107-655A-2H-4, 59–70 cm) showing characteristic sedimentary structures and coloration. See text for discussion of these features.

Sedimentary Instability

In addition to the volcanogenic turbiditic layers (see Table 3), sedimentary instability is denoted by the occurrence of several debris flows in Sections 107-655A-2H-4 and -5 (9.05–9.40 mbsf), Sections 107-655A-3H-6 and -7 (21.4–22.3 mbsf), Section 107-655A-6X-5 (48.1–48.6 mbsf), and possibly in Section 107-655A-6X-2 (43.7–43.8 mbsf). Reworked fragments of marly nannofossil oozes of various color sometimes contain a mixture of micro- and nannofossils indicating a variety of geologic ages for these mud pebbles (see "Biostratigraphy" section, this chapter). Due to intense drilling disturbances, one cannot be certain whether all of the observed structures in the debris flow at Sections 107-655A-3H-6 and -7 are primary or caused by drilling, but pieces of a sapropelic layer are present within this flow. The only true tensional microfault was observed within the debris flow from 9.05 to 9.40 mbsf.

The occurrence of debris flows is somewhat surprising near the top of a topographic high which is apparently about 250 m high. Possibly, uplift of the hill and tilting of the basaltic basement are very recent, but this interpretation is not supported by seismic reflection profiles.

Limestones Within the Basalt Sequence

Indurated limestones occur in the basalt flows in three different ways: (1) thin layers in contact with chilled basalt; (2) in cracks within basalt that is not chilled at the contacts, and (3) as very thin elongate veins.

1. In this case fine-grained limestone is in contact with the chilled margins of vesicular basalt (e.g., interval 107-655A-11X-1,

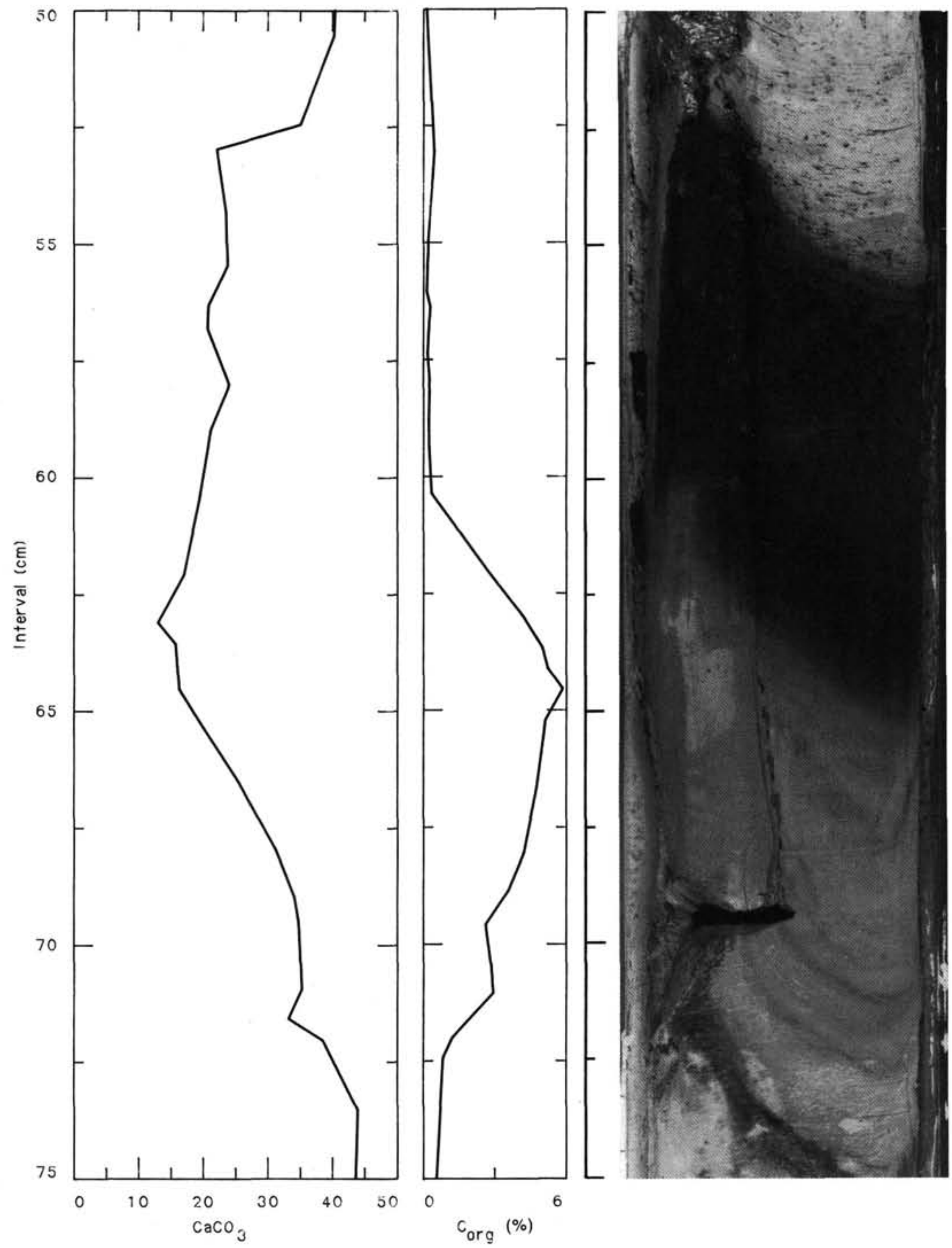

Figure 9. Sapropel layer (Core 107-655A-3H-1, 52–72 cm), moderately disturbed during drilling, showing characteristic sedimentary structures and coloration. The carbonate and organic carbon content obtained from samples taken from the left side of the working core half are graphed alongside the core photograph.

32 cm; interval 107-655A-12X-1, 75 cm) (Fig. 10). This limestone is basically gray, but a thin reddish zone containing palagonite separates the indurated limestone from the chilled margins of the basalt. Some isolated pieces of limestone (5 cm in size) exhibiting a reddish crust also occur. The first limestone type is interpreted to represent former carbonate ooze interbedded between basalt flows (e.g., interval 107-655A-10X-1, 76–80 cm, interval 107-655A-12X-1, 22 cm); it is essentially contemporary with eruption of the pillow lavas.

2. The second type of limestone within the basalts is white, yellowish, or pale gray (e.g., interval 107-655A-11X-1, 32–64 cm; interval 107-655A-12X-1, 29 cm) and lacks chilled margins with the basalt (Fig. 10 and 11). This sediment is sometimes perpendicular to the orientations of chilled margins (Fig. 10). The width of the limestone varies from less than 1 mm to 2 cm. Microfossils or nannofossils are occasionally present (see "Biostratigraphy" section, this chapter). This second limestone type is interpreted to be an filling of ooze that percolated down into

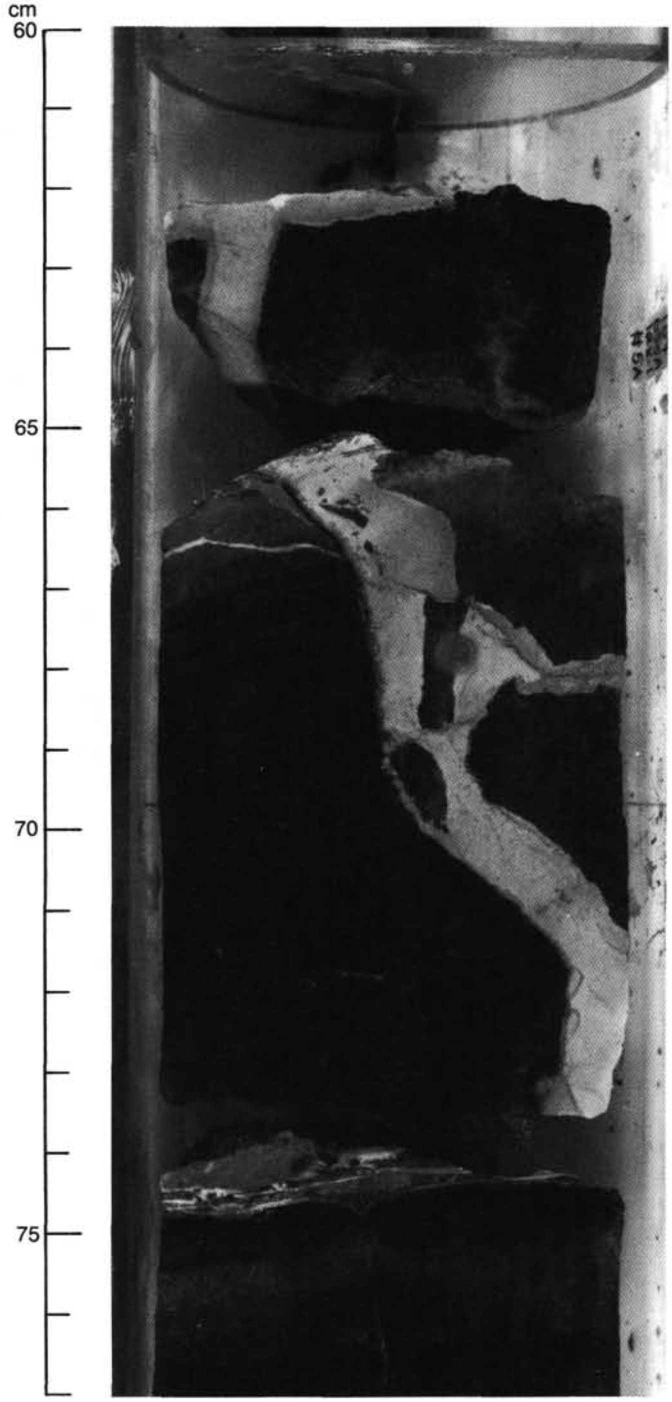

Figure 10. Contact between basalt and limestone (Core 107-655A-12X-1, 60–77 cm, 89.4 mbsf). Chilled margin of a probable basaltic pillow at 75 cm and gray limestone at 74.5 cm are separated by a 2–5-mm reddish zone with calcite and palagonite. From 62 to 73 cm, white limestone fills former fractures in basalt.

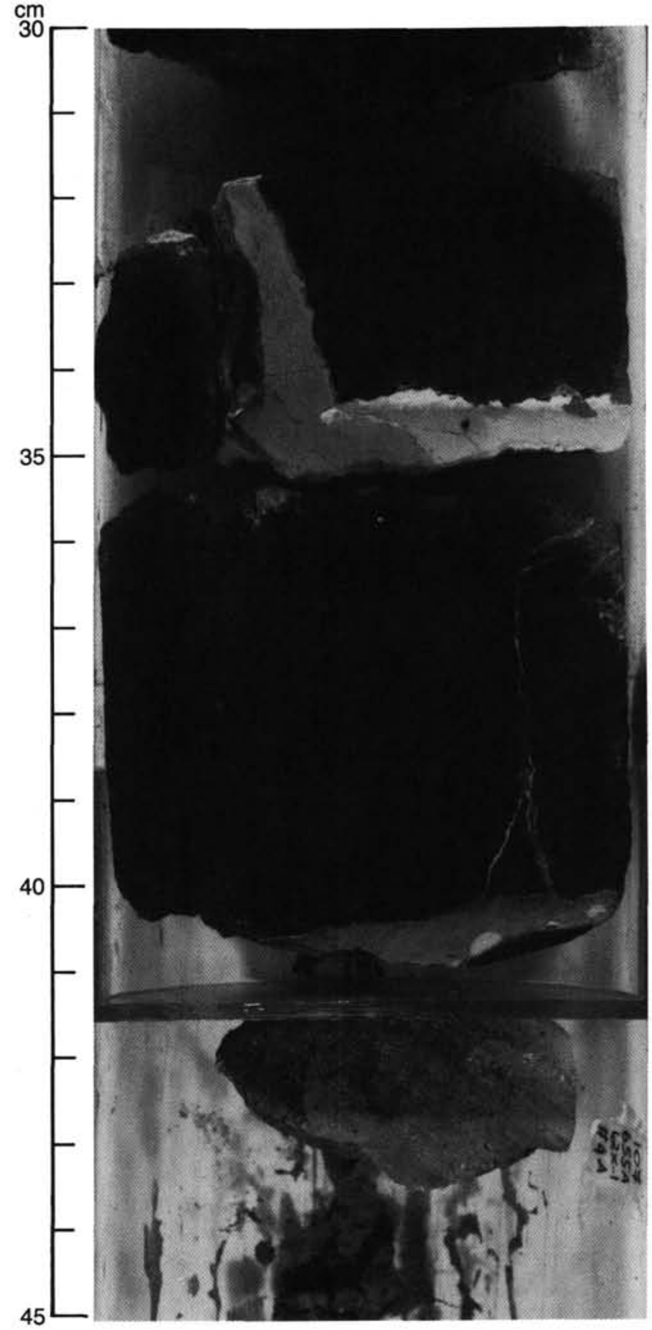

Figure 11. Two successive calcareous fillings in basalt (Core 107-655A-12X-1, 30–45 cm, 89.4 mbsf). At 35 cm, two successive calcareous fillings in the basalts are shown by different colors in the limestone and no chilled margin between basalt and limestones; between 36 and 40 cm a very thin microcrystalline carbonate filling represents *in-situ* precipitated carbonates.

fractured basalt. In some cases, (interval 107-655A-11X-1, 32 cm), two successive generations of fill can be observed (Fig. 11, between 32 and 35 cm).

3. Finally, some very thin veins (less than 1 mm thick) of microcrystalline carbonates probably originated by *in-situ* precipitation from seawater that circulated within basalt fractures (Fig. 11, between 36 and 40 cm; see "Igneous Petrology" section, this chapter).

IGNEOUS PETROLOGY

Holes 655A and 655B Basement

Basalt was encountered in Hole 655A at 80 mbsf, below sediments of middle Pliocene age. The sediment becomes gradually dark brown in color for an interval of about 10–20 cm just above the contact, which is marked by an altered chilled glass margin. The basalt was drilled down to 90.4 mbsf at Hole 655A, for a thickness of 10.4 m, and down to 196.1 mbsf at Hole 655B (rotary drill) for a thickness of 120 m.

Macroscopic Description and Textures

Chilled glass margins were observed throughout the basalt unit. The glassy rims generally show curved shapes, suggesting that they mark the surface of pillows. The distribution of chilled margins indicate that the whole unit consists of many pillow basalt flows, each roughly 2 m thick on average. The glassy rims frequently grade upward into a crust of palagonite and palagonite breccias cemented by carbonates and occasionally by zeolites. In some cases fresh basaltic glass (sideromelane) is preserved.

Throughout the unit, but particularly in approximately the upper 30 m, fractures and veins filled with carbonate were observed in the basalt. In some cases the carbonates consist of micritic sediments, which probably penetrated spaces between pillows and fractures in the rock after emplacement of the basalt on the seafloor. Foraminiferal tests and nannofossils were observed in these sediments. In other cases, particularly within thin veins, the carbonate probably originated by precipitation from seawater circulating within fractures.

The basalt appears to be generally aphanitic, though occasionally phenocrysts (as large as 1-2 mm) of plagioclase can be observed. In thin section the texture of the rock ranges from porphyritic to glomeroporphyritic.

Mineralogy and Chemistry

The modal composition of the basalt appears to be relatively constant throughout the unit, though the degree of alteration varies from mild to strong in different portions of the unit. Phenocrysts of Ca-plagioclase, occasionally associated with euhedral olivine, are set in a groundmass where, in addition to alteration products, smaller plagioclase laths, olivine, and, rarely, an augitic clinopyroxene can be recognized. The plagioclase and olivine phenocrysts are relatively fresh except in a few samples. Close to chilled margins the phenocrysts are set in a glassy matrix with occasional, scattered plagioclase needles.

A few preliminary major element analyses suggest that Site 655 basalt has tholeiitic affinity and is rather similar to basalts drilled at DSDP Site 373 (Hsü, Montadert, et al., 1978) and at Site 651, also within the Vavilov Basin.

Age

The age of the basalt can be constrained based on identification of foraminifers and nannofossils contained in the carbonate sediments trapped within the rock. Among the foraminifers, the presence of *Globorotalia puncticulata*, *Sphaeroidinellopsis* sp., and of *Globorotalia margaritae* in sediments just above the basalt indicates the top of the MPl3 foraminiferal biozone. Among the nannofossils, the presence of *Sphenolithus abies* and *Reticulofenestra pseudoumbilica* indicates the NN15 nannofossil biozone (see "Biostratigraphy" section, this chapter). This information, coupled with paleomagnetic data indicating that the entire basalt unit is reversely magnetized (see "Paleomagnetics" section, this chapter), suggests that the basalt was emplaced within the upper part of the Gilbert magnetic epoch, and has an age which lies between 3.5 and 3.6 m.y. This estimate will have to be verified by absolute age determinations.

BIOSTRATIGRAPHY

Summary

It was expected that the location of Site 655 on top of the Gortani Ridge would provide a sequence void of turbiditic layers. However, the incomplete Quaternary series shows debris flows mixed with Pliocene/Pleistocene sediments, and reworking from older strata.

The determination of the biozones is difficult due to the scarcity or absence of certain index fossils. The results are summarized in Figure 12.

Late Pliocene sediments (of about 3.2 m.y.) overlie vesicular basalts. Micro- and nannofossils are destroyed in the lowermost sediments due to diagenesis.

Planktonic Foraminifers

Quaternary

The lower Quaternary (*Globigerinoides cariacoenis* zone) has been recorded in 107-655A-3H, CC (22.3 mbsf). *Globigerinoides obliquus* occurs until interval 107-653A-3H-2, 72-74 cm (14.9 mbsf). The Pliocene/Pleistocene boundary is recognized in interval 107-655A-3H, CC (22.3 mbsf) by the first peak of left-coiled *Neogloboquadrina pachyderma*.

Globorotalia truncatulinoides excelsa is sporadically present from interval 107-655A-2H-3, 35-38 cm (6.36 mbsf). *Globigerina cariacoensis* is rare.

Holocene was observed at the top of Core 107-655A-1H with the characteristic planktonic assemblage described by Cifelli (1975) from plankton tows and by Parker (1955), Todd (1958), and Thunell (1978) from surface sediments.

Globorotalia truncatulinoides excelsa is sinistrally coiled. Pteropods with transparent shells are frequent and in a state of almost good preservation. The presence of *Hyalocylix striata* and *Styliola subula* characterizes the sediments younger than 4,000 years. No living benthic foraminifers were found.

The Pleistocene/Holocene boundary should be within Core 107-655A-1H.

Pleistocene

Core 107-655A-1H, CC (3.1 mbsf) shows a temperate warm assemblage; 107-655A-2H, CC (12.7 mbsf) and 107-655A-3H, CC (22.3 mbsf) are both temperate. Identification of isotopic stages is not possible at the moment and will remain difficult because both cores should be early Pleistocene in age when climate changes were frequent, but of lower amplitude than in the late Pleistocene (Thunell and Williams, 1981).

Pliocene

Age determination for the Pliocene is based on the zonation given by Cita (1973; 1975).

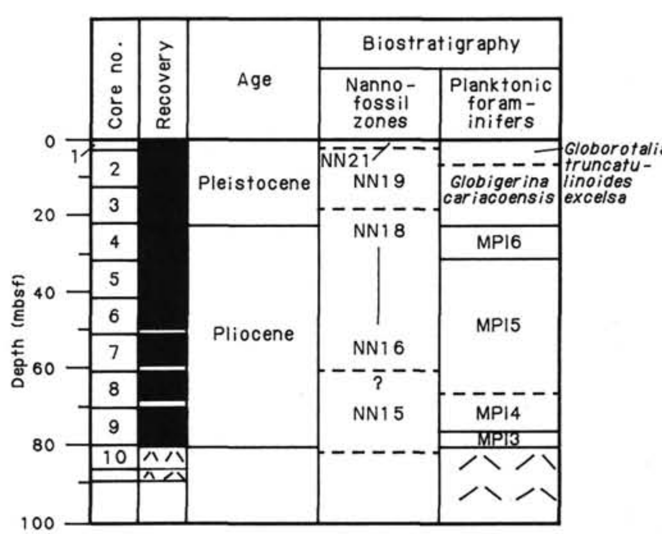

Figure 12. Biostratigraphic determinations made at Site 655.

Upper Pliocene interval is present between about 22.5 mbsf (Sections 107-655A-3H, CC) and 76.3 mbsf (107-655A-9X, CC) where the last *Globorotalia margaritae* occurs. Between 76.3 and 79.8 mbsf the lower Pliocene is present with *Globorotalia puncticulata* and rare and scattered *Globorotalia margaritae*.

MPl6 (*Globorotalia inflata*) biozone was not recorded between 22.5 mbsf and 29.1 mbsf (Core 107-655A-4H-5, 80–84 cm) samples but was at 39.1 mbsf (interval 107-655A-4H-5, 128–130 cm). The extent of the zone will be verified during shore-based studies.

MPl5 (*Globigerinoides elongatus*) biozone is present between about 29.1 mbsf (107-655A-4H, CC) and 59 mbsf (107-655A-7H-6, 36–38 cm), where the last *Sphaeroidinellopsis* sp. was recognized. MPl4 was recognized between 59 mbsf and 76.3 mbsf (107-655A-9H-5, 70–72 cm) where the last *G. margaritae* was recognized. MPl3 is present between 76.3 mbsf and the base of the sequence where *Globorotalia margaritae* and *G. puncticulata* occur together.

Partial dissolution and recrystallization of foraminiferal tests is noted. At 10–11 cm in Section 107-655A-9X, CC, dissolution is very strong. At 6–7 cm in Section 107-655A-9H, CC dissolution seems weaker; small perforations in the wall of mid-sized foraminiferal shells and fragmentation of the large ones can be observed. This phenomenon is comparable with that known from sediments deposited between lysocline and carbonate compensation depth (Berger, 1970; Be et al., 1975) but, at Site 655 it is linked not to the depth but to the proximity of the basalt. How far from the basalt the dissolution occurs will be studied on shore.

In carbonate intervals recovered from within the basaltic unit, planktonic foraminifers and nannofossils are present in thin sections and smear slides. *Globorotalia puncticulata* and rare *Sphaeroidinellopsis* sp. specimens were recognized. *Globorotalia margaritae* is not present in thin sections. In the nannofossil assemblage *Sphenolithus abies* and *Reticulofenestra pseudoumbilica* have been recognized. Therefore the carbonate intervals belong to the MPl4 foraminiferal biozone and to the NN15 nannoplankton biozone. Since the sediments are reverse-magnetized, they must belong to the upper part of Gilbert magnetic Epoch, with an age of about 3.6–3.4 m.y.

Benthic Foraminifera

Benthic foraminifers occurred from the top down to 80 mbsf of Hole 655A. In all the samples between the top and 70 mbsf (Section 107-655A-8H, CC), fairly abundant well-preserved specimens are present. Only a sample at 79.8 mbsf (Section 107-655A-9X, CC) yields ill-preserved and recrystallized specimens.

The top sample of Core 107-654A-1H includes several specimens of *Articulina tubulosa*, *Ammolagena clavata*, and *Glomospira charoides*, accompanied by some displaced specimens of *Miliolinella circularis*, *Elphidium macellum*, and *Asterigerinita mamilla*.

Between 3.1 mbsf (Section 107-655A-1H, CC) and 79.8 mbsf (Section 107-655A-9X, CC), many species were found, and displaced specimens are very rare. The bottom level of *Articulina tubulosa* is placed at 22 mbsf (Section 107-655A-3H, CC) at the very base of *Globigerina cariacoensis* zone. A maximum in the species diversity as found in the Pliocene of Sites 652, 653, and 654 can be recognized in Core 107-655A-8H (60.6–70.2 mbsf). The disappearance level of *Cibicidoides italicus* is found at interval 107-655A-8H-4, 67–69 cm, in the lower part of MPl5 zone of planktonic foraminifers.

Nannoplankton

At Hole 655A the Pleistocene sequence is incomplete. The very condensed or eroded series of nannoplankton zone NN21 (*Emiliania huxleyi* zone) was recognized from the top to sample 107-655A-1H-2, 113 cm directly underlain by zone NN19 (*Pseudoemiliania lacunosa* zone) from sample 107-655A-1H-2, 120 cm to sample 107-655A-3H-1, 144 cm (3.0–14.1 mbsf). Nannoplankton are diluted by detrital carbonates and reworked species within the turbiditic layers of zone NN21. The assemblages are often of low diversity with the dominance of *Syracosphaera mediterraneae* and *Helicosphaera carteri*. Sediments of zone NN19 are generally rich in well-preserved nannoplankton. The acme zone of the small *Gephyrocapsa* was recognized from sample 107-655A-2H-1, 82 cm, to sample 107-655A-3H-1, 130 cm. The extinction level of *Helicosphaera sellii* lies in sample 107-655A-2H-2, 120 cm within the small *Gephyrocapsa* zone.

Sapropel layers are concentrated around the Jaramillo magnetic event (Sections 107-655A-2H-4 to 107-655A-3H-1), and the Pliocene/Pleistocene boundary (Sections 107-655A-3H and -4H). The nannofossils are almost entirely dissolved in the sapropel of sample 107-655A-2H-4, 65 cm.

Large specimens of *Braarudosphaera bigelowi* are common in the sapropel of sample 107-655A-2H-6, 93 cm and within the uppermost Pliocene (Sample 107-655A-3H-5, 110 cm). This observation, indicating a decrease of salinity of surface water, is comparable with the results obtained from the other sites. In Sections 3 and 4 of Core 107-655A-3H mixing of Pliocene and Pleistocene sediments occurs.

The Pliocene/Pleistocene boundary is not determined precisely due to some mixing of Pliocene and Pleistocene sediments within this interval of the sequence. Most probably it lies between sample 107-655A-3H-5, 60 cm and sample 107-655A-3H-5, 110 cm (at about 19.3 mbsf).

Discoasters are rare within the upper part of the Pliocene and they are restricted to certain levels. They become common from sample 107-655A-6H-6, 40 cm downsection (lower NN16). The last *Discoaster tamalis* was observed in sample 107-655A-4H-2, 50 cm.

The highest occurrence of the small *Reticulofenestra pseudoumbilica* lies in sample 107-655A-7H-5, 120 cm at the base of the sedimentary sequence. It was also observed within the sediments included in the basalt where they are of normal size, indicating that the sediments deposited just upon the basalt are of late early Pliocene age (zone NN15) of about 3.4–3.6 m.y.

Nannofossils are very rare or entirely destroyed by diagenesis in the sediments overlying the basalt. These sediments are rich in secondary dolomite.

PALEOMAGNETICS

A large proportion of the samples from the Pliocene/Pleistocene section recovered at Hole 655A was found to carry a remanence with a steeply dipping positive inclination. Many of these samples maintained this remanence direction after alternating field (AF) demagnetization at peak fields of 200 Oe. Thermal treatment will be required to generate a clear magnetic stratigraphy at this site. A predominance of negative inclinations in Cores 107-655A-5H and 107-655A-6H suggests that these cores are within the Matuyama Epoch.

The basalts recovered at Hole 655B are characterized by natural remanent magnetization (NRM) intensities of 5.10^{-2} to 10^{-3} G/cm^3. The median destructive fields are mostly in the 300–400 Oe range indicating moderate coercivities, higher than those usually associated with young ocean ridge basalts but consistent with those affected by several million years of low-temperature oxidation. The entire 110-m section of these "pillow" basalts was found to carry a very stable single-component reversed magnetization, the inclination of the characteristic remanence being negative. The inclination values lie in the 50°–60° range, close to expected values, indicating no tectonic disruption of the pillow stack. This reversed remanence is consistent with foraminiferal identifications in intercalated limestones, which suggest that eruption of the basalts occurred at a time interval correlative to the 460,000-yr reversed chron at the top of the Gilbert Epoch.

Bulk susceptibility values were measured using the Bartington discrete sample sensor. Values lie in the range 6.10^{-4}–1.10^{-4} G/Oe, which is within the wide range of susceptibility values recorded in young oceanic basalts.

PHYSICAL PROPERTIES

Introduction

Cores 1H to 12X in Hole 655A and cores 1R to 12R in Hole 655B were used for shipboard analysis of GRAPE density, bulk density, porosity, grain density, and velocity. Thermal conductivity was measured on all sections of Hole 655A. Shear strength measurements were done on each core of Hole 655A. The different methods of analysis are described in the "Explanatory Notes" chapter, this volume.

Results

Index Properties and Compressional Velocity

Porosity, bulk density, grain density, and compressional velocity from Hole 655A and Hole 655B are plotted relative to sub-bottom depth in Figures 13 and 14 and are listed in Tables 4–7.

In Hole 655A, grain density is highly variable from the mud line to the bottom of the hole. The data from Hole 655B, in the basalt, show an alternation of high (2.8–3.2 g/cm³) and low (2.5–2.7 g/cm³) values and a generally increasing downsection trend.

The bulk density values are in good agreement with the porosity values and reflect the same trend along the cores. Two main physical property units can be distinguished in Site 655:

1. Unit 1. This unit extends from the seafloor to the bottom of Hole 655A and corresponds to the sedimentary cover of the

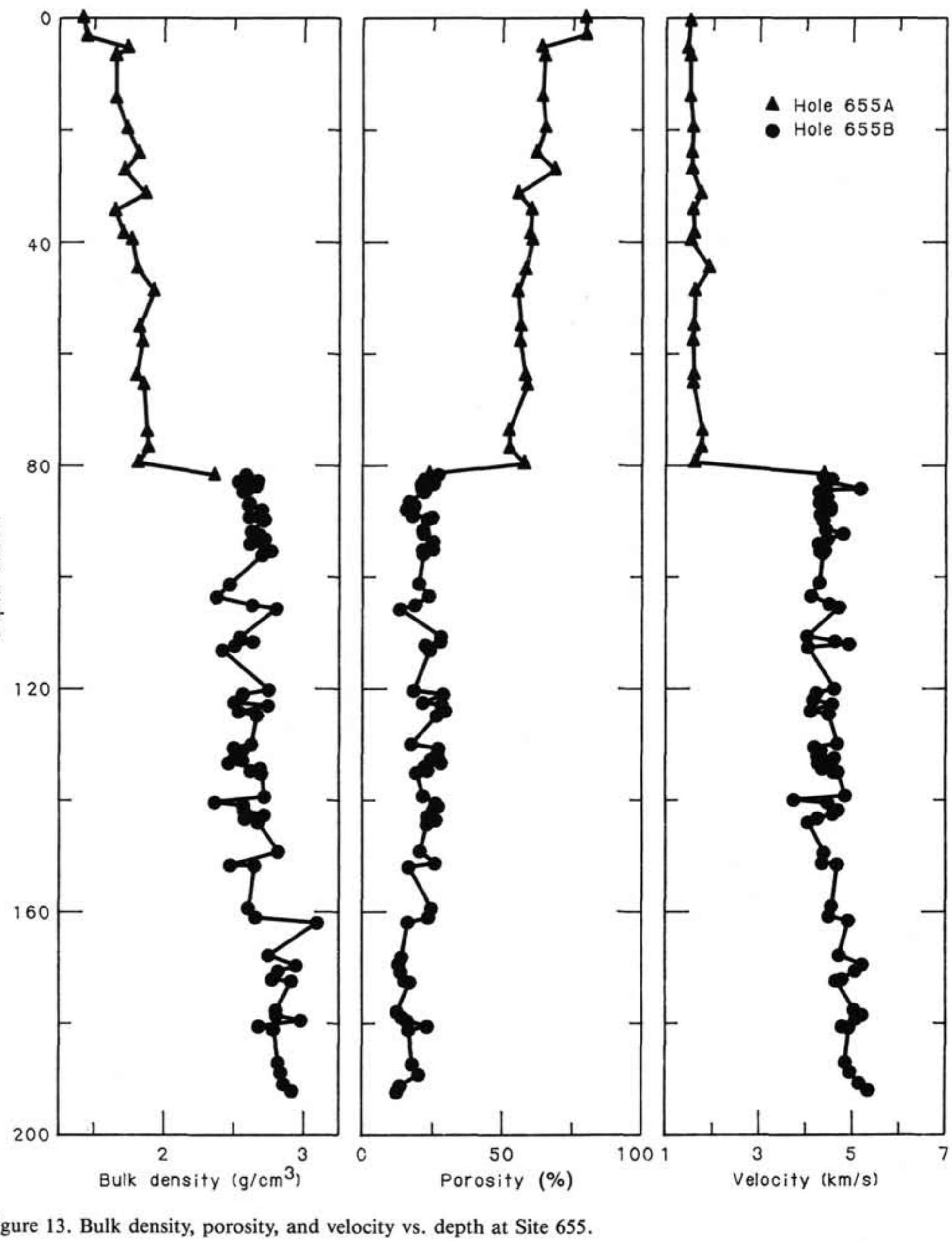

Figure 13. Bulk density, porosity, and velocity vs. depth at Site 655.

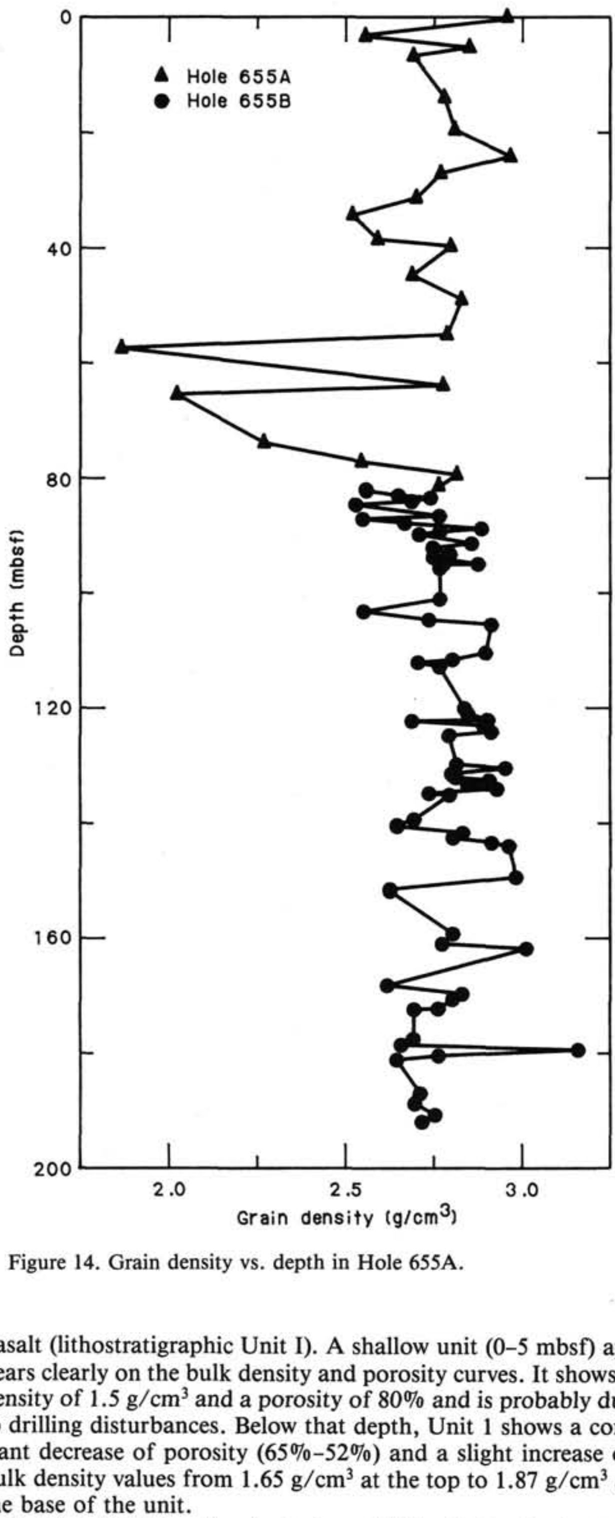

Figure 14. Grain density vs. depth in Hole 655A.

basalt (lithostratigraphic Unit I). A shallow unit (0–5 mbsf) appears clearly on the bulk density and porosity curves. It shows a density of 1.5 g/cm^3 and a porosity of 80% and is probably due to drilling disturbances. Below that depth, Unit 1 shows a constant decrease of porosity (65%–52%) and a slight increase of bulk density values from 1.65 g/cm^3 at the top to 1.87 g/cm^3 at the base of the unit.

2. Unit 2. This unit extends from 81.35 mbsf to the bottom of Hole 655B and corresponds to the basalt. Unit 2 shows alternations of high and low values of bulk density and porosity (Figs. 15 and 16). Two main subunits can be recognized in the basalt:

A. Subunit 2a (from the top of the basalt to about 140 mbsf). This subunit shows scatter in the bulk density and porosity values; 2.7 g/cm^3 (high value) and 2.4 g/cm^3 (low value) for the bulk density data, and 28% (high value) and 20% (low value) for porosity.

Table 4. Physical properties index, Hole 655A.

Core section	Interval or piece no.	Depth sub-bottom (m)	Bulk density (g/cm^3)	Porosity (%)	Grain density (g/cm^3)
1H-C	5-8	2.97	1.44	79.8	2.55
2H-2	48-51	5.08	1.74	63.9	2.85
2H-3	48-51	6.58	1.65	65.1	2.69
3H-1	123-126	13.93	1.65	64.4	2.78
3H-5	75-78	19.45	1.73	65.4	2.81
4H-2	33-37	24.13	1.81	62.3	2.97
4H-4	19-23	26.99	1.71	68.7	2.77
4H-7	3-6	31.33	1.86	56.0	2.70
5H-2	87-90	34.27	1.65	60.8	2.52
5H-5	47-50	38.36	1.71	59.9	2.59
5H-6	24-27	39.64	1.76	60.7	2.80
6H-3	24-27	44.74	1.80	58.4	2.69
6H-5	129-132	48.79	1.91	55.8	2.83
7H-3	80-83	54.90	1.82	56.8	2.79
7H-5	44-46	57.54	1.84	56.6	1.86
8H-3	10-13	63.70	1.80	58.2	2.78
8H-4	30-33	65.40	1.84	59.3	2.02
9X-7	22-25	79.42	1.81	57.9	2.82

B. Subunit 2b (140–196 mbsf). This subunit shows an increase of bulk density and a decrease of porosity with depth. The bulk density ranges from 2.4–2.7 g/cm^3 (at the top) to 2.7–2.85 g/cm^3 (at the bottom). The porosity ranges from 20%–28% at 140 mbsf to 12%–19% at the bottom of the hole.

The compressional wave velocity plot (Fig. 13) shows two main trends:

1. Unit 1. From the mud line to the bottom of Hole 655A, this unit corresponds to the sedimentary cover of the basement. The velocities measured on samples show a slight increase from 1.49 km/s at the mud line to 1.79 km/s at the bottom of the hole and an average value of 1.62 km/s.

2. Unit 2. This unit was sampled in Hole 655B and is composed of basalt. Plot of the data shows (Fig. 17) an alternation of high and low velocities. The abnormal (high and low) data always correspond to breccia and/or limestone-dolostone samples without correlation between lithologies and velocities. The measurements done on homogeneous basaltic samples justify two subunits:

A. Subunit 2a (80–145 mbsf). This subunit shows an alternation of high (4.8–5.2 km/s) and low (4.2–4.5 km/s) velocities. Nevertheless, the average velocity seems to remain constant all along this subunit.

B. Subunit 2b (145–196 km/s). This unit presents an increasing trend which ranges from 4.7 km/s to 5.3 km/s for the high velocities and from 4.3 km/s to 4.9 km/s for the low velocities.

Both vertical and radial velocities were measured on the sampled basalts of Hole 655B (Fig. 17). The following observations can be noted: (1) The breccia and limestone-dolostone samples present an important acoustic anisotropy, without any particular spatial orientation; (2) Anisotropy of the basaltic samples varies in intensity; however, increase in intensity of this anisotropy vs. depth was noted. For most of the measurements, the vertical velocity is higher than the radial velocity.

Shear Strength

Measurements were recorded all along Hole 655A cores (Fig. 18 and Table 8). The data show an increase in shear strength vs. depth from the seafloor (3 kPa) to 65 mbsf (137 kPa). Below 65 mbsf, the shear strength decreases abruptly, probably because

Table 5. Physical properties index, Hole 655B.

Core section	Interval or piece no.	Depth sub-bottom (m)	Bulk density (g/cm³)	Porosity (%)	Grain density (g/cm³)
1R-1	2	81.35	2.50	27.3	2.56
1R-1	4	82.00	2.59	21.6	2.56
1R-1	7	82.64	2.43	26.1	2.65
1R-2	5	83.08	2.58	21.0	2.75
1R-2	10	83.81	2.52	21.0	2.69
1R-3	1	84.29	2.48	22.4	2.53
1R-4	8	86.34	2.53	16.9	2.77
1R-4	12B	86.91	2.52	19.0	2.55
1R-5	2	87.50	2.64	16.3	2.67
1R-5	9	88.61	2.60	18.2	2.89
1R-6	4	89.07	2.51	25.4	2.77
1R-6	7	89.40	2.65	22.7	2.71
2R-1	4	91.26	2.55	21.4	2.86
2R-1	13B	92.00	2.60	22.2	2.75
2R-2	16	93.00	2.64	24.2	2.80
2R-2	5	93.64	2.52	25.1	2.75
2R-3	12	94.84	2.61	24.5	2.88
2R-3	13	94.94	2.71	21.2	2.78
2R-4	4	95.59	2.61	22.1	2.77
3R-1	2A	100.81	2.40	20.0	2.77
3R-2	4C	103.04	2.31	24.0	2.55
3R-3	3A	104.45	2.55	19.3	2.74
3R-4	1C	105.17	2.71	13.5	2.92
4R-1	2	110.24	2.47	28.4	2.90
4R-1	11	111.17	2.56	28.1	2.81
4R-2	2A	111.81	2.43	22.6	2.71
4R-2	7	112.56	2.35	24.3	2.77
5R-1	2B	119.80	2.65	18.6	2.84
5R-1	8B	120.55	2.48	29.0	2.85
5R-2	9	121.93	2.42	27.0	2.91
5R-2	11	122.10	2.43	21.2	2.69
5R-3	1A	122.58	2.66	28.3	2.90
5R-3	12	123.84	2.44	28.9	2.92
5R-4	4	124.37	2.58	26.4	2.80
6R-1	8	129.71	2.54	17.5	2.82
6R-1	13	130.24	2.42	26.9	2.96
6R-2	5	131.02	2.47	26.7	2.81
6R-2	14	131.80	2.42	26.7	2.82
6R-3	2	132.37	2.47	24.6	2.92
6R-3	7	132.96	2.38	28.2	2.85
6R-4	1B	133.75	2.61	21.1	2.94
6R-4	8A	134.49	2.53	24.1	2.74
6R-4	11B	134.87	2.60	19.2	2.80
7R-1	3	139.20	2.63	21.5	2.70
7R-1	11	140.01	2.28	26.3	2.65
7R-2	3	140.52	2.49	27.7	2.65
7R-2	11C	141.53	2.50	25.8	2.84
7R-3	7	142.41	2.64	23.1	2.81
7R-3	14B	143.16	2.49	27.4	2.92
7R-4	6	143.83	2.58	22.7	2.97
8R-1	9A	149.19	2.72	20.2	2.99
8R-2	14	151.17	2.38	26.8	2.63
8R-3	2	151.45	2.56	16.6	2.63
9R-1	7E	158.76	2.51	24.9	2.81
9R-2	18	160.74	2.56	24.0	2.78
9R-3	3	161.39	3.00	15.9	3.02
10R-1	3	167.74	2.64	13.9	2.62
10R-2	2	169.28	2.84	12.9	2.84
10R-2	11	170.33	2.71	13.5	2.81
10R-3	13	171.85	2.67	15.3	2.77
10R-4	2	172.12	2.81	17.3	2.70
11R-1	2A	177.51	2.69	12.1	2.70
11R-1	5A	178.35	2.71	13.9	2.66
11R-2	8	179.20	2.87	16.3	3.17
11R-2	23	180.35	2.56	23.4	2.77
11R-3	11	180.95	2.69	16.1	2.65
12R-1	2	186.90	2.71	17.6	2.72
12R-2	3A	188.78	2.73	19.6	2.70
12R-3	7	190.78	2.75	13.0	2.76
12R-4	8	191.93	2.81	12.1	2.72

of drilling disturbances (overpressures). Two trends seem to be present from the seafloor to 38 mbsf and from 38 mbsf to 65 mbsf.

Thermal Conductivity

Thermal conductivity was routinely measured on each section (sometimes more frequently) of Hole 655A. The results are plotted on Fig. 18 and are listed in Table 9. The data show an increasing thermal conductivity from 2.20 × 10^{-3} cal/(°C × cm × s) at the seafloor to 3.10 × 10^{-3} cal/(°C × cm × s) at about 20 mbsf. The thermal conductivity remains constant at about 2.85 × 10^{-3} cal/(°C × cm × s) from 20 to 53 mbsf. A small step to 3.0 × 10^{-3} cal/(°C × cm × s) is noted at this depth, then the thermal conductivity gently decreases to 2.80 × 10^{-3} cal/(°C × cm × s) at 65 mbsf. The bottom of the hole is marked by an increase of thermal conductivity which goes up to 3.2 × 10^{-3} cal/(°C × cm × s). In summary, four thermal conductivity intervals can be distinguished: 0–20 mbsf, 20–53 mbsf, 53–65 mbsf, and 65–80 mbsf.

Table 6. Compressional velocity, Hole 655A.

Core section	Interval (cm)	Depth sub-bottom (m)	Compressional velocity (km/s)
1H-1	19–22	0.19	1.494
2H-2	48–51	5.08	1.446
2H-3	48–51	6.58	1.536
3H-1	123–126	13.93	1.512
3H-5	75–78	19.45	1.561
4H-2	33–36	24.13	1.570
4H-4	20–23	27.00	1.559
4H-7	3–6	31.33	1.752
5H-2	87–90	34.27	1.593
5H-5	47–50	38.37	1.599
5H-6	24–27	39.64	1.542
6H-3	24–27	44.74	1.924
6H-5	129–132	48.79	1.645
7H-3	80–83	54.90	1.609
7H-5	44–47	57.54	1.601
8H-3	10–13	63.70	1.606
8H-4	30–33	65.40	1.600
9X-3	55–58	73.75	1.788
9X-5	56–59	76.76	1.779
9X-7	22–25	79.42	1.612

Conclusion

The physical properties measured at Site 655 show two main units which are in good agreement with the lithology:

1. An upper unit, from the seafloor to the top of the basalt at about 80 mbsf (Hole A). This unit corresponds to the Pliocene-Pleistocene sediments and is characterized by homogeneous physical properties, as expected. However, the variability of the grain density should be noted.
2. A lower unit, drilled in Hole 655B, is composed of basalt. This unit is characterized by an alternation of high and low values of grain density, bulk density, porosity, and velocity. All the curves indicate the same organization. The basalt is composed of pillows or flows, and a close relation between the physical properties of the samples analysed and their position in the pillows and/or flows can be suspected. High velocity always occurs in samples showing high bulk density and low porosity. Such samples may indicate the central part of the pillows and/or flows. Samples with low velocity and density are probably from the peripheral part of the basaltic pillows and/or flows.

The basalt can be divided into two physical properties subunits: 80–140 mbsf and 140-196 mbsf. More precise investigations are required to study the relation between the composition of the basalt, its mineral orientation, its vesicularity, and the variations observed in the physical properties.

GEOCHEMISTRY

A few carbonate analyses were carried out to facilitate the work of the sedimentologists. Results are listed in Table 10 and plotted vs. depth in Figure 19, together with results of a few organic carbon determinations. Because ideal sapropel layers in

Table 7. Compressional velocity, Hole 655B.

Core section	Piece no.	Depth sub-bottom (m)	Compressional velocity (km/s) Axis B-C (radial)	Axis A (vertical)
1R-1	2	81.35	4.377	4.815
1R-1	7	82.64	4.445	4.366
1R-2	5	83.08	4.404	4.394
1R-2	10	83.81	5.175	5.151
1R-3	1	84.29	4.252	4.376
1R-3	13	85.26	4.453	4.475
1R-4	8	86.34	4.297	4.424
1R-4	12B	86.91	4.498	4.679
1R-5	2	87.50	4.583	4.463
1R-5	9	88.61	4.428	4.483
1R-6	4	89.07	4.327	4.418
1R-6	7	89.40	4.423	4.483
2R-1	4	91.26	4.426	4.417
2R-1	13B	92.00	4.820	4.632
2R-2	16	93.00	4.468	4.565
2R-2	5	93.64	4.262	4.340
2R-3	12	94.84	4.277	4.236
2R-3	13	94.94	4.485	4.672
2R-4	4	95.59	4.342	4.524
3R-1	2A	100.81	4.261	4.197
3R-2	4C	103.04	4.099	4.138
3R-3	3A	104.45	4.480	4.501
3R-4	1C	105.17	4.699	4.804
4R-1	2	110.24	4.013	4.006
4R-1	11	111.17	4.617	4.668
4R-2	2A	111.81	4.927	4.318
4R-2	7	112.56	4.070	5.239
5R-1	2B	119.80	4.635	4.595
5R-1	8B	120.55	4.197	3.734
5R-2	9	121.93	4.122	4.250
5R-2	11	122.10	4.299	4.273
5R-3	1A	122.58	4.571	4.543
5R-3	12	123.84	4.079	4.107
5R-4	4	124.37	4.513	4.343
6R-1	8	129.71	4.682	4.686
6R-1	13	130.24	4.134	3.715
6R-2	5	131.02	4.313	4.395
6R-2	14	131.8	4.220	4.242
6R-3	2	132.37	4.699	4.824
6R-3	3	132.96	4.297	4.311
6R-4	1B	133.75	4.324	4.322
6R-4	8A	134.49	4.553	4.533
6R-4	11B	134.87	4.685	4.600
7R-1	3	139.20	4.849	4.999
7R-1	11	140.01	3.730	3.877
7R-2	3	140.52	4.467	4.452
7R-2	11C	141.53	4.669	4.446
7R-3	7	142.41	4.573	4.656
7R-3	14B	143.16	4.238	4.217
7R-4	6	143.83	4.025	4.146
8R-1	9A	149.19	4.378	4.347
8R-2	14	151.17	4.359	4.333
8R-3	2	151.45	4.669	4.769
9R-1	7E	158.76	4.549	4.586
9R-2	18	160.74	4.466	4.436
9R-3	3	161.39	4.903	5.089
10R-1	3	167.74	4.726	4.947
10R-2	2	169.28	5.241	5.317
10R-2	11	170.33	5.085	5.106
10R-3	13	171.85	4.795	5.078
10R-4	2	172.12	4.658	4.719
11R-1	2A	177.51	5.049	5.212
11R-1	5A	178.35	5.210	5.249
11R-2	8	179.20	5.087	5.248
11R-2	23	180.35	4.782	4.813
11R-3	11	180.95	4.968	4.895
12R-1	2	186.90	4.866	4.926
12R-2	3A	188.78	4.956	5.103
12R-3	7	190.78	5.166	5.180
12R-4	8	191.93	5.370	5.417

the Pleistocene sequence of Cores 2H and 3H were disturbed, a special sampling technique was employed to allow for very closely spaced samples. Results of C_{org} and $CaCO_3$ analyses from the dense sampling of Samples 107-655A-2H-4, 63–78 cm at 8.2 mbsf, and 107-655A-3H-1, 52–76 cm at 13.3 mbsf are also given in Table 10 and depicted with a close-up photograph in Figure 8 (see

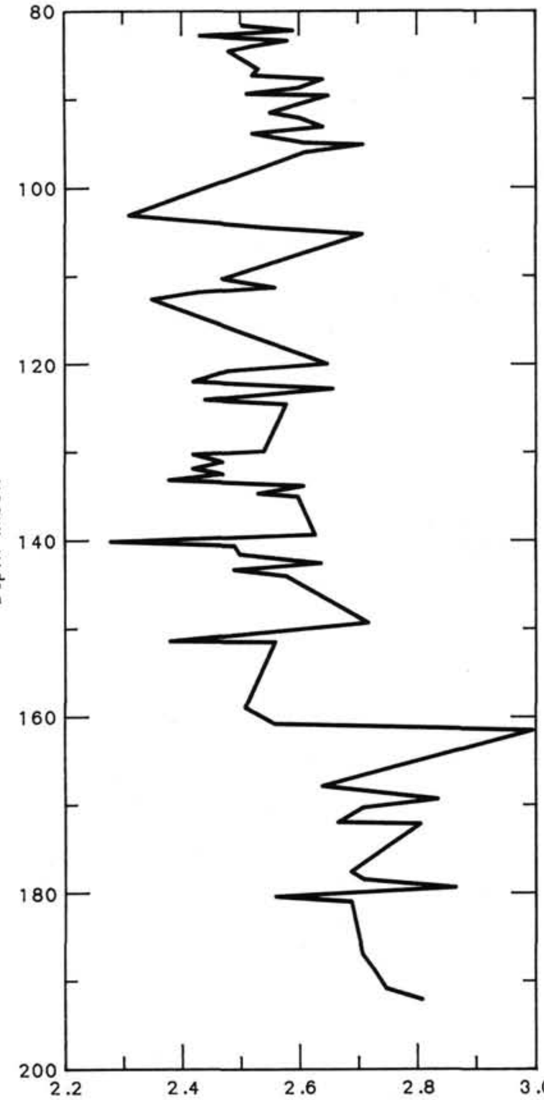

Figure 15. Bulk density vs. depth in Hole 655B.

"Lithostratigraphy" section, this chapter). Because only two samples were taken for interstitial water analyses, these were not analyzed on board.

DOWNHOLE MEASUREMENTS

Heat Flow

Introduction

Segments of Gortani Ridge and their buried prolongations display a local negative heat flow anomaly when compared to the average regional heat flow (Fig. 20). Heat flow values less than 30 mW/m^2 and even down to zero were measured mainly on the western side and near the bathymetric base of the structure (Figs. 21A and B). Heat flow values rise sharply eastward, i.e., toward the center of the Vavilov Basin.

Data

Three heat flow measurements have been performed at Site 655 during the Advanced Piston Coring operations using the Von Herzen temperature measurement probe. Temperature records are of excellent quality. Measurement 1 (base of Core 107-

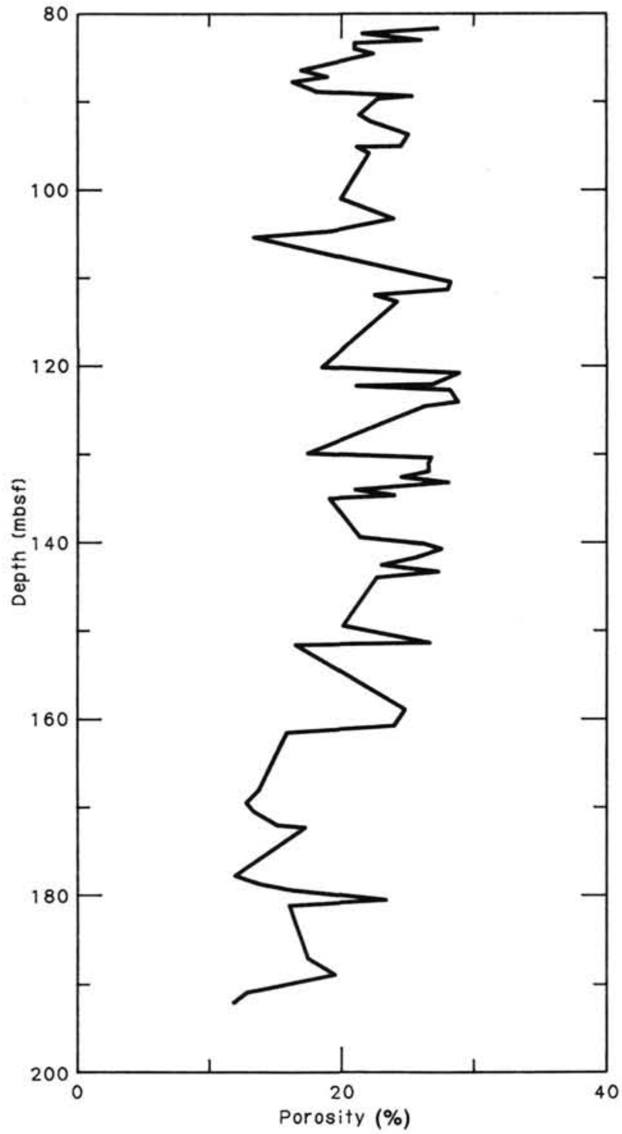

Figure 16. Porosity vs. depth in Hole 655B.

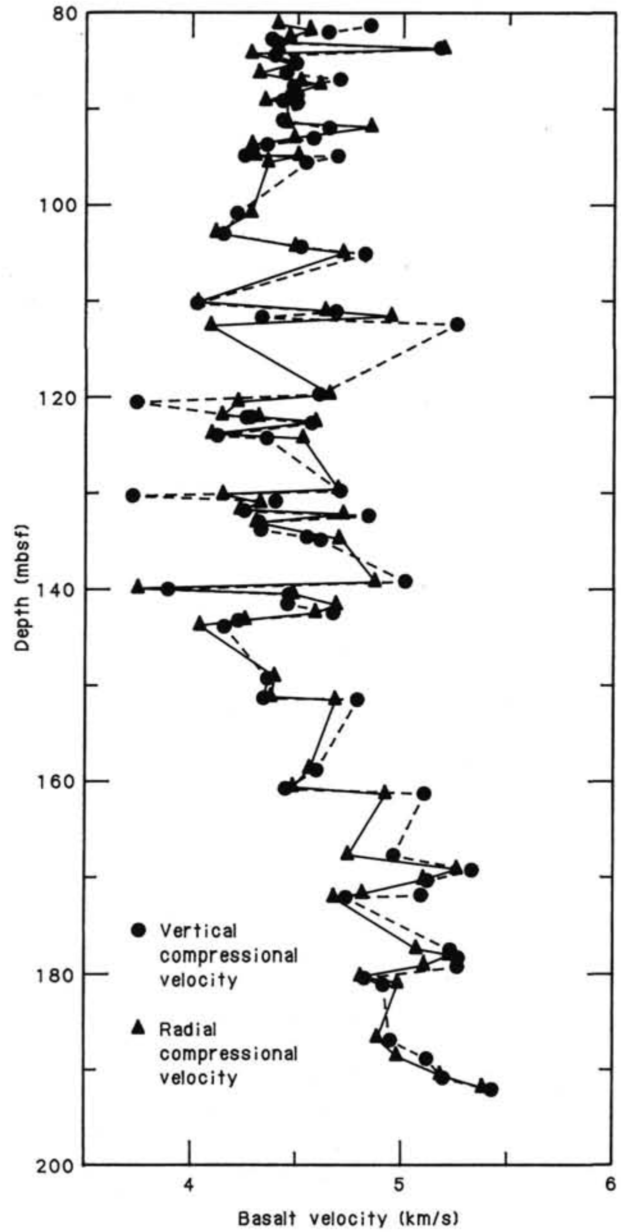

Figure 17. Vertical and radial velocity vs. depth in Hole 655B.

655A-4H, 31.9 mbsf) gives a temperature of 15.77° ± 0.02°C; measurement 2 (base of Core 107-655A-6H, 51.1 mbsf) indicates a 17.05° ± 0.02°C temperature; measurement 3 (base of Core 107-655A-8H at 70.2 mbsf) is 18.10° ± 0.02°C.

A bottom water temperature of 13.22 ± 0.01°C was measured during these three operations.

Temperatures records vs. time are presented in Figures 22 and 23A, and values are plotted vs. depth on Figure 23B, illustrating the geothermal gradient.

At Site 655 the geothermal gradient does not fit a straight line, but instead slowly decreases toward the deepest measured interval. The quantitative variations of interval gradients are reported in Table 11.

Thermal conductivity has been measured on board on sampled cores, using the needle probe method; 49 measurements are plotted in Figure 18. The means, as well as the mean for each interval of temperature measurement, are listed in Table 12.

Conclusion

The thermal conductivity increases slightly toward the base of the sedimentary series. Nevertheless, even taking into account the highest thermal conductivity value of 1.304 $W/m^2/s$ (3.24 10^{-3} cal/(°C × cm × s), obtained from Core 107-655A-9X, within the last (2–3) interval of measurements, heat flow decreases from 88.6 for the 0–1 interval to 71.5 mW/m^2 for the 2–3 interval (see Table 11).

We propose, as a mean heat flow value for Site 655, a value of:

$$85 \pm 4 \text{ mW/m}^2 = 2.03 \pm 0.01 \text{ HFU.}$$

Considering the geological environment and the structural setting of Site 655, as well as previous shallow probe heat flow determinations, we may propose that the decrease of heat flow with depth is an effect of the proximity of the basaltic basement in which bulk thermal conductivity is commonly about three times greater than the sediments in which the temperatures were measured. Such a lateral conductive effect is probably amplified near the ridge flanks, where hydrothermal circulation through

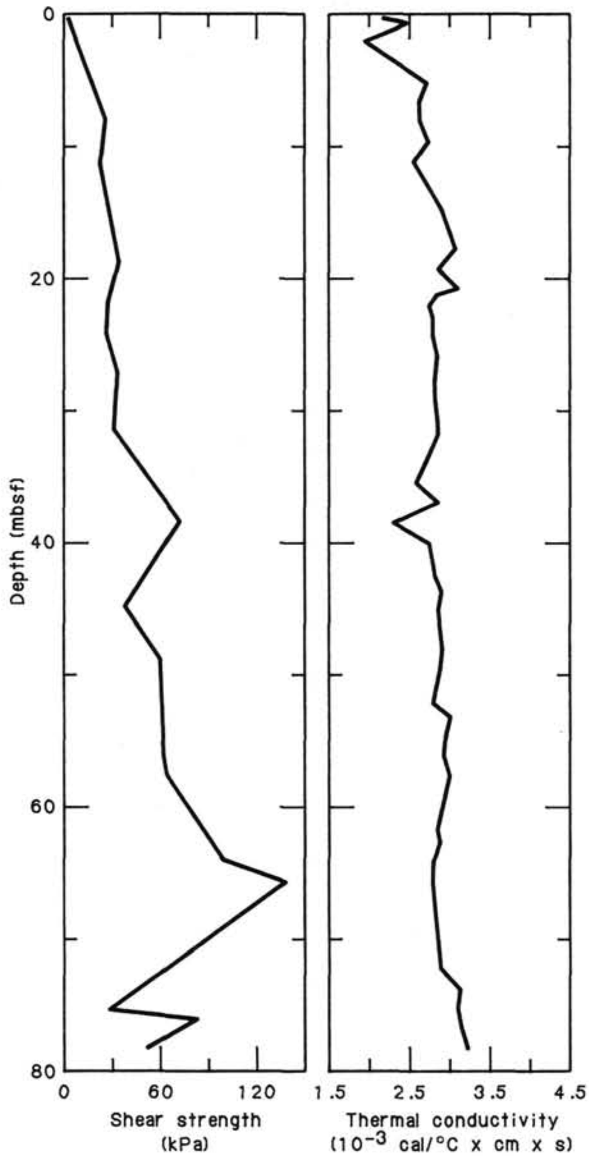

Figure 18. Shear strength and thermal conductivity vs. depth in Hole 655A.

Table 8. Shear strength, Hole 655A.

Core section	Interval (cm)	Depth sub-bottom (m)	Shear strength (kPa)
1H-1	42	0.42	3.25
2H-4	29	7.89	26.39
2H-6	60	11.20	22.54
3H-5	4	18.74	34.11
3H-7	4	21.74	27.41
4H-2	27	24.07	26.60
4H-4	25	27.05	33.70
4H-7	7	31.37	31.27
5H-5	35	38.25	72.12
5H-6	23	39.62	64.11
6H-3	22	44.72	37.88
6H-5	132	48.76	59.74
7H-4	50	56.10	61.92
7H-5	50	57.60	64.11
8H-3	28	63.88	99.00
8H-4	49	65.59	137.69
9X-4	62	75.32	28.45
9X-4	136	76.06	83.07
9X-6	48	78.18	52.35

Table 9. Thermal conductivity, Hole 655A.

Core section	Interval (cm)	Depth sub-bottom (m)	Thermal conductivity (10^{-3} cal/cm^2/s)
1H-1	25	0.25	2.193
1H-1	50	0.50	2.476
1H-1	100	1.00	2.346
1H-2	50	2.00	1.959
2H-2	50	5.10	2.728
2H-3	50	6.60	2.635
2H-4	50	8.10	2.648
2H-5	50	9.60	2.741
2H-6	50	11.10	2.571
3H-2	50	14.70	2.916
3H-4	50	17.70	3.090
3H-5	50	19.20	2.867
3H-6	50	20.70	3.118
3H-6	100	21.20	2.854
3H-7	30	22.00	2.759
4H-1	60	22.90	2.802
4H-2	50	24.30	2.795
4H-3	50	25.80	2.860
4H-4	100	27.80	2.821
4H-5	100	29.30	2.842
4H-6	100	30.80	2.861
4H-7	40	31.70	2.864
5H-2	50	33.90	2.712
5H-3	50	35.40	2.606
5H-4	50	36.90	2.867
5H-5	50	38.40	2.320
5H-6	50	39.90	2.766
6H-1	100	42.50	2.825
6H-2	50	43.50	2.903
6H-3	50	45.00	2.866
6H-4	50	46.50	2.890
6H-5	50	48.00	2.916
6H-6	50	49.50	2.890
7H-1	100	52.10	2.810
7H-2	50	53.10	3.021
7H-3	50	54.60	2.968
7H-4	50	56.10	2.941
7H-5	50	57.60	3.024
8H-1	100	61.60	2.859
8H-2	50	62.60	2.896
8H-3	50	64.10	2.815
8H-4	50	65.60	2.804
9X-2	50	72.20	2.901
9X-3	50	73.70	3.150
9X-4	50	75.20	3.118
9X-5	50	76.70	3.165
9X-6	50	78.20	3.240

basalt fractures is likely to cause the large cooling effect observed on and around this basement structure.

LOGGING OPERATIONS

Introduction

Logging operations at Hole 655B commenced at 0115 on 13 February. Two logging runs were planned: resistivity-velocity-gamma ray-caliper (DIL-LSS-GR-CALI) and borehole televiewer (BHTV). Borehole televiewer logging was planned as an aid in delineating present-day stress directions.

The resistivity velocity run reached total depth (195 mbsf) at 0330 with only minimal difficulty. Measurements were recorded logging up and the tool was returned on deck at 0630. The caliper log indicated excellent hole conditions. Schlumberger's automatic velocity-picking software failed to pick first arrivals accurately, so that reprocessing of the waveforms was needed onshore. The real-time data are reported in the section at the end of this chapter.

The borehole televiewer was lowered from the rig at 0728. At 30 m below the drill floor the tool failed completely; troubleshooting attempts at the surface indicated that the failure was probably caused by shorted conductors in the cable head. As a

Table 10. Summary of carbonate concentrations measured at Site 655.

Sample	Depth (mbsf)	$CaCO_3$ (%)	C_{org} (%)
2H-2, 48-51	5.1	41.9	
2H-4, 63-78	8.2	27.1	3.51
2H-4, 82-83	8.4	56.0	
2H-6, 48-51	11.1	51.5	
3H-1, 52-76	13.3	16.71	5.69
3H-1, 126-132	14.0	51.9	
3H-5, 75-78	19.5	43.3	
4H-2, 33-37	24.1	52.0	
4H-4, 19-23	27.0	45.0	
4H-7, 3-6	31.3	49.4	0.01
5H-1, 25-26	32.2	25.7	
5H-1, 72-73	32.7	33.8	
5H-2, 87-90	34.3	63.0	
5H-2, 132-133	34.7	28.6	
5H-5, 47-50	38.4	13.7	0.07
5H-6, 24-27	39.6	49.1	
6H-3, 24-27	44.7	63.6	
6H-5, 129-132	48.8	42.3	0.09
7H-3, 80-83	54.9	53.5	
7H-5, 47-49	57.6	60.0	0.01
8H-3, 10-11	63.7	50.1	0.11
8H-4, 30-33	65.4	51.4	
9H-1, 55-59	71.3	65.8	
9H-5, 56-59	77.3	65.6	0.01
9H-7, 22-25	79.9	61.8	

Detailed analyses of $CaCO_3$ and C_{org} in two Pleistocene saproprels: Samples 2H-4, 63-78 cm and 3H-1, 52-76 cm in 0.5-cm intervals

Sample no.	$CaCO_3$ (%)	C_{org} (%)
2H-4, 1	38.55	0.08
2	39.70	0.21
3	40.29	0.10
4	37.94	0.32
5	37.13	0.58
6	35.75	0.97
7	28.88	2.20
8	31.40	1.79
9	19.48	0.37
10	25.73	1.20
12	32.09	1.05
13	28.44	2.53
14	26.46	3.60
15	31.48	2.96
16	27.05	3.51
17	28.10	2.91
18	27.35	2.68
19	25.16	0.47
3H-1, 1	43.97	0.63
2	38.28	1.09
3	33.04	2.17
4	35.07	3.00
6	34.68	2.60
7	34.15	3.43
8	31.65	4.21
8A	31.14	4.29
9	25.93	4.79
10	20.99	5.06
11	16.71	5.69
12	15.72	5.05
13	13.49	4.28
15	17.32	2.73
17	18.30	1.33
18	19.65	0.34
19	21.27	0.25
20	24.06	0.22
21	20.63	0.27
22	23.77	0.11
23	23.67	0.27
24	22.08	0.51
26	34.90	0.42
28	40.16	0.13

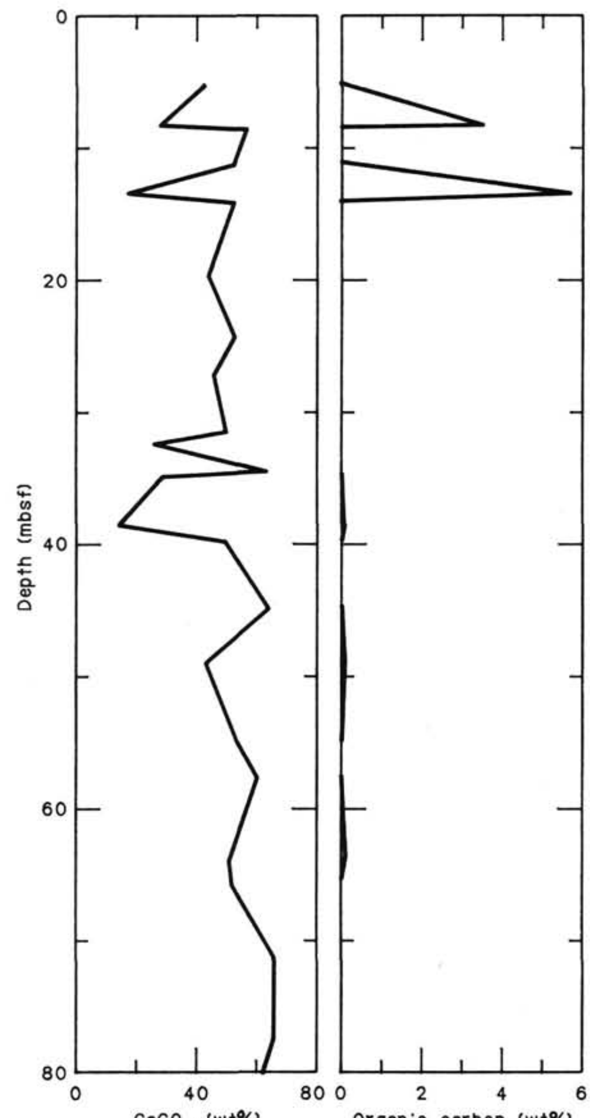

Figure 19. Percentages of carbonate and organic carbon plotted vs. depth for Hole 655A.

strict time allocation did not permit reheading the cable, logging operations were terminated at 0900 on 13 February.

Discussion of Results

A summary of the logging tools is given in Table 13. A brief description of the principles governing each of the measurements is given in the "Explanatory Notes" chapter, this volume.

The gamma ray log displayed in Figure 24 is corrected for borehole effects; this correction compensates for attenuation of gamma ray count rates caused by variations in hole size and by drilling fluid. The average log value of 16 $\pm$ 2 GAPI units is high when compared to values (<18 GAPI) in other relatively fresh basalts (Salisbury et al., 1979; Mathews et al., 1984). The higher gamma ray count rates observed at Site 655 suggest the presence of potassium-rich alteration products lining or filling some of the fractures observed in the cores.

Three different resistivity measurements were made, each with a different depth of investigation into the formation. Resistivity differences between induction (deep and medium) and focused logs reflect the ability of the induction devices to "see" vesicu-

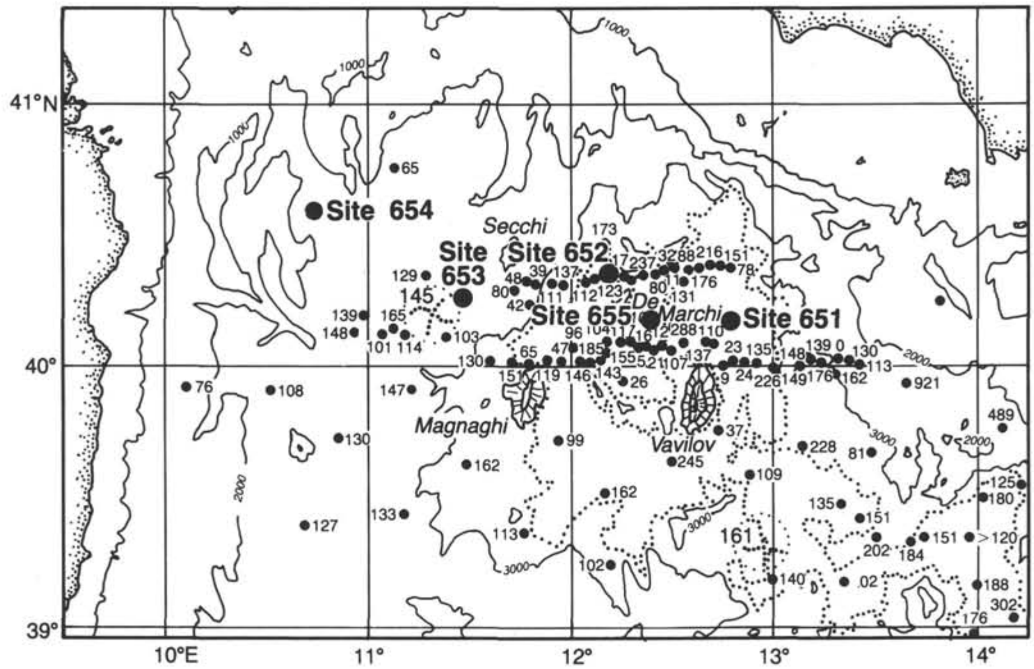

Figure 20. Location map and background heat flow measurements. Points and values are heat flow shallow-probe measurements plotted after Della Vedova et al. (1984). They outline the cross sections of Rehault et al. (1984, Figs. 2 and 3).

lar pores; such pores are inaccessible to current-passing devices like the spherically-focused log.

Sonic waveforms from 8-, 10-, and 12-ft receivers are shown in Figures 25–27. All traces are normalized to the same maximum amplitude. Two distinct phases are present in the waveforms: the compressional wave and the Stoneley wave. In reprocessing of the waveforms we seek to correctly pick the first onset of acoustic energy; this fastest wave is the compressional wave. In crystalline rocks, the compressional wave velocity is most sensitive to porosity and the distribution of pore shapes. The late phase is the Stoneley wave, a guided phase which travels at or near the borehole fluid velocity. Shear energy is recognizable in the waveforms, but the first shear arrival cannot be easily distinguished. The highly variable compressional and Stoneley wave attenuation carries much information about the *in-situ* mechanical properties and will be studied in detail in our future work.

Two different schemes were attempted in reprocessing the sonic waveforms; the first scheme (third track of Fig. 25) uses the redundancy of several waveforms to create a velocity log uncompensated for sonde tilt or washout; the second algorithm attempts to repick the first arrivals using a cross-correlation algorithm (fourth track of Fig. 24).

Even after reprocessing, the velocities do not show very good correlation with resistivity or gamma ray curves. There is no evidence that low velocity anomalies correlate to brecciated or highly fractured intervals. Log velocities are lower than core velocities, primarily a measurement scale effect. The average computed log velocity from the reprocessed far receiver data (far right track of Fig. 24) is 4.16 km/s, compared with 4.54 km/s core velocity. These velocities are consistent with the high porosities (10%–30%) recorded in shipboard physical properties measurements.

The logged interval includes 115 m of basaltic flows, the sediment-basalt interface, and 10 m of the overlying sediment. On the basis of resistivity, caliper, and gamma ray measurements, three distinctive units are present in the basalts.

Upper zone: 81.5–125 mbsf. This is a higher resistivity, lower radioactivity zone. Fractures and voids between pillows are filled mainly with carbonates. Since gamma ray value is higher than the average value in relatively fresh basalts from other sites drilled in oceanic basalts (Salisbury et al., 1979; Mathews et al., 1984), potassium-rich alteration products are likely present, maybe in the early stages (palagonite crust after glass). A gradual increase in porosity between 113 and 130 mbsf is suggested by the decreasing resistivity and is consistent with core physical properties.

Intermediate zone: 125–160 mbsf. This zone is marked by lower resistivities and higher gamma ray count rates. We interpret this as higher porosity and more prevalent alteration. Basaltic breccia was recovered in this interval, as well as altered glasses.

Lower zone: 160–195 mbsf. This zone is marked by high resistivity and gamma ray values similar to the overlying intermediate zone. A general decrease in porosity with depth is inferred, and is consistent with slight increases in velocity.

DISCUSSION AND CONCLUSIONS

The Pliocene-Pleistocene Sediments

The location of Site 655 on a topographic high, well above the ponded turbidites, offered an opportunity to recover a pelagic Pliocene-Quaternary sequence to address stratigraphic questions unanswered at Site 653. However, the sediment turned out to be thinner than predicted and younger and less continuous than hoped.

The sediments recovered range from lower Quaternary to the uppermost lower Pliocene. The Pleistocene sequence includes six sapropels or sapropelic layers. In two of the best-developed sapropels, organic carbon content increases to a peak at the center of the sapropel whereas carbonate content decreases to a minimum at nearly the same level. Poor preservation of calcareous nannofossils in the center of the sapropel suggests that the carbonate low is a dissolution phenomenon during sulfate reduction. Together, the sapropels of Sites 652, 653, 654, and 655 may be used to constrain the depth range and lateral extent of episodes of enhanced preservation of marine organic matter, pos-

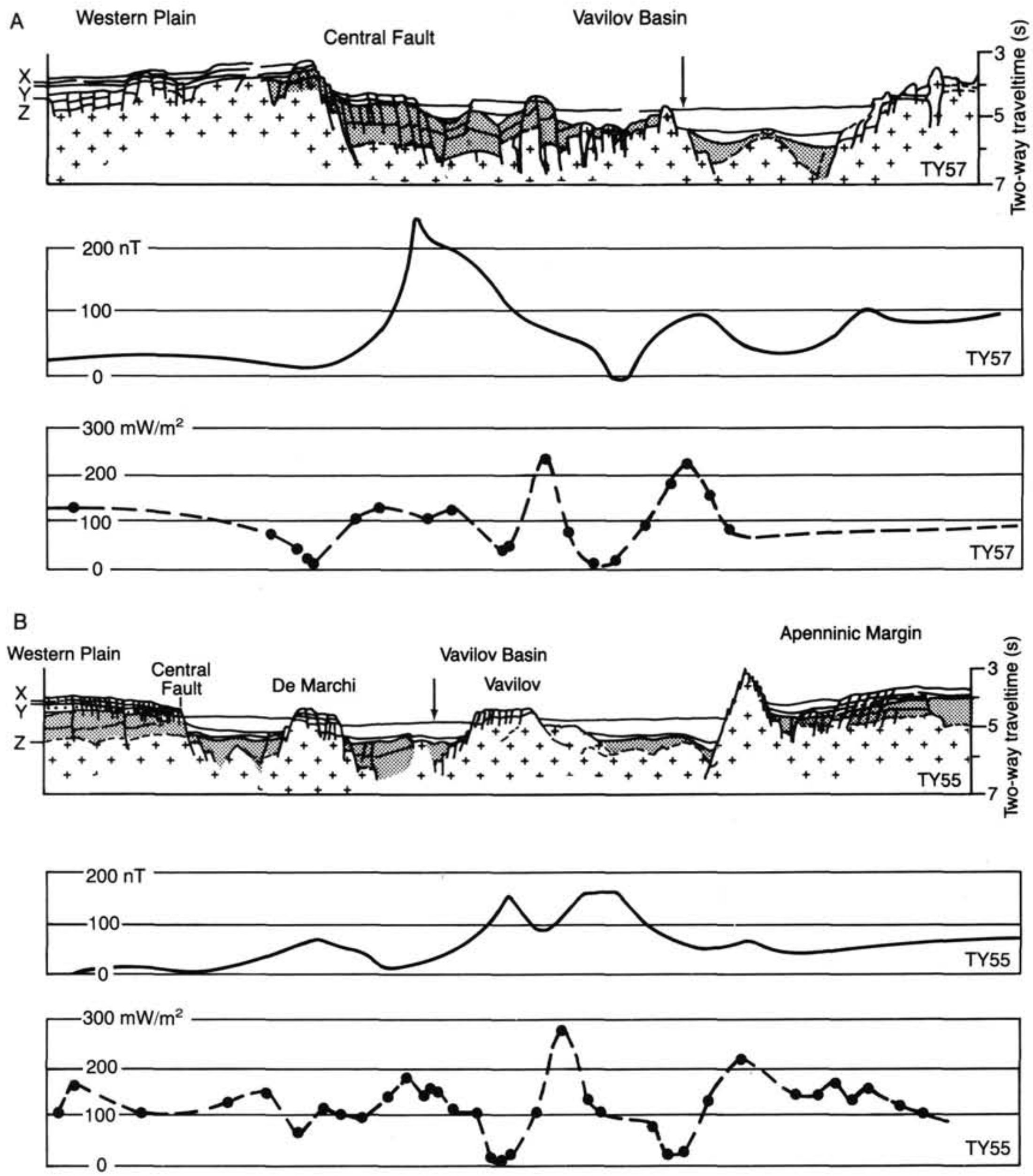

Figure 21. A. Subsurface geologic structure deduced from TY57 air-gun reflection profile with superimposed magnetic anomalies and heat flow measurements (after Bolis et al., 1981; Rehault et al., 1984, 1985). The arrow points to the northern segment of Gortani Ridge, drilled at Site 655 (see Fig. 20 for location). B. Superficial geologic structure deduced from TY55 air-gun reflection profile with superimposed magnetic anomalies and heat flow distribution. The arrow points to the southern termination of the ridge on which Site 655 was drilled (see Fig. 20 for location).

sibly resulting from anoxia of bottom water in the Tyrrhenian Sea.

The observation of sand layers and normally-graded beds interpreted as turbidites is puzzling, given Site 655's hilltop location. These turbidites may be locally redeposited from the slightly higher portion of the ridge which lies west and south of the site; their mineralogy suggests a local provenance. It is also possible that large volume, thick turbidity currents from a more distant source flowed uphill and deposited turbidites on the topographic high.

The lowermost 6 m of hemipelagic sediments above the contact with basalt show a downsection color change from pale yellow to brown. A 5-cm-thick dolostone directly overlies the basalt. The thickness of the anomalous "basal" sediments and degree of difference between the "basal" sediments and the overlying "normal" sediments is less at Site 655 than at either of the earlier sediment/basalt contacts recovered (Site 650 or 651).

Basement

Prior to Leg 107, it had been suggested that Gortani Ridge was a protrusion of upper mantle material, analogous to the serpentinite ridge drilled at Site 637 on the Atlantic margin off Galicia (Boillot et al., 1985). Although we have not conclusively ruled out the possibility that the ridge may have a core of serpentinite/peridotite under a carapace of basalt, the recovery of 120 m of basalt makes this hypothesis unlikely.

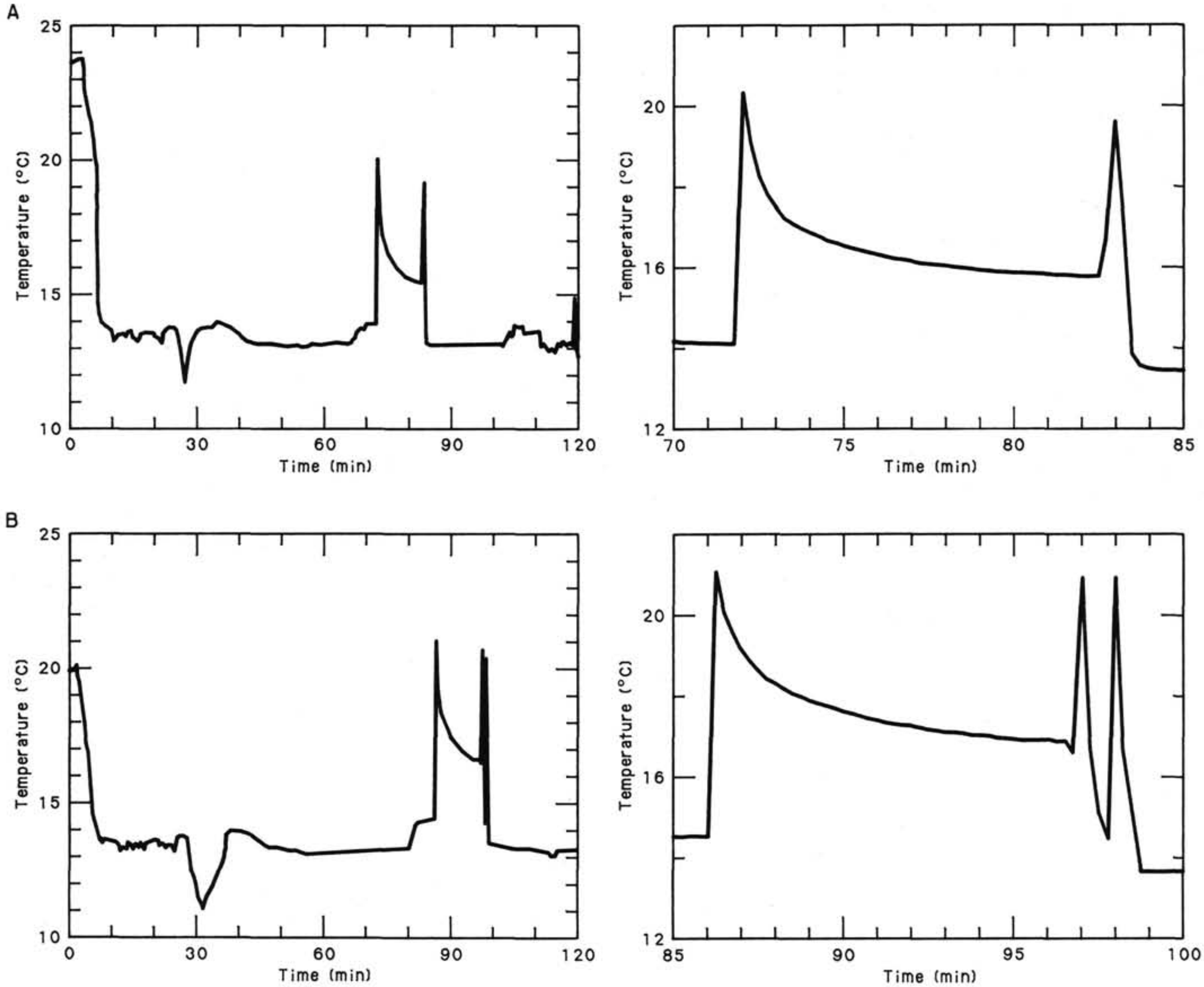

Figure 22. Temperature records at station: A. HF1 (31.9 mbsf). B. HF2 (51.1 mbsf).

The curved, glassy rims observed throughout the basalt section suggest that the ridge is constructed of successive flows of pillow basalts. The consistent magnetic inclination values of 50°–60° are close to that expected, indicating that the pillow stack has not been tectonically disrupted, as might be expected had the ridge been emplaced diapirically or by faulting.

After the extremely heterogeneous basement at Site 651 in the axis of Vavilov Basin, a striking aspect of the Site 655 basement was how little vertical variability was observed. We cored only basalt, and even within the basalt there was little vertical change in either structure or modal composition. Overall, the Site 655 basalt is less altered than that recovered at Site 650 or 651; in some cases fresh glass (sideromelane) is preserved on the pillow rims. The lesser degree of alteration may result from lower post-emplacement temperatures, caused by the thinner sediment cover (80 m at Site 655 vs. 602 m at Site 650 and 388 m at Site 651) and less steep thermal gradient (less than 9°C/100 m as opposed to 14°C/100 m at Site 650).

The age of the basalts is constrained by the observation of reversed magnetic inclination throughout the basalt column, and by the identification of biozones MPl3/NN15 in calcareous rocks within cracks of the basalt. Together, these observations suggest that the basalt erupted during the upper half of the reversed polarity event at the top of the Gilbert magnetic Epoch (3.4–3.86 m.y. ago). This is at least 1.5 m.y. older than the inferred age of the oldest basalt recovered from the Marsili Basin (Site 650). The estimated ages and the inferred oceanic-type geochemistry of Site 655 basalts, if confirmed by shore-based analysis, will support the concept that the Vavilov Basin is floored with tholeiitic, oceanic-type upper crust.

REFERENCES

Be, A.W.H., Morse, J. W., and Harrison, S. M., 1975. *In* Sliter, W. V., Be, A.W.H., and Berger, W. H., (Eds.), *Dissolution of deep-sea carbonates*. Cushman Found. Foraminiferal Res. Spec. Publ., 13:27–55.

Berger, W. H., 1970. Planktonic Foraminifera: Selective Solution and the lysocline. *Mar. Geol.*, 8:111–138.

Boillot, G., Grimaud, S., Mauffret, A., Mougenot, D., Mergoil-Daniel, J., Kornprobst, J., and Torrent, G., 1980. Ocean-continent boundary off the Iberian margin: a serpentinite diapir west of the Galicia bank. *Earth Planet. Sci. Lett.*, 48:23–34.

Boillot, G., Winterer, E. L., Meyer, A. W., et al., 1985. Ocean Drilling Program: Evolution of a passive margin. *Nature*, 317:115-116.

Bolis, G., Capelli, V., and Marinelli, M., 1981. Aeromagnetic data of the Italian area: instrumental to a better comprehension of the basement main characteristic in Italy. *AGIP-EAEG* (43rd meeting), Venezia.

Bonatti, E., Hamlyn, P. R., and Ottonello, G., 1981. The upper mantle beneath a young oceanic rift: peridotites from the island of Zabargad, Red Sea. *Geology*, 9:474-479.

Cifelli, R., 1974. Planktonic Foraminifera from the Mediterranean and adjacent Atlantic waters (Cruise 49 of the Atlantis II, 1969). *J. Foraminiferal Res.*, 4,4:171-183.

Cita, M. B., 1973. Pliocene biostratigraphy and chronostratigraphy, *In* Ryan, W.B.F., Hsü, K. J., et al., *Init. Repts. DSDP*, 13. Washington (U.S. Govt. Printing Office), 1343-1379.

———, 1975. Studi sul Pliocene e gli strati di passaggio dal Miocene al Pliocene. VIII. Planktonic foraminiferal biozonation of the Mediterranean Pliocene deep sea record. A revision. *Riv. Ital. Paleontol. Stratigr.*, 81:527-544.

Mathews, M., Salisbury, M. H., and Hyndman, R. D., 1984. Basement logging on the Mid-Atlantic ridge, Deep Sea Drilling Project Hole 395A. *In* Hyndman, R. D., Salisbury, M. H., et al., *Init. Repts. DSDP*, 78B, Pt. 2: Washington (U.S. Govt. Printing Office), 717-730.

Moussat, E., Rehault, J. P., Fabbri, A., and Mascle, G., 1985. Evolution géologique de la Mer Tyrrhénienne, *C. R. Acad. Sci. Ser.* A, 301:491-496.

Parker, F. L., 1955. Distribution of planktonic Foraminifera in some Mediterranean sediments. *In Papers in Marine Biology and Oceanography Deep-Sea Res.* (Vol. 3 suppl.): London (Pergamon), 204-212.

Recq, M., Rehault, J. P., Steinmetz, L., and Fabbri, A., 1984. Amincissement de la croute et accrétion au centre du bassin Tyrrhénien d'aprés la sismique réfraction. *Mar. Geol.*, 55:411-428.

Rehault, J. P., Tisseau, C. and Fouchet, J. P., 1984. Structure, subsidence et flux thermique de la Mer Tyrrhéniénne Centrale: éssais de modélisation. CIESM (29th meeting) 11-19 October 1984, Lucerne.

Rehault, J. P., Moussat, E., and Fabbri, A., 1987. Structural evolution of the Tyrhenian back-arc basin. *Mar. Geol.*, 74:123-150.

Salisbury, M. H., Donelly, T., and Francheteau, J., 1979. Geophysical logging in Deep Sea Drilling Project Hole 417D. *In* Donnelly, T., Francheteau, J., et al., *Init. Repts. DSDP*, 51, 52, 53, Pt. 2: Washington (U.S. Govt. Printing Office), 705-713.

Steinmetz, L., Ferrucci, F., Hirn, A., Morelli, C., and Nicolich, R. 1983. A 550 km long moho traverse in the Tyrrhenian Sea from O.B.S. recorded Pn waves, *Geophys. Res. Lett.*, 10:428-431.

Thunell, R. C., 1978. Distribution of Recent planktonic foraminifera in surface sediments of the Mediterranean Sea. *Mar. Micropaleontol.*, 3:147-173.

Thunell, R. C., and Williams, D. F., 1983. The stepwise development of Pliocene-Pleistocene paleoclimatic and paleoceanographic conditions in the Mediterranean: Oxygen isotopic studies of DSDP Sites 125 and 132. *Utrecht Micropaleontol. Bull.*, 30:111-127.

Todd, R., 1958. Foraminifera from Western Mediterranean Deep-Sea cores. *Rept. Swed. Deep-Sea Exped.*, 3:169-215.

Table 11. Interval temperature, gradient, thermal conductivity, and heat flow at Site 655.

Measured interval	Sub-bottom interval (m)	Temperature difference (°C)	Thermal gradient (°C/km)	Thermal conductivity ($Wm^{-1}c^{-1}$)	n	Heat flow (mW/m^2)	Heat flow HFU
0-1	31.9	2.54	79.62	1.113		88.6	2.12
1-2	19.2	1.28	66.66	1.159		77.3	1.85
2-3	19.1	1.05	54.97	1.213		66.7	1.6
				(1.3)	5	71.15	1.7
0-2	51.1	3.83	74.95	1.136		85.1	2.03
0-3	70.2	4.88	69.5	1.161		80.7	1.93

Table 12. Thermal conductivity harmonic means for each core and temperature interval measured.

Core number	Number of measurements	Thermal conductivities ($W\ m^{-1}c^{-1}$) harmonic means: Per core	Interval measured
1	4	0.939 ± 0.04	1.113 ± 0.1
2	6	1.099 ± 0.04	
3	7	1.226 ± 0.04	
4	7	1.187 ± 0.01	
5	5	1.111 ± 0.05	1.159 ± 0.05
6	6	1.206 ± 0.02	
7	5	1.237 ± 0.03	1.213 ± 0.03
8	4	1.190 ± 0.02	
9	5	1.304 ± 0.05	1.304 ± 0.05

Table 13. Summary of log measurements at Hole 655B.

Mnemonic	Tool	Measurement	Unit	Depth (mbsf)
CALI	Caliper	Hole size	in.	70.0-185.0
GR	Natural Gamma Ray	Natural radioactivity	GAPI	70.0-187.0
DIL	Dual Induction	Deep, medium, and focused resistivity	Ω·m	70.0-194.5
LSS	Long Spacing Sonic	Sonic transit time (Short and long spacing)	μs/ft	70.0-182.5

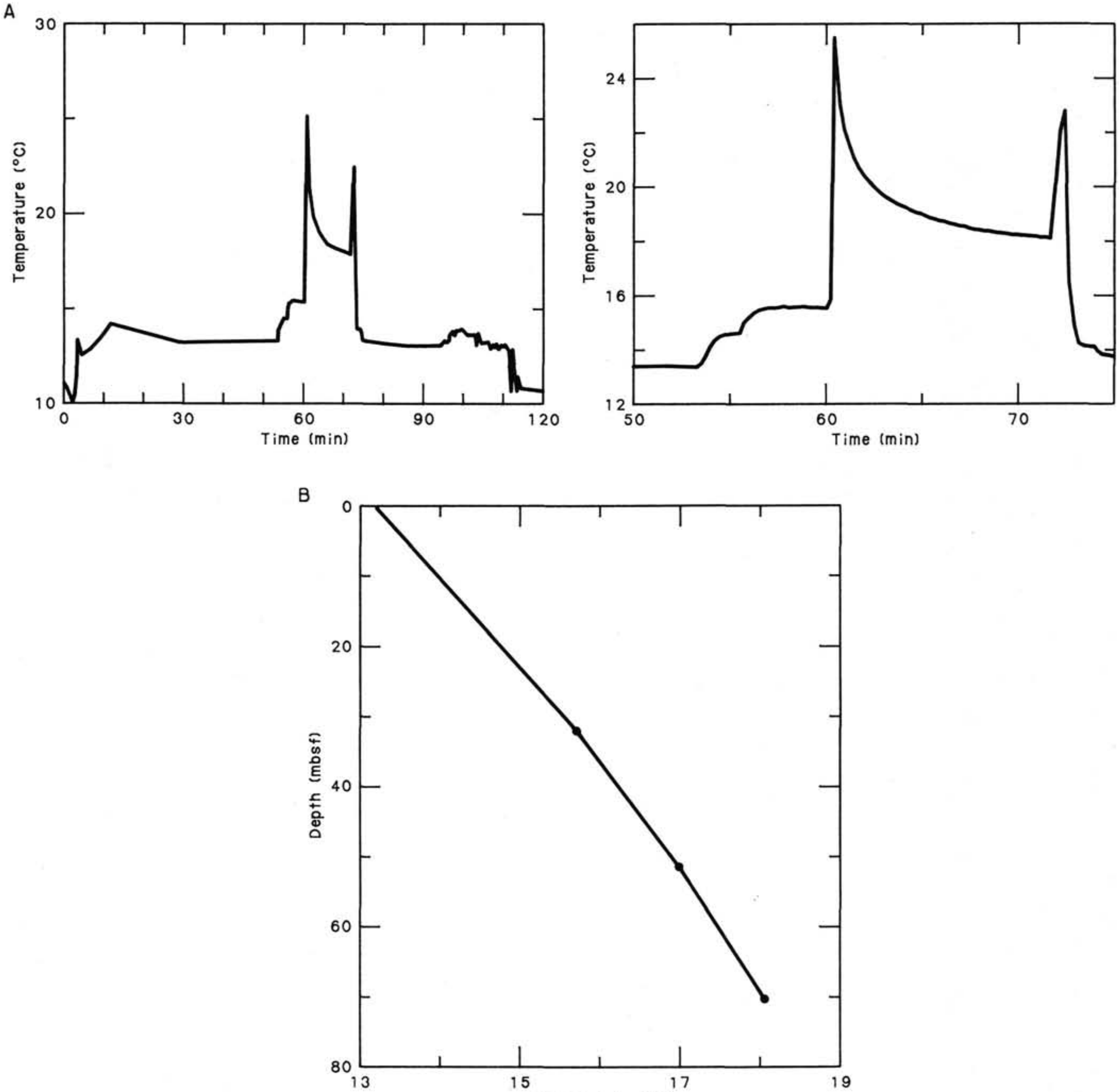

Figure 23. A. Temperature records at station HF3 (70.2 mbsf). B. Plot of sediment temperature vs. depth in Hole 655A (equivalent of geothermal gradient).

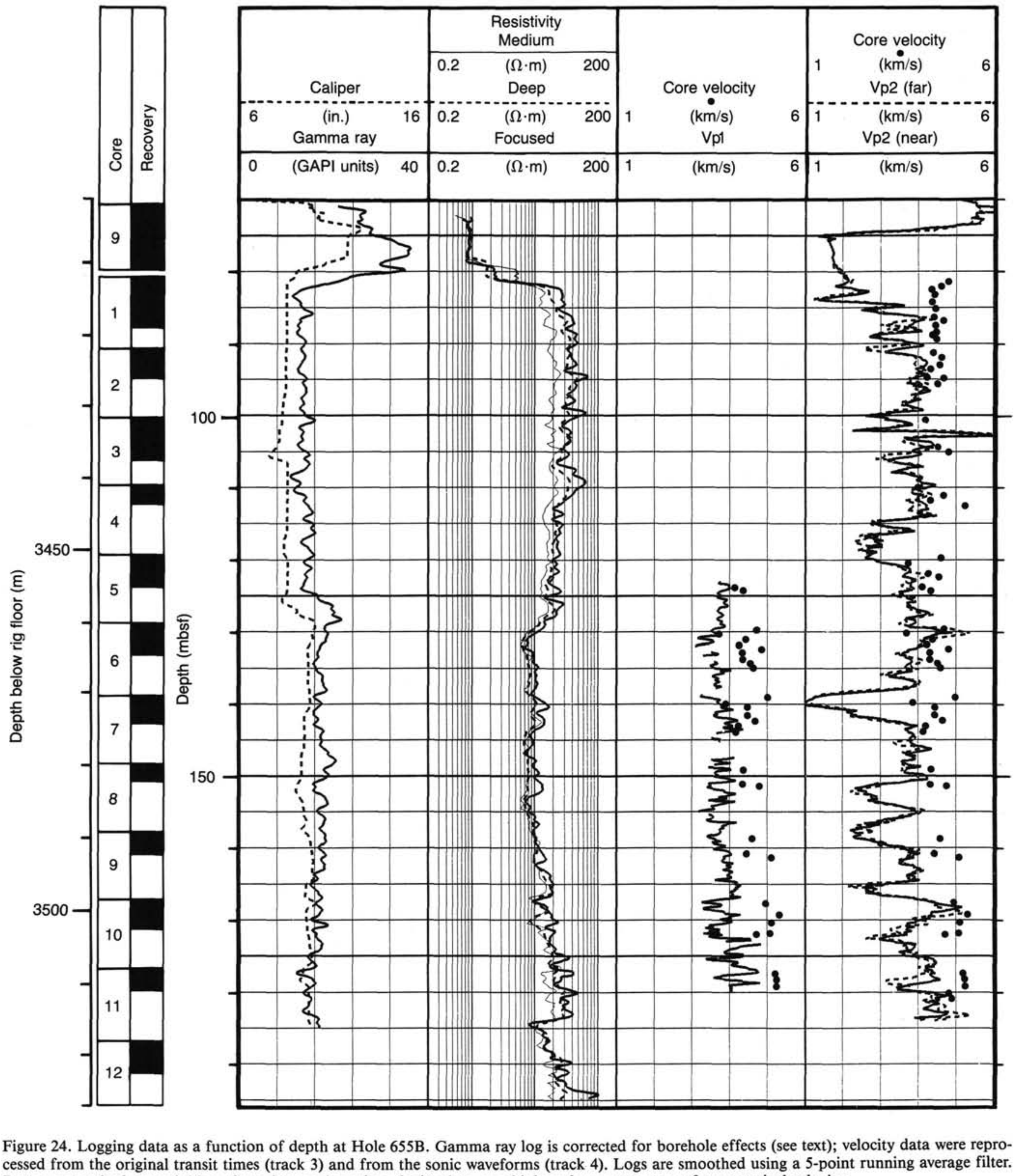

Figure 24. Logging data as a function of depth at Hole 655B. Gamma ray log is corrected for borehole effects (see text); velocity data were reprocessed from the original transit times (track 3) and from the sonic waveforms (track 4). Logs are smoothed using a 5-point running average filter. Data are acquired every 0.15 m. Superimposed on the velocity data are shipboard measurements of core vertical velocity.

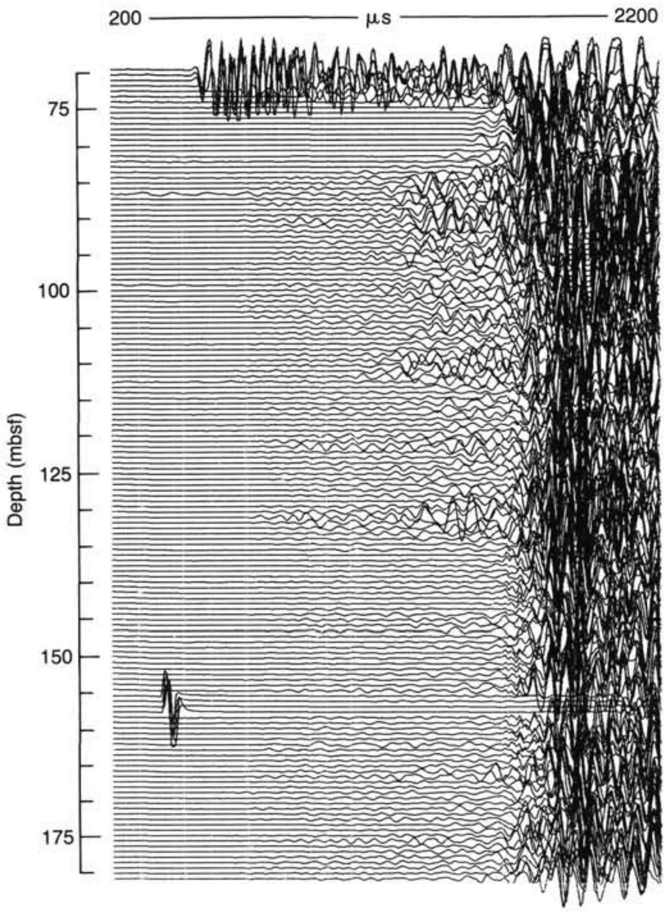

Figure 25. Acoustic waveforms recorded by the long spacing sonic tool are displayed for a source receiver spacing of 8 ft. The sediment-basalt interface and the bottom of the drill pipe are seen clearly at 75 and 82 mbsf, respectively. The first arrival travels at the formation compressional-wave velocity. The late high-amplitude arrival is a Stoneley wave, traveling at a velocity close to that of the borehole fluid. Attenuation of the Stoneley wave is often due to more intense fracturing in the formation.

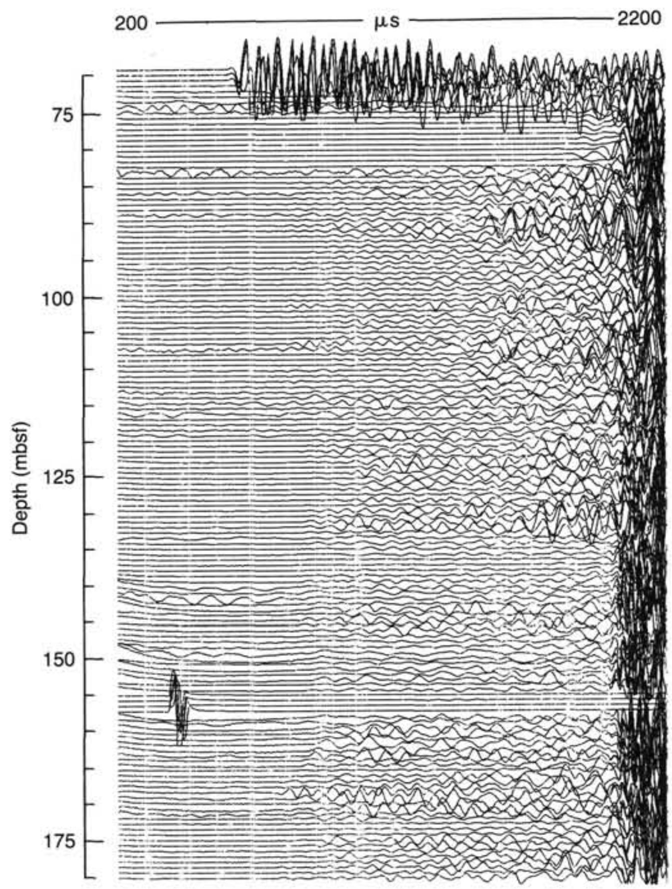

Figure 26. Acoustic waveforms recorded by the long spacing sonic tool are displayed for a source receiver spacing of 10 ft. The sediment-basalt interface and the bottom of the drill pipe are seen clearly at 75 and 82 mbsf, respectively. The first arrival travels at the formation compressional-wave velocity. The late high-amplitude arrival is a Stoneley wave, traveling at a velocity close to that of the borehole fluid. Attenuation of the Stoneley wave is often due to more intense fracturing in the formation.

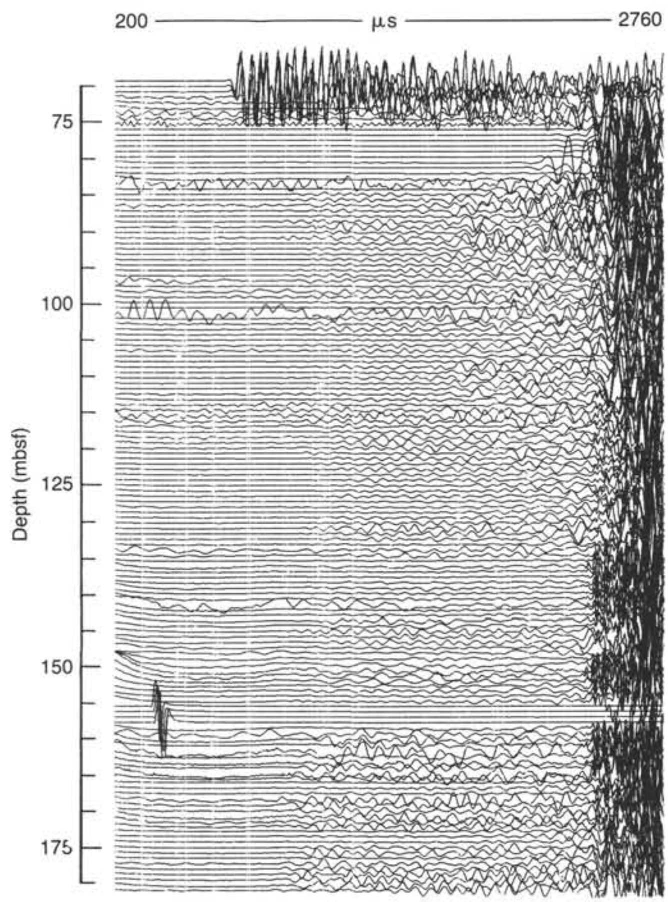

Figure 27. Acoustic waveforms recorded by the long spacing sonic tool are displayed for a source receiver spacing of 12 ft. The sediment-basalt interface and the bottom of the drill pipe are seen clearly at 75 and 82 mbsf, respectively. The first arrival travels at the formation compressional-wave velocity. The late high-amplitude arrival is a Stoneley wave, traveling at a velocity close to that of the borehole fluid. Attenuation of the Stoneley wave is often due to more intense fracturing in the formation.

Summary Log for Hole 655B

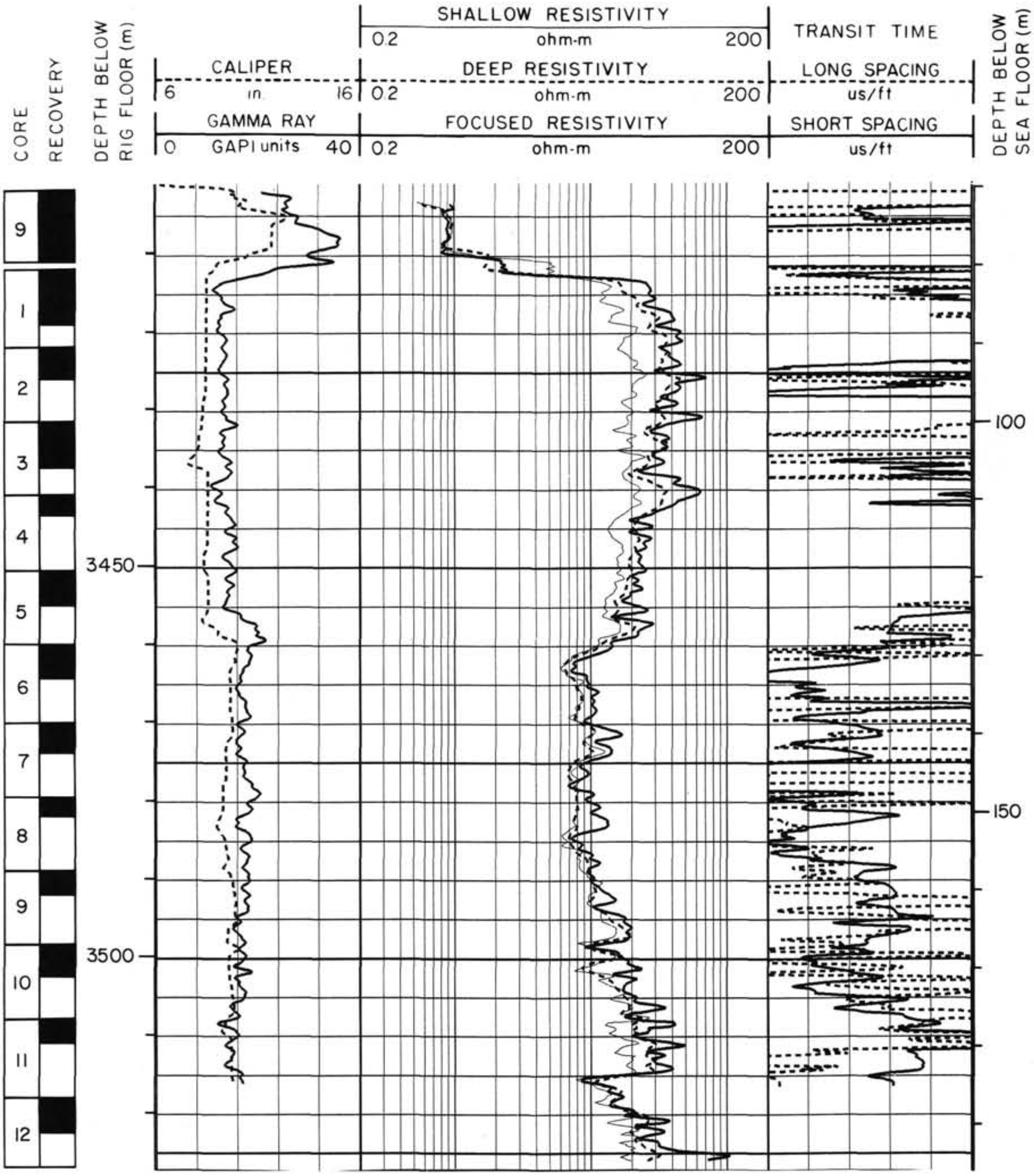

SITE 655 HOLE A CORE 1 H CORED INTERVAL 3290.0-3293.1 mbsl; 0-3.1 mbsf

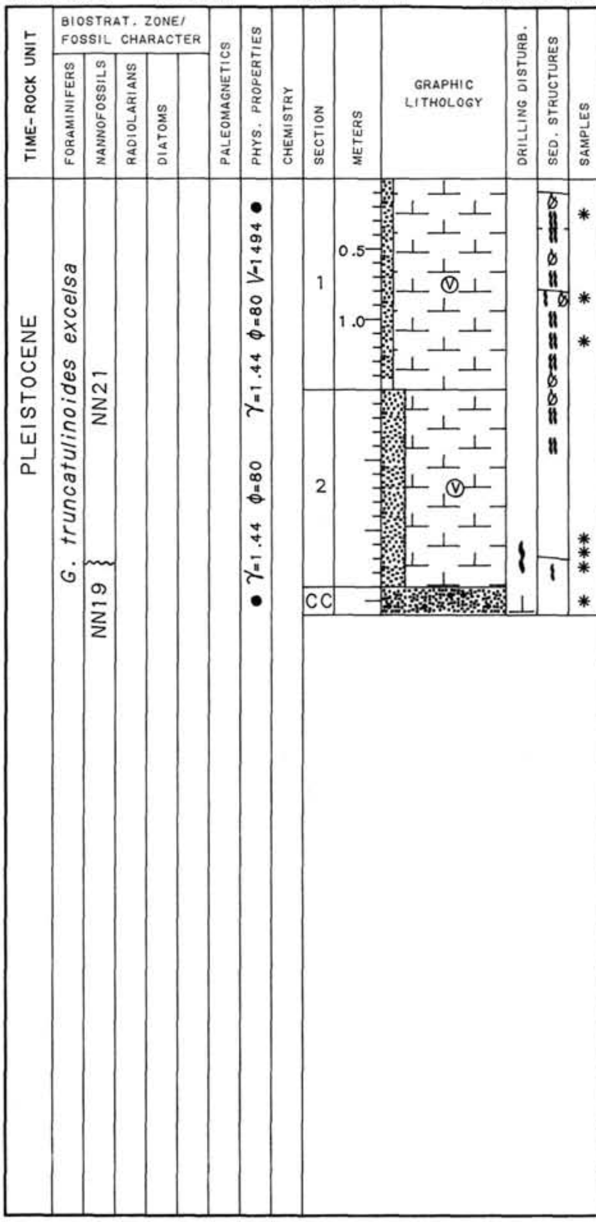

LITHOLOGIC DESCRIPTION

MARLY NANNOFOSSIL OOZE

Marly nannofossil ooze, alternating yellowish brown (10YR 5/4), pale brown (10YR 6/3), grayish brown (10YR 5/2, 2.5Y 5/2), light brownish gray (2.5Y 6/2), and dark grayish brown (2.5Y 4/2); moderately bioturbated, interbedded with numerous dark gray (10YR 4/1), 0.5- to 3.0-cm thick, well-sorted, detrital sand (quartz, feldspar, and lithoclast) layers; a few of the layers are biogenic calcareous sand. Fragments of pteropod shells are found in Section 1. Pumice layers with fragments as large as 1 cm occur at Section 1, 55–58 cm, and Section 2, 86–88 cm.

Section 2, 135–142 cm, and CC, 0–20 cm, contain a pale yellow (2.5Y 7/4) volcanic ash and calcareous silty sand with a more indurated, light yellowish brown interval (CC, 16–18 cm), which was fractured by drilling.

SMEAR SLIDE SUMMARY (%):

	1, 25 D	1, 87 M	1, 114 D	2, 105 M	2, 113 M	2, 123 D	CC, 18 D
TEXTURE:							
Sand	8	90	8	25	10	5	50
Silt	10	5	12	40	30	15	30
Clay	82	5	80	35	60	80	20
COMPOSITION:							
Quartz	3	20	2	8	2	1	7
Feldspar	11U25	Tr	12	1	—	—	—
Rock fragments (including limestone)	—	25	—	7	Tr	—	—
Mica	Tr	-10	Tr	3	2	—	2
Clay	51	—	43	27	45	31	17
Volcanic glass	5	—	3	Tr	1	2	25
Calcite	2	15	—	4	3	—	—
Dolomite	—	—	2	—	—	—	5
Accessory minerals	—	5	1	2	2	1	—
Manganese micronodules	2	—	—	—	3	—	2
Zeolites	1	—	—	—	—	—	—
Foraminifers	5	—	3	6	6	8	3
Nannofossils	28	—	40	25	25	50	8
Diatoms	—	—	Tr	—	1	—	—
Radiolarians	2	—	—	Tr	Tr	1	—
Sponge spicules	Tr	—	2	2	Tr	1	—
Fish remains (ortholith? teeth?)	—	—	—	1	—	—	—
Micrite	—	—	4	3	7	5	30
Limonite	—	—	—	—	1	—	—
Other opaques	—	—	—	—	1	—	—

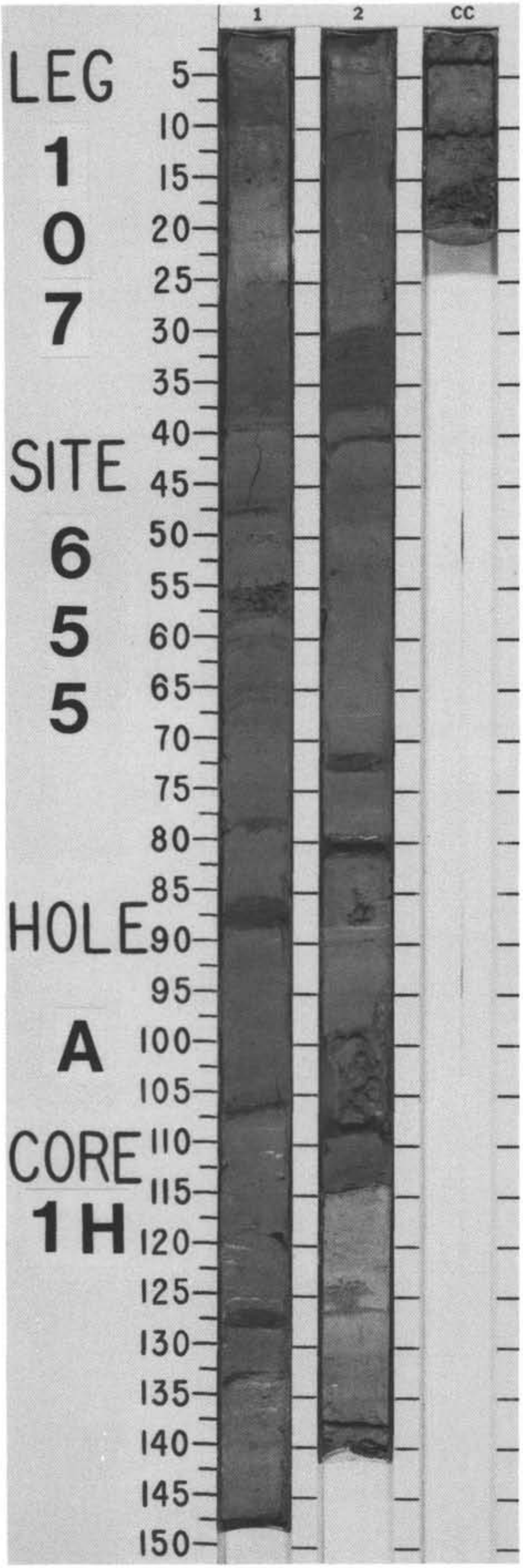
LEG 1 0 7
SITE 6 5 5
HOLE A
CORE 1 H
1
2
CC
5
10
15
20
25
30
35
40
45
50
55
60
65
70
75
80
85
90
95
100
105
110
115
120
125
130
135
140
145
150

SITE 655 HOLE A CORE 2 H CORED INTERVAL 3293.1-3302.7 mbsl; 3.1-12.7 mbsf

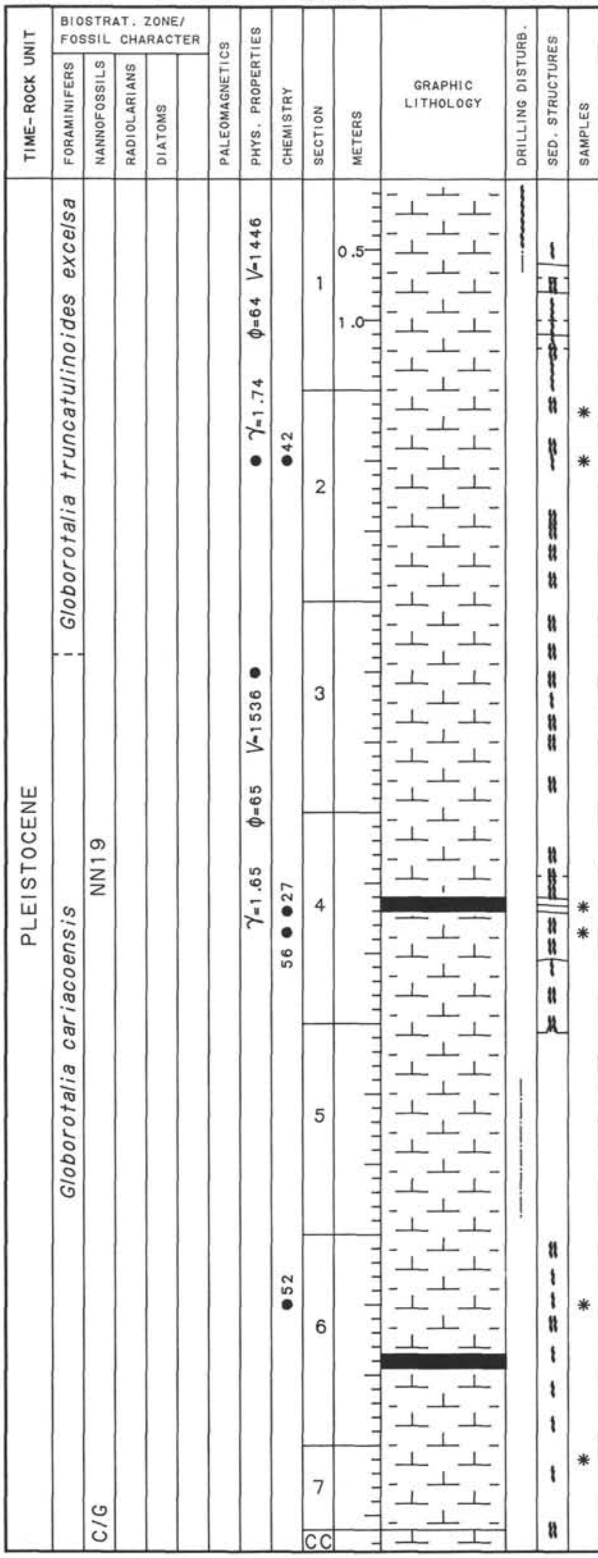

LITHOLOGIC DESCRIPTION

MARLY NANNOFOSSIL OOZE and SAPROPELS

Marly nannofossil ooze, with numerous alternations of light brownish gray (2.5Y 6/2) with light gray (2.5Y 7/2, 5Y 7/2 and 6/1), brown (10YR 5/3), and light olive-gray (5Y 6/2); moderately bioturbated. Foraminifers and pteropods abundant. Section 4, 146–150 cm, and Section 5, 0–32 cm, is a debris-flow composed of multicolored mud pebbles in a pale olive (5Y 6/3) mud matrix. Section 2, 17–18 cm, is a zeolitic sand, and Section 7, 7–10 cm, is a sandy siltstone. Micronodules commonly occur, and in Section 3, a 1-mm-thick, olive-brown (2.5Y 4/4) iron manganese crust was observed.

Sapropels: Section 4, 58–100 cm, is a well-developed sapropel; 58–59 cm is olive (5Y 4/4) and finely bioturbated; 59–64.5 cm is greenish gray (5GY 5/1) and laminated; 64.5–67 cm is black (5Y 2.5/1) and laminated; 67–70 cm is dark olive-gray (5Y 3/2) and laminated; 70–100 cm is gray (5Y 5/1) and bioturbated. Section 6, 75–115 cm, is a probable sapropelic layer; 75–85 cm is light yellowish brown (2.5Y 6/4); 85–89 cm is greenish gray (2GY 6/1); 89–90 cm is grayish green (5G 5/2); 90–95 cm is gray (5Y 5/1), and 95–115 cm is olive-gray (5Y 5/2). The entire interval is moderately bioturbated.

SMEAR SLIDE SUMMARY (%):

	2, 17 M	2, 50 D	4, 67 M	4, 82 D	6, 46 D	7, 9 M
TEXTURE:						
Sand	80	25	20	5	4	30
Silt	10	25	25	5	6	20
Clay	10	50	55	90	90	50
COMPOSITION:						
Quartz	5	3	1	1	1	15
Mica	—	—	—	—	—	4
Clay	13	18	23	26	30	23
Volcanic glass	—	2	—	—	—	3
Dolomite	—	1	3	2	1	1
Accessory minerals	—	1	3	1	Tr	2
Zeolites	60	—	—	1	—	5
Gypsum	5	—	—	—	—	—
Micrite	10	10	15	5	—	10
Foraminifers	5	12	2	4	3	2
Nannofossils	2	50	45	60	65	30
Radiolarians	—	2	—	—	—	—
Sponge spicules	—	—	Tr	—	—	—
Silicoflagellates	—	—	—	—	—	2
Micronodules	—	1	4	—	—	3
Opaques	—	—	4	—	—	—

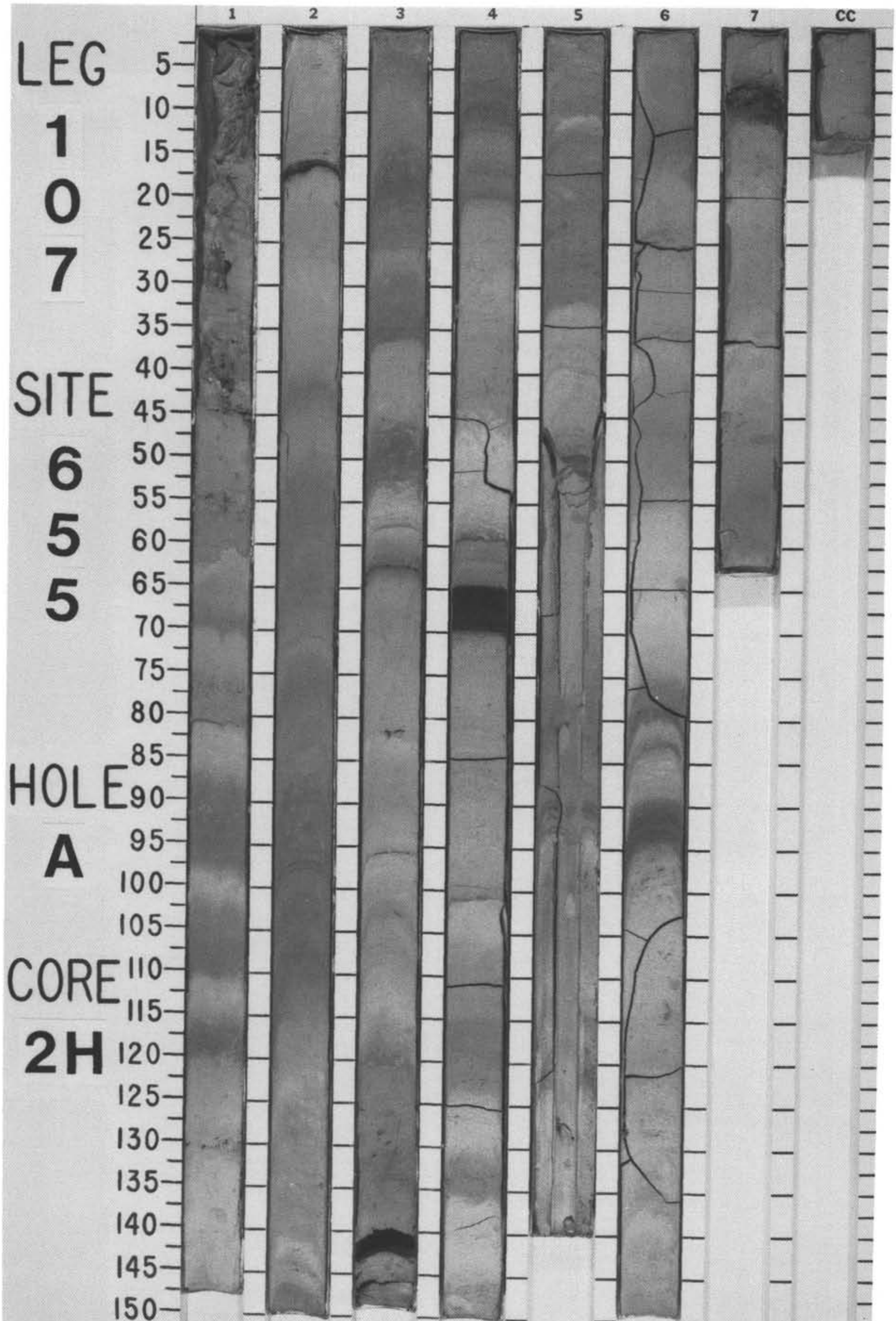
LEG
107
SITE
655
HOLE
A
CORE
2H
1
2
3
4
5
6
7
CC
5
10
15
20
25
30
35
40
45
50
55
60
65
70
75
80
85
90
95
100
105
110
115
120
125
130
135
140
145
150

SITE 655 HOLE A CORE 3 H CORED INTERVAL 3302.7-3312.3 mbsl; 12.7-22.3 mbsf

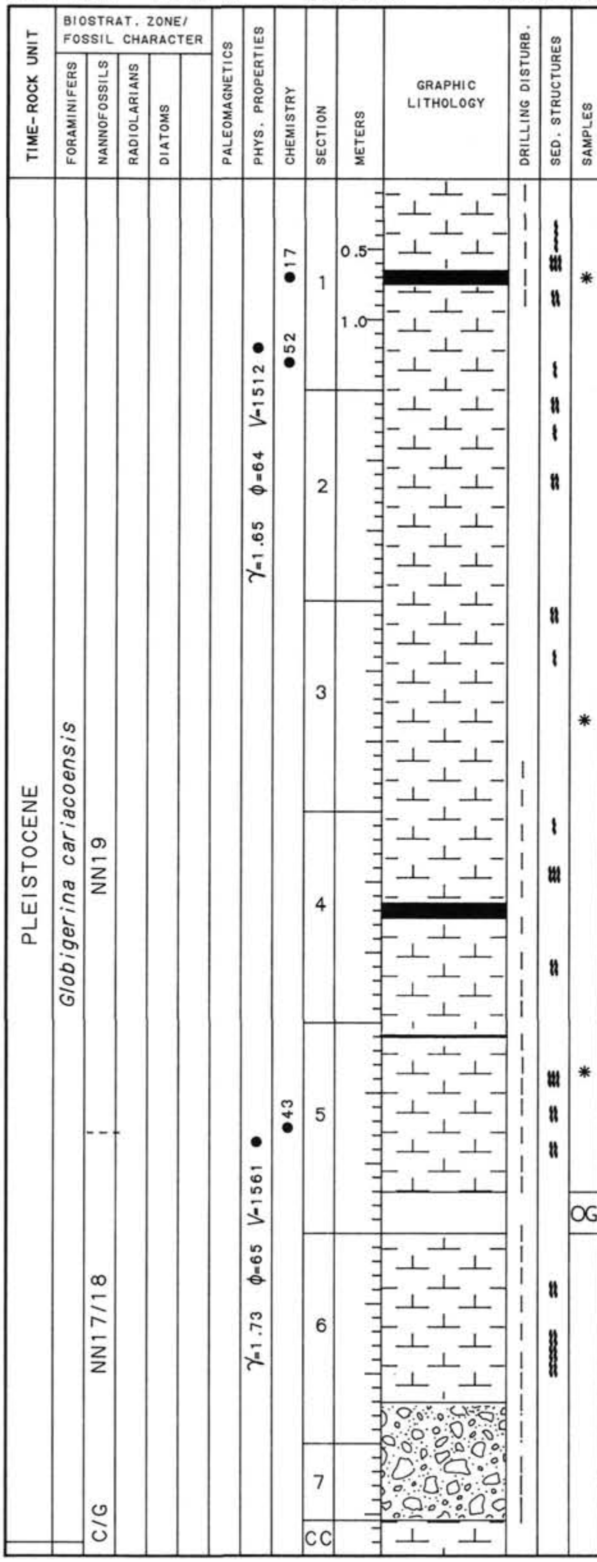

LITHOLOGIC DESCRIPTION

MARLY NANNOFOSSIL OOZE and SAPROPELS

Marly nannofossil ooze, mainly light gray (5Y 7/1, 2.5Y 7/2), with gray (5Y 6/1), light olive-brown (2.5Y 6/2), and pale yellow (5Y 7/4); contains a small percentage of detrital quartz and abundant foraminifers. Sections 4 and 5 show alternations of darker bioturbated 10 cm-thick zones and lighter homogeneous zones of variable thickness. In Section 5, 30 cm, a very dark olive-brown (2.5Y 3/2) silty layer occurs. The bottom of Section 6 and Section 7 show debris highly disturbed by drilling.

Sapropels: Section 1, 62–72 cm, is black (5Y 5/2) and 10 cm thick; Section 1, 143–145 cm is olive-gray (5Y 4/2) and 2 cm thick; Section 4, 67–75 cm is dark olive-gray (5Y 3/2) and 10 cm thick; Section 5, 12–14 cm, is dark olive-gray (5Y 3/2) and 2 cm thick. Each is followed upsection by a zone of gradational change in color with diagenetic fronts as thick as 20 cm.

SMEAR SLIDE SUMMARY (%):

	1, 68 M	3, 80 D	5, 30 M
TEXTURE:			
Sand	15	4	20
Silt	20	4	20
Clay	65	92	60
COMPOSITION:			
Quartz	4	2	6
Feldspar	—	—	3
Clay	37	46	43
Volcanic glass	—	—	3
Calcite/dolomite	5	Tr	3
Accessory minerals	2	Tr	2
Micronodules	3	—	—
Opaques	—	—	5
Zeolites	—	—	8
Foraminifers	3	2	Tr
Nannofossils	40	45	15
Sponge spicules	1	1	2
Silicoflagellates	—	2	Tr
Micrite	5	2	10

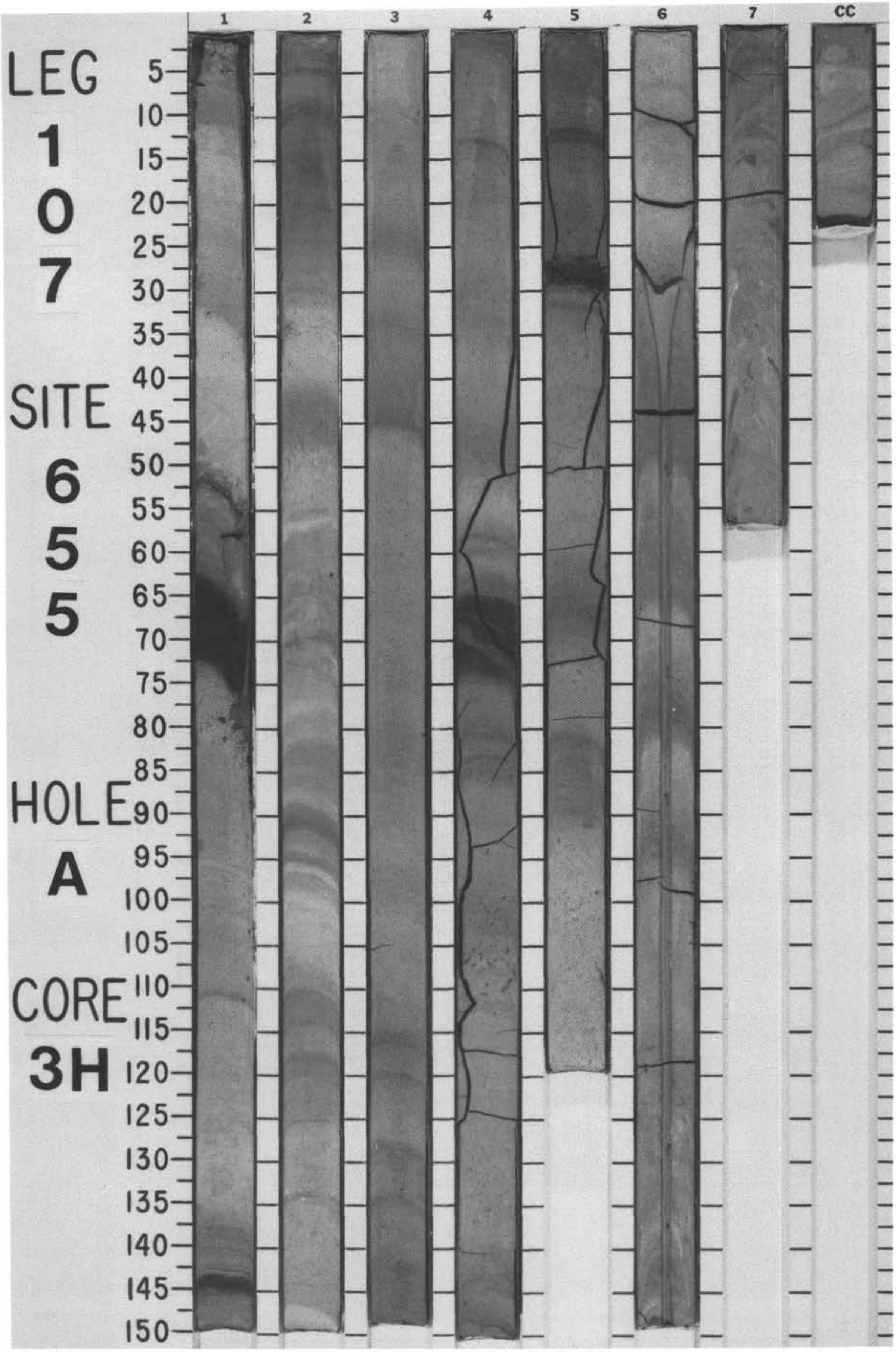
LEG
107
SITE
655
HOLE
A
CORE
3H
1
2
3
4
5
6
7
CC
5
10
15
20
25
30
35
40
45
50
55
60
65
70
75
80
85
90
95
100
105
110
115
120
125
130
135
140
145
150

SITE 655 HOLE A CORE 4 H CORED INTERVAL 3312.3-3321.9 mbsl; 22.3-31.9 mbsf

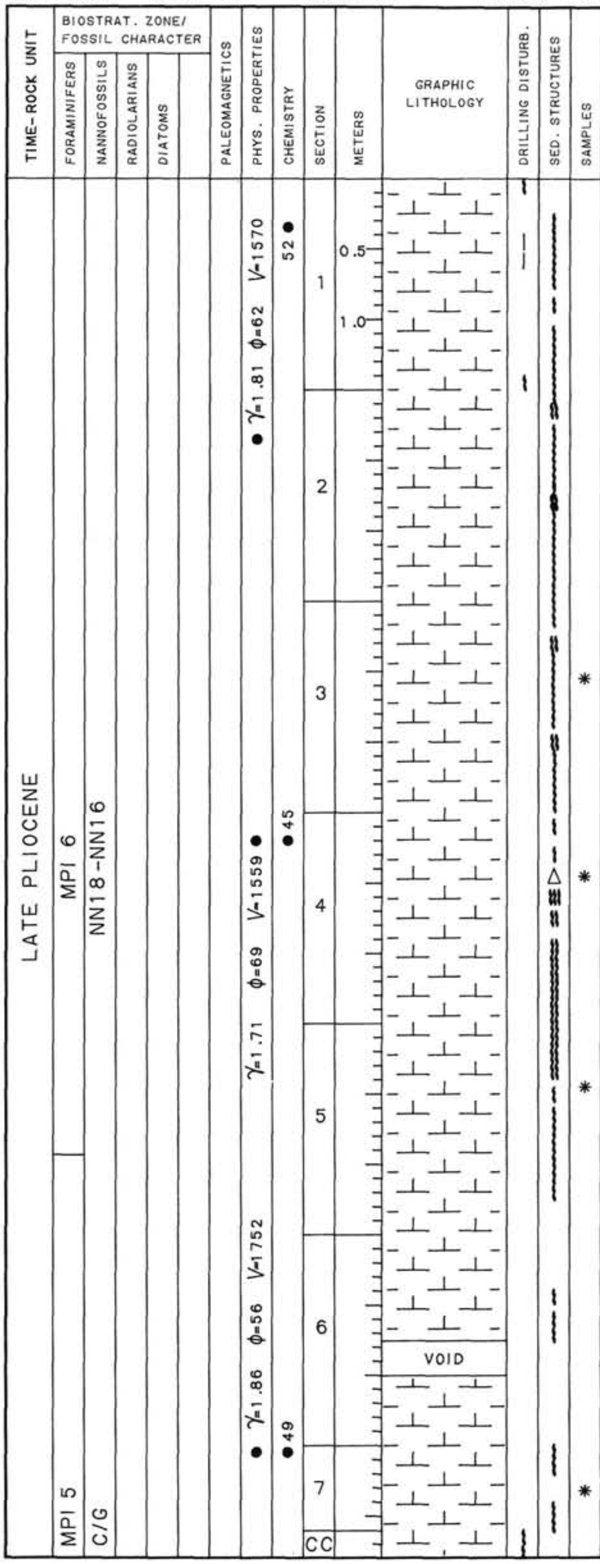

LITHOLOGIC DESCRIPTION

MARLY NANNOFOSSIL OOZE

Marly nannofossil ooze, light gray (2.5Y 7/2, 5Y 7/2); some foraminifer-rich layers or pockets occur randomly in Sections 1 through 4 and more rarely in Sections 5 and 6; bioturbation is common. In Section 4, 50 cm, a 3 cm-thick, gray (2.5Y 6/0) volcanic ash layer occurs. From Section 3 to base there are many color alternations; in Sections 3 and 4 alternating colors are white (2.5Y 8/2) and pale yellow (2.5Y 7/4); from Section 5, 90 cm, to the base alternation becomes frequent; each interval is ‹10 cm thick, and colors are more variable with pinkish tones dominating: pinkish white (7.5YR 8/2, 5YR 8/2), pink (7.5YR 7/4 and 8/4, 5YR 7/3 and 7/4), pinkish gray (7.5YR 7/2), and reddish yellow (7.5YR 7/1).

SMEAR SLIDE SUMMARY (%):

	3, 55 M	4, 43 M	5, 49 M	7, 31 D
TEXTURE:				
Sand	2	10	32	1
Silt	10	80	10	14
Clay	88	10	58	85
COMPOSITION:				
Quartz	4	3	1	Tr
Feldspar	2	5	—	Tr
Mica	Tr	3	—	—
Clay	36	10	31	42
Volcanic glass	—	53	—	—
Accessory minerals	1	Tr	—	—
Zeolites	3	1	5	2
Pyroxene	—	Tr	—	—
Foraminifers	4	4	31	5
Nannofossils	50	16	35	50
Intraclasts	—	3	1	1

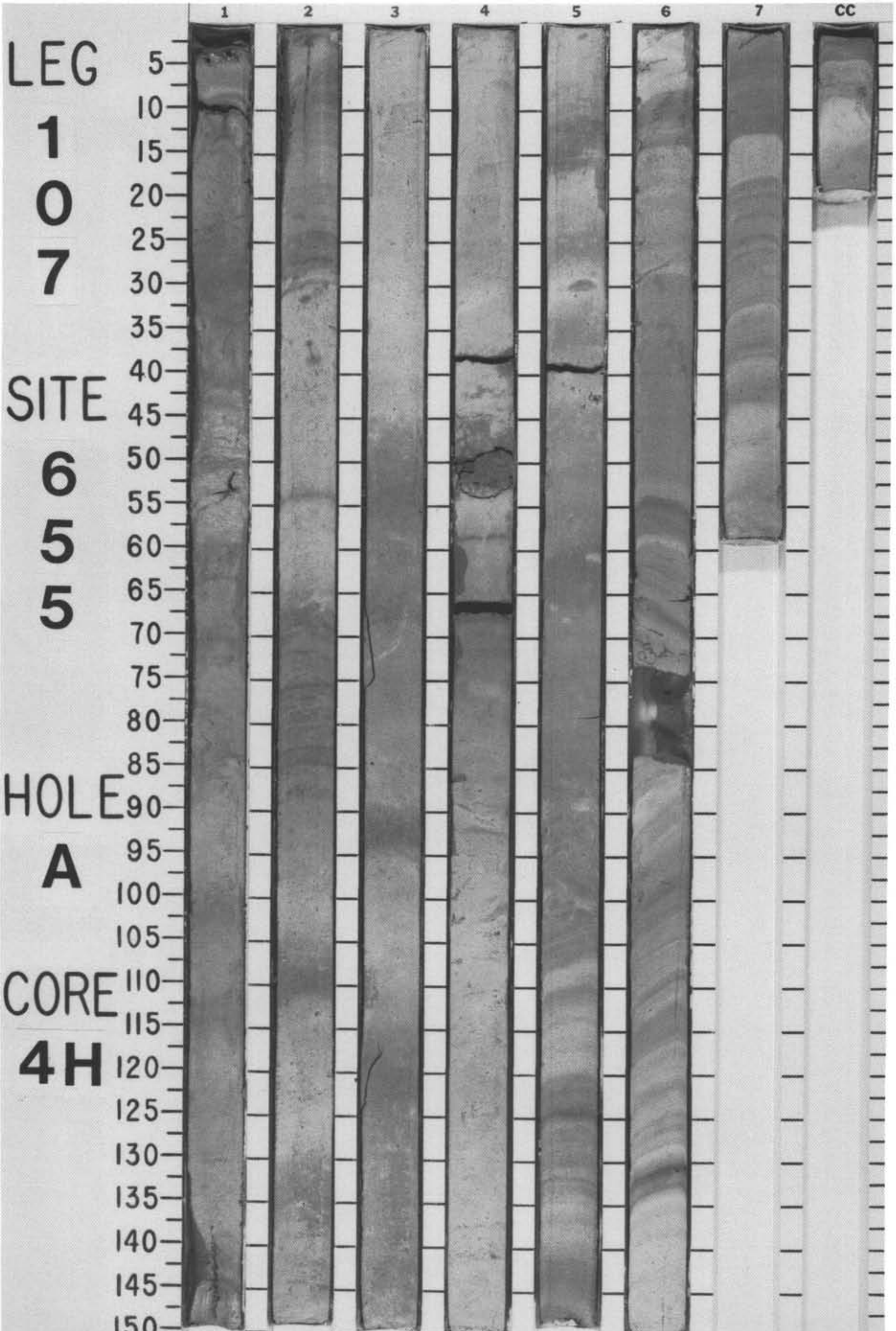
LEG 107
SITE 655
HOLE A
CORE 4H
1
2
3
4
5
6
7
CC

SITE 655 HOLE A CORE 5 H CORED INTERVAL 3321.9-3331.5 mbsl; 31.9-41.5 mbsf

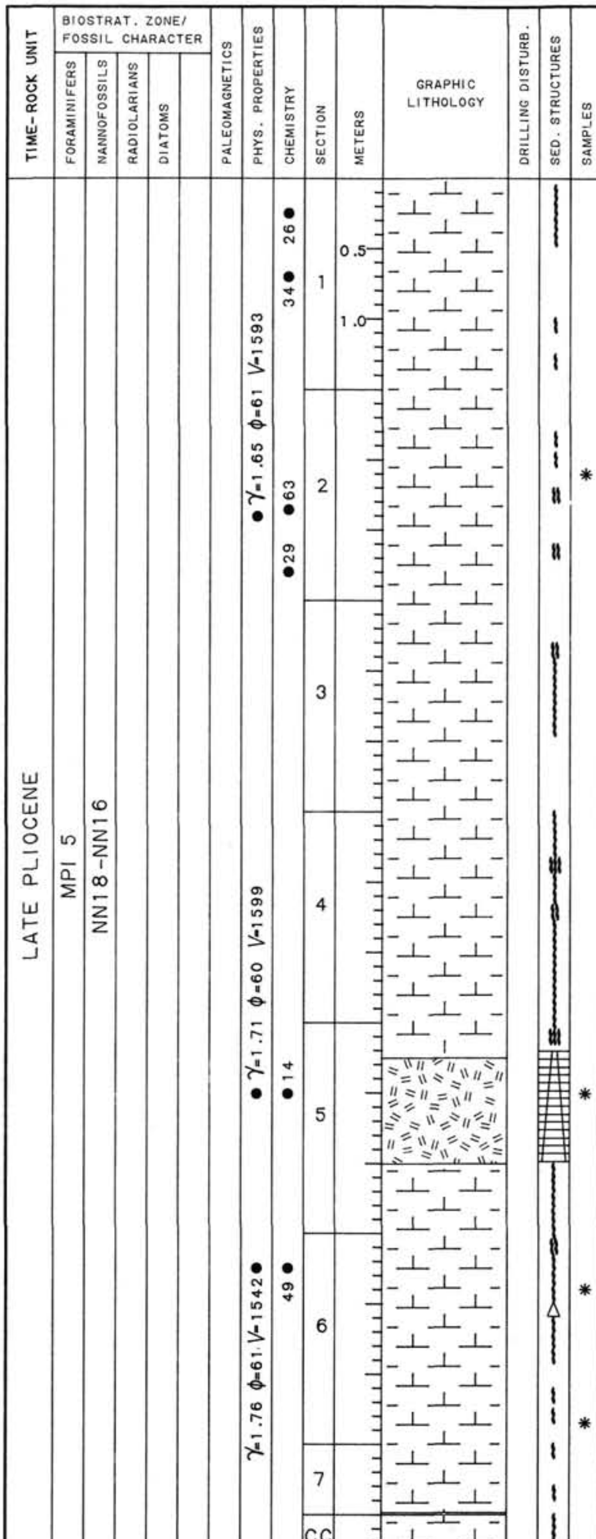

LITHOLOGIC DESCRIPTION

MARLY NANNOFOSSIL OOZE and VOLCANICLASTIC TURBIDITE

The sediment is mainly a clear, bioturbated nannofossil ooze with scattered foraminifers. Section 1, 0–75 cm, shows color variations from dominant pink (7.5YR 7/4) to pale yellow (2.5Y 7/4) and reddish brown (7.5YR 7/6); the remaining colors are predominantly yellow (5Y 8/6) and white (2.5Y 8/2).

Section 5, 15–100 cm, thick turbiditic sequence of volcaniclastic material, rich in black, heavy minerals (pyroxene); 44–75 cm, contains numerous well-preserved laminations as much as 1 cm-thick; 75–98 cm is massive sand enriched in heavy minerals.

Section 6, 38 cm, is a 2 cm-thick graded layer of foraminifer sand; Section 6, 143 cm, is a 2 cm-thick layer of altered volcanic glass.

SMEAR SLIDE SUMMARY (%):

	2, 65 D	5, 48 D	6, 39 M	6, 145 M
TEXTURE:				
Sand	—	60	31	25
Silt	15	30	15	60
Clay	85	10	54	15
COMPOSITION:				
Quartz	2	15	2	6
Feldspar	—	8	—	12
Mica	Tr	—	—	—
Clay	37	10	19	15
Volcanic glass	—	47	Tr	45
Calcite/dolomite	—	—	4	—
Accessory minerals	—	—	2	—
Pyroxenes	—	5	—	Tr
Zeolites	Tr	Tr	—	12
Foraminifers	10	2	25	2
Nannofossils	50	3	40	8
Sponge spicules	—	—	—	Tr
Intraclasts	1	3	8	—
Micrite	—	7	—	—

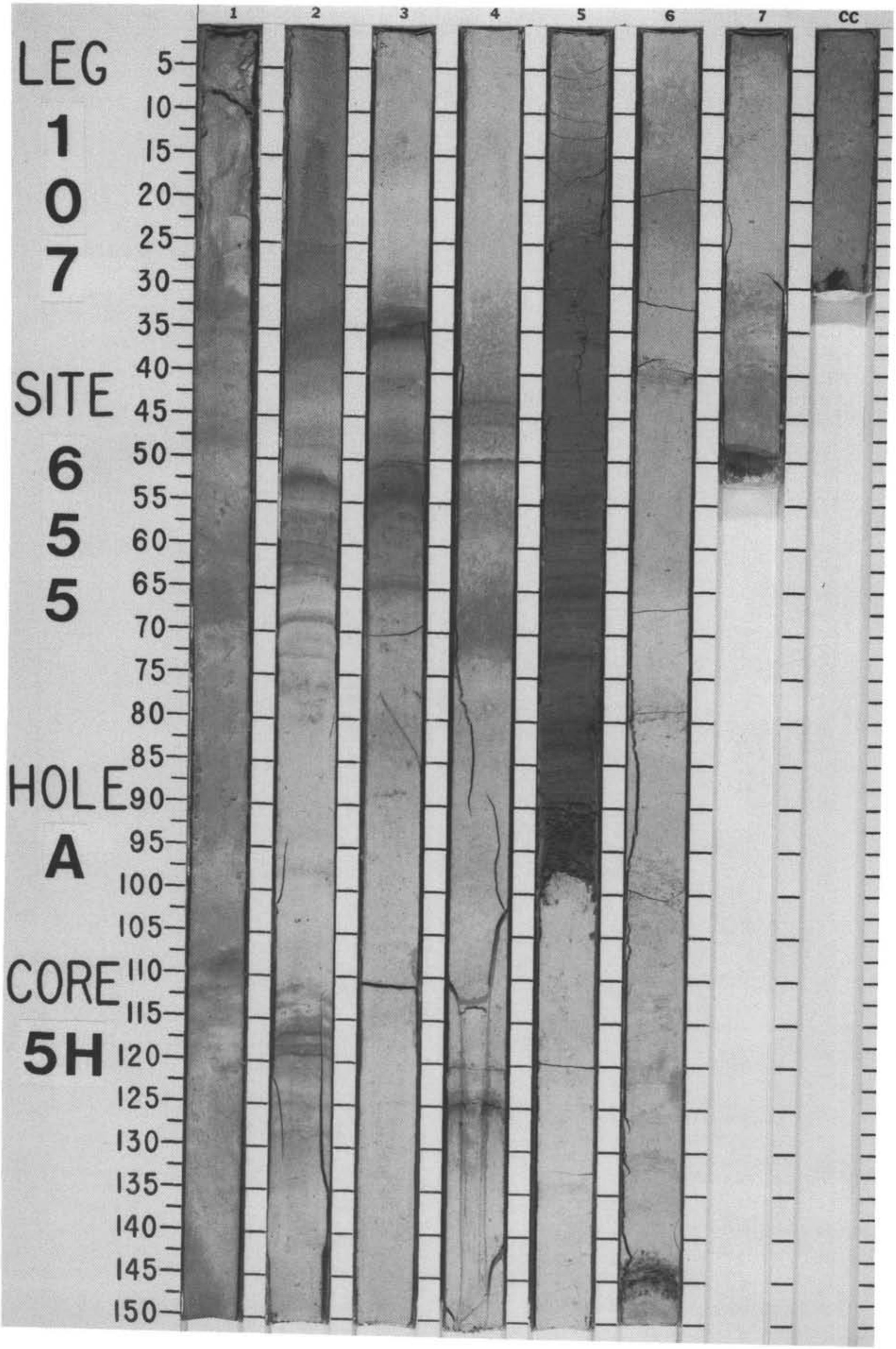
LEG 107
SITE 655
HOLE A
CORE 5H
1
2
3
4
5
6
7
CC
5
10
15
20
25
30
35
40
45
50
55
60
65
70
75
80
85
90
95
100
105
110
115
120
125
130
135
140
145
150

SITE 655 HOLE A CORE 6 H CORED INTERVAL 3331.5-3341.1 mbsl; 41.5-51.1 mbsf

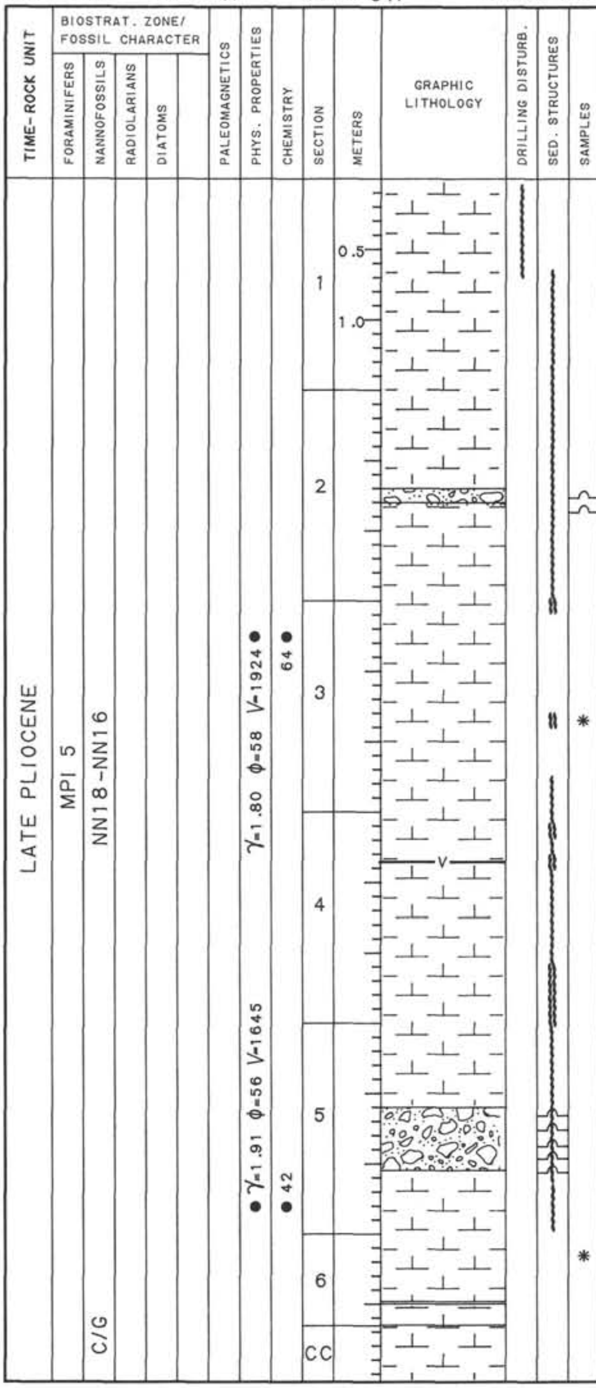

LITHOLOGIC DESCRIPTION

NANNOFOSSIL OOZE, DEBRIS FLOW, and VOLCANIC ASH

Nannofossil ooze in Section 1 is light gray (2.5Y 7/2), pale yellow (2.5Y 7/4), and pink (7.5YR 7/4); in Section 2 it is light brown (7.5YR 6/4) to pinkish gray (7.5YR 7/6); in Section 3 it is pink (7.5YR 7/4), reddish yellow (7.5YR 7/6), and reddish brown (10R 6/6); in Section 4 it is white (5Y 8/1) and light gray (5Y 7/1) except for 70–120 cm, which is pink (7.5YR 7/4–6/4–6/6); in Section 5 it is light gray (5Y 7/2) to pale yellow (5Y 7/3); and in Section 6 and the CC it is light olive-gray (5Y 6/2). The whole interval is bioturbated.

One 45-cm-thick debris flow occurs in Section 5, 60–105 cm, with reworked pebbles of marly nannofossil ooze as large as 3.5 cm in diameter; a second debris flow, which is not easily identifiable because of intense burrowing, possibly exists in Section 2, 60–72 cm.

A volcanic ash layer occurs in Section 4, 38 cm.

SMEAR SLIDE SUMMARY (%):

	3, 83 D	6, 19.5 D
TEXTURE:		
Sand	14	7
Silt	25	10
Clay	61	83
COMPOSITION:		
Quartz	9	2
Feldspar	4	—
Mica	1	—
Clay	33	24
Calcite/dolomite	1	—
Accessory minerals	—	1
Zeolites	Tr	—
Foraminifers	4	23
Nannofossils	45	46
Micrite	3	—
Bioclasts	—	4

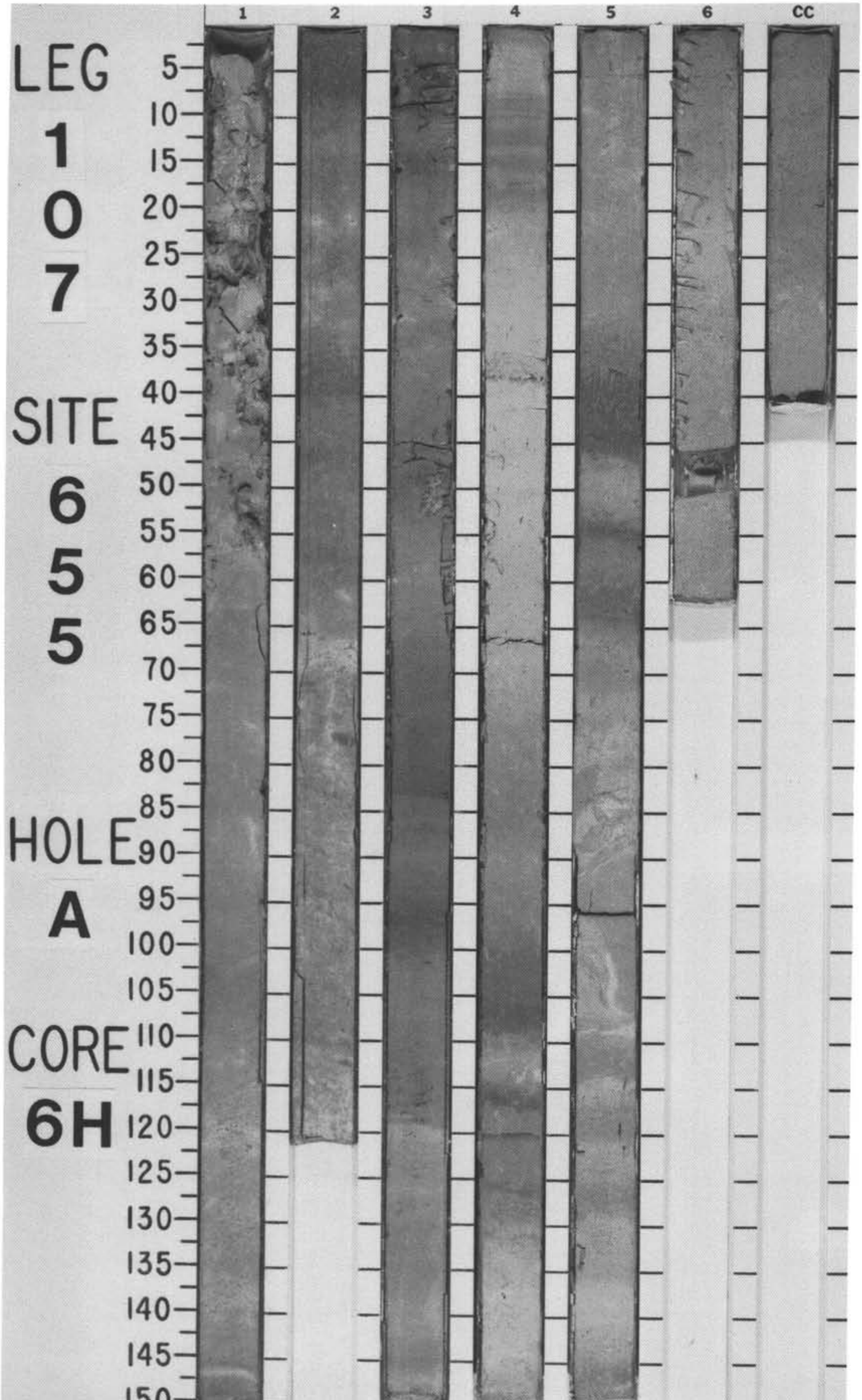
LEG
1
0
7
SITE
6
5
5
HOLE
A
CORE
6H
1
2
3
4
5
6
CC

SITE 655 HOLE A CORE 7 H CORED INTERVAL 3341.1-3350.6 mbsl; 51.1-60.6 mbsf

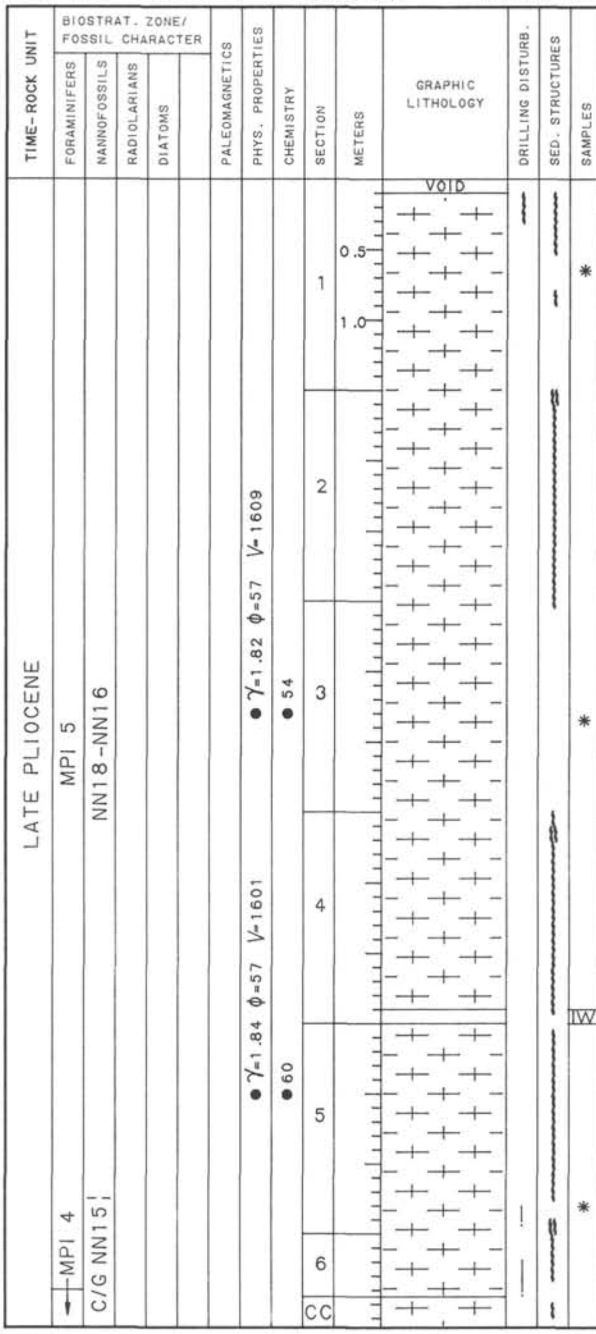

LITHOLOGIC DESCRIPTION

FORAMINIFER-NANNOFOSSIL OOZE

Banded foraminifer-nannofossil ooze shows variations in color that are generally gradational. Section 1 is dominantly light gray (2.5Y 7/2), yellow (2.5Y 7/6), and light yellowish brown (2.5Y 6/4) at the top, and brownish yellow (10YR 6/6), very pale brown (10YR 7/4), and white (10YR 8/2) at the base. Section 2 shows variations from white (10YR 8/1) to yellow (10YR 7/6). Section 3 is mainly white (10YR 8/1), with two thin yellow intervals (10YR 7/16). Section 4 is very pale brown (10YR 7/4–7/3) or pale brown (10YR 6/3) with a light gray (5Y 7/2) interval at 30–70 cm. Sections 5, 6, and CC are light yellowish brown (2.5Y 6/4).

SMEAR SLIDE SUMMARY (%):

	1, 70 D	3, 82 D	5, 132 M
TEXTURE:			
Sand	4	5	5
Silt	16	10	45
Clay	80	85	50
COMPOSITION:			
Quartz	2	3	Tr
Feldspar	1	1	—
Clay	35	46	30
Volcanic glass	—	—	Tr
Accessory minerals	1	1	Tr
Zeolites	1	1	Tr
Foraminifers	12	12	20
Nannofossils	46	34	40
Sponge spicules	—	—	Tr
Micrite	2	—	10
Bioclasts	—	2	—

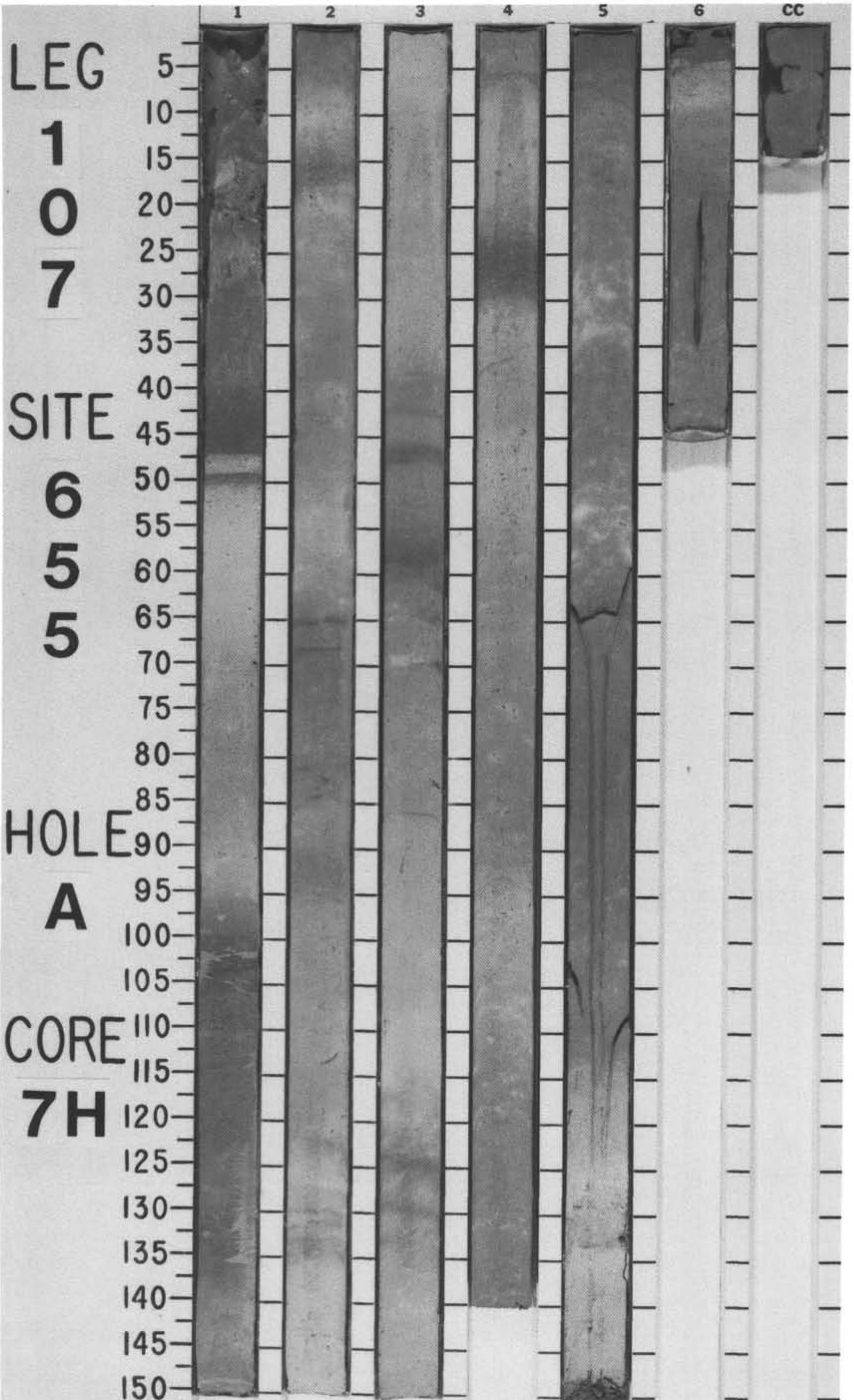
LEG
107
SITE
655
HOLE
A
CORE
7H
1
2
3
4
5
6
CC
5
10
15
20
25
30
35
40
45
50
55
60
65
70
75
80
85
90
95
100
105
110
115
120
125
130
135
140
145
150

SITE 655 HOLE A CORE 8 H CORED INTERVAL 3350.6-3360.2 mbsl; 60.6-70.2 mbsf

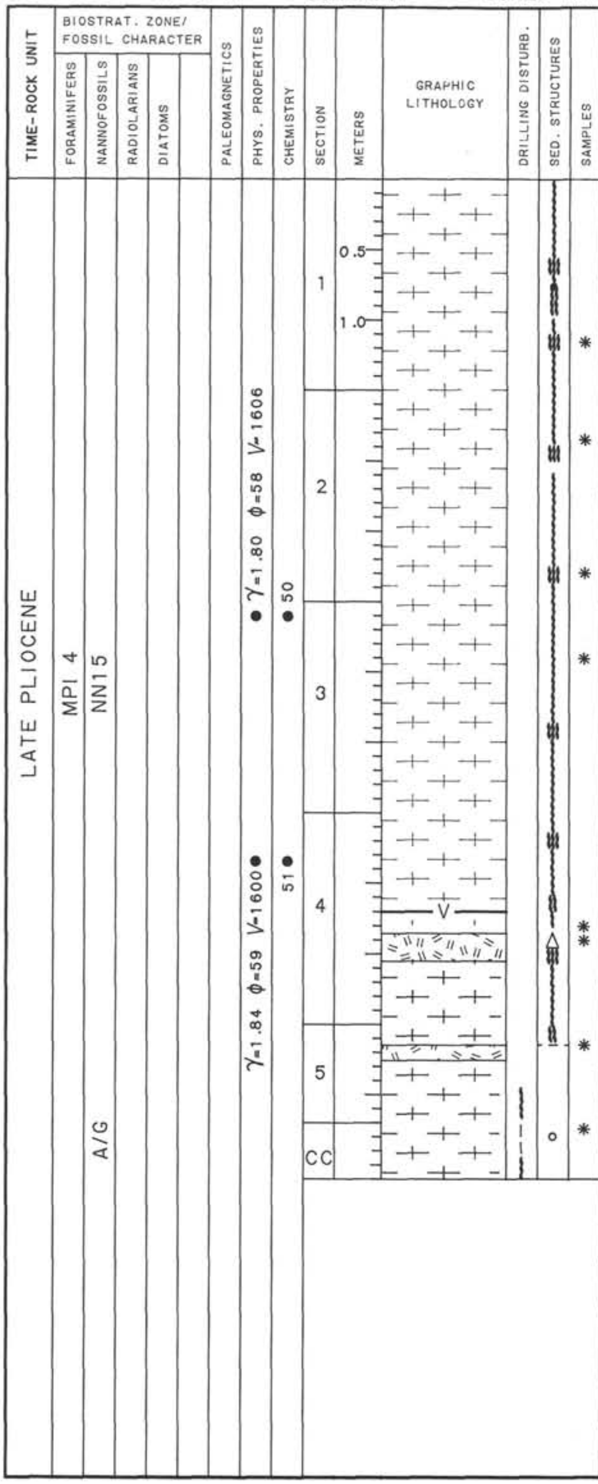

LITHOLOGIC DESCRIPTION

FORAMINIFER-NANNOFOSSIL OOZE, ASH LAYERS, and SANDY SILT

The dominant lithology is foraminifer-nannofossil ooze containing up to 20% dolomite; predominantly gray (5Y 6/2), with zones of very pale yellow (10YR 7/2–7/1), yellow (10YR 7/6), and pink (5YR 7/3) in Section 1, 70–110 cm, and Section 2, 50–60 cm; reddish yellow (7.5YR 6/6) in Section 2, 10–50 cm.

Ash layers 8–10 cm-thick are present in Section 4, 88–106 cm, and Section 5, 15–23 cm; a 1 cm-thick layer is found in Section 4, 70 cm; ash layers are very dark gray (2.5Y 3/0).

In CC, 10 cm, a rock fragment occurs.

SMEAR SLIDE SUMMARY (%):

	1, 127 D	2, 38 D	2, 135 M	3, 45 M	4, 80 M	4, 97 M
TEXTURE:						
Sand	20	10	10	20	10	25
Silt	20	10	10	30	—	50
Clay	60	80	80	50	90	25
COMPOSITION:						
Quartz	Tr	2	Tr	15	10	12
Feldspar	Tr	Tr	Tr	5	Tr	6
Clay	18	15	25	20	20	6
Volcanic glass	—	—	—	—	—	35
Calcite/dolomite	20	10	10	5	10	—
Accessory minerals	5	20	5	10	—	—
Zeolite	2	—	Tr	10	—	20
OxFe	—	—	5	—	—	—
Pyroxene	—	—	Tr	—	—	Tr
Foraminifers	15	20	13	15	10	8
Nannofossils	25	25	30	30	50	—
Sponge spicules	Tr	—	Tr	—	—	—
Silicoflagellates	—	—	2	—	—	—
Micrite	15	8	15	—	—	—
Pellets	—	—	—	—	—	2
Intraclasts	—	—	—	—	—	8
Span	—	—	—	—	—	3

	5, 20 M	CC, 7 M
TEXTURE:		
Sand	45	33
Silt	25	20
Clay	30	47
COMPOSITION:		
Quartz	32	15
Feldspar	6	3
Mica	Tr	Tr
Clay	4	25
Volcanic glass	22	4
Calcite/dolomite	—	2
Zeolites	20	—
Pyroxene	1	—
Foraminifers	2	5
Nannofossils	Tr	28
Micrite	—	15
Intraclasts	6	—
Span	—	1
Glauconite	—	2

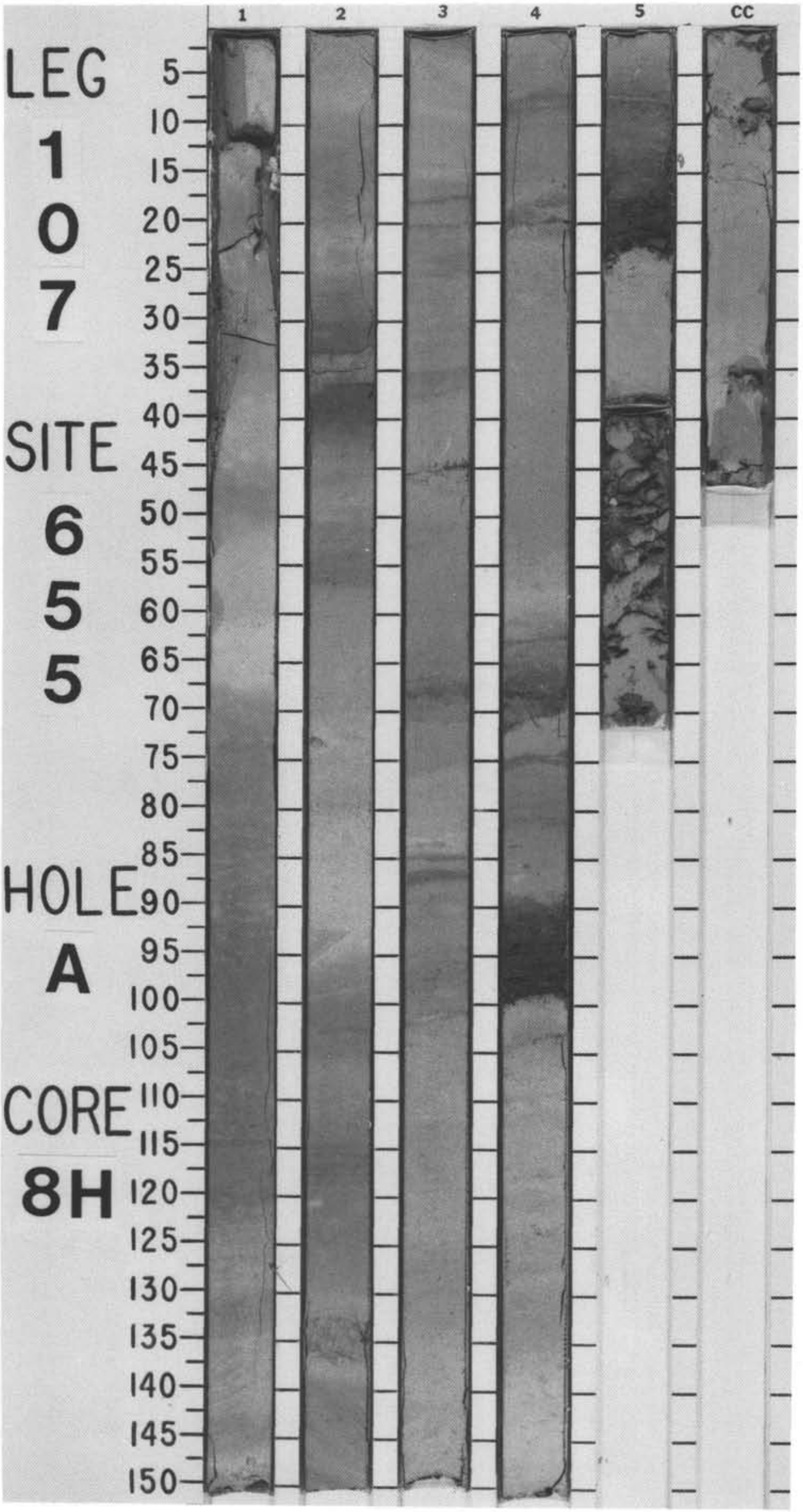
LEG
107
SITE
655
HOLE
A
CORE
8H
1
2
3
4
5
CC

SITE 655 HOLE A CORE 9 X CORED INTERVAL 3360.2-3369.9 mbsl; 70.2-79.9 mbsf

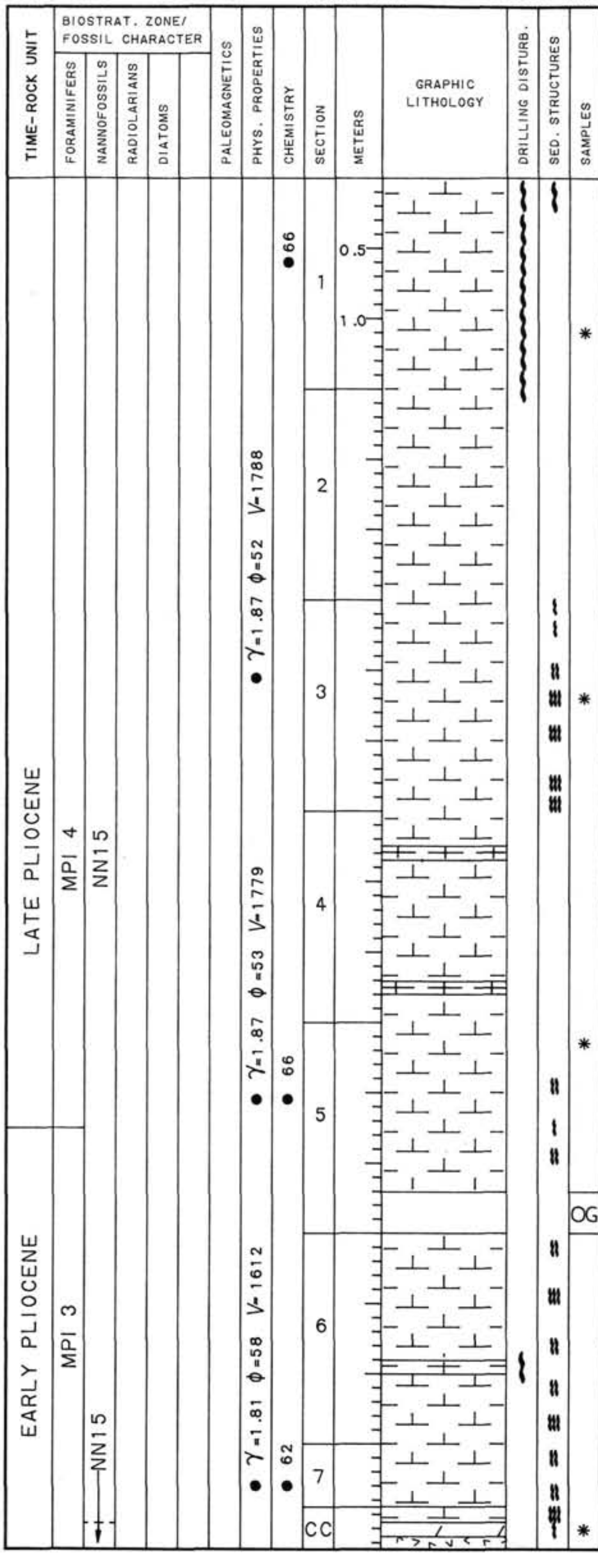

LITHOLOGIC DESCRIPTION

NANNOFOSSIL OOZE, BASAL DOLOMITIC MUDSTONE, and BASALT

Nannofossil ooze, grading from light brownish gray (2.5Y 6/2) to light olive-gray (5Y 6/2) in Section 1, 0–150 cm, and in Section 2, 0–102 cm, and becoming pale yellow (2.5Y 7/4) below. In the remainder of the core, brownish yellow (10YR 6/6), light yellowish brown (10YR 6/4), yellow (10YR 7/6), yellowish brown (10YR 5/4, 5/6), brown (10YR 5/3), and very pale brown (10YR 7/3) are the dominant colors. This yellow-brown ooze is strongly to moderately bioturbated with intervals intensely bespeckled with black (FeS_2-rich) coloring that produces a 'leopard-skin' pattern. Foraminifers and pteropods are abundant and are often found as sandy stringers or layers within the ooze.

The CC contains the basal contact between the overlying dark yellowish brown (10YR 4/4) dolomitic mudstone (CC, 16–24 cm), and the black pebbles and fragments of vesicular basalt.

SMEAR SLIDE SUMMARY (%):

	1, 112 D	3, 72 D	5, 15 M	CC, 22 M
TEXTURE:				
Sand	1	2	45	1
Silt	40	40	30	84
Clay	59	58	25	15
COMPOSITION:				
Feldspar	—	Tr	—	—
Volcanic glass	1	1	Tr	—
Dolomite	3	4	5	99
Accessory minerals	1	1	—	—
Opaques	Tr	—	—	—
Foraminifers	5	4	47	—
Nannofossils	90	90	48	—
Sponge spicules	—	—	Tr	—
Fish remains	—	—	—	1

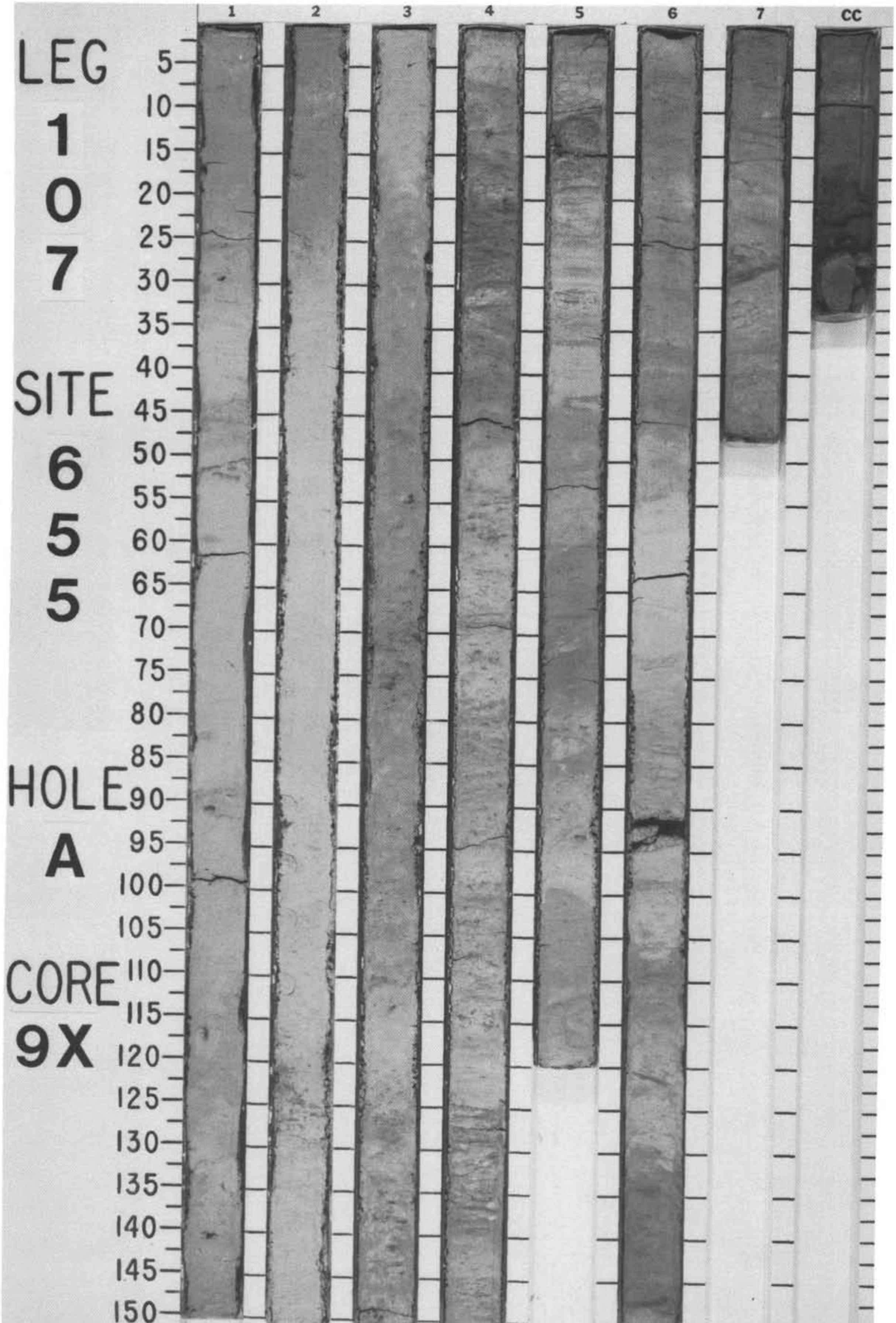
LEG 107
SITE 655
HOLE A
CORE 9X
1
2
3
4
5
6
7
CC

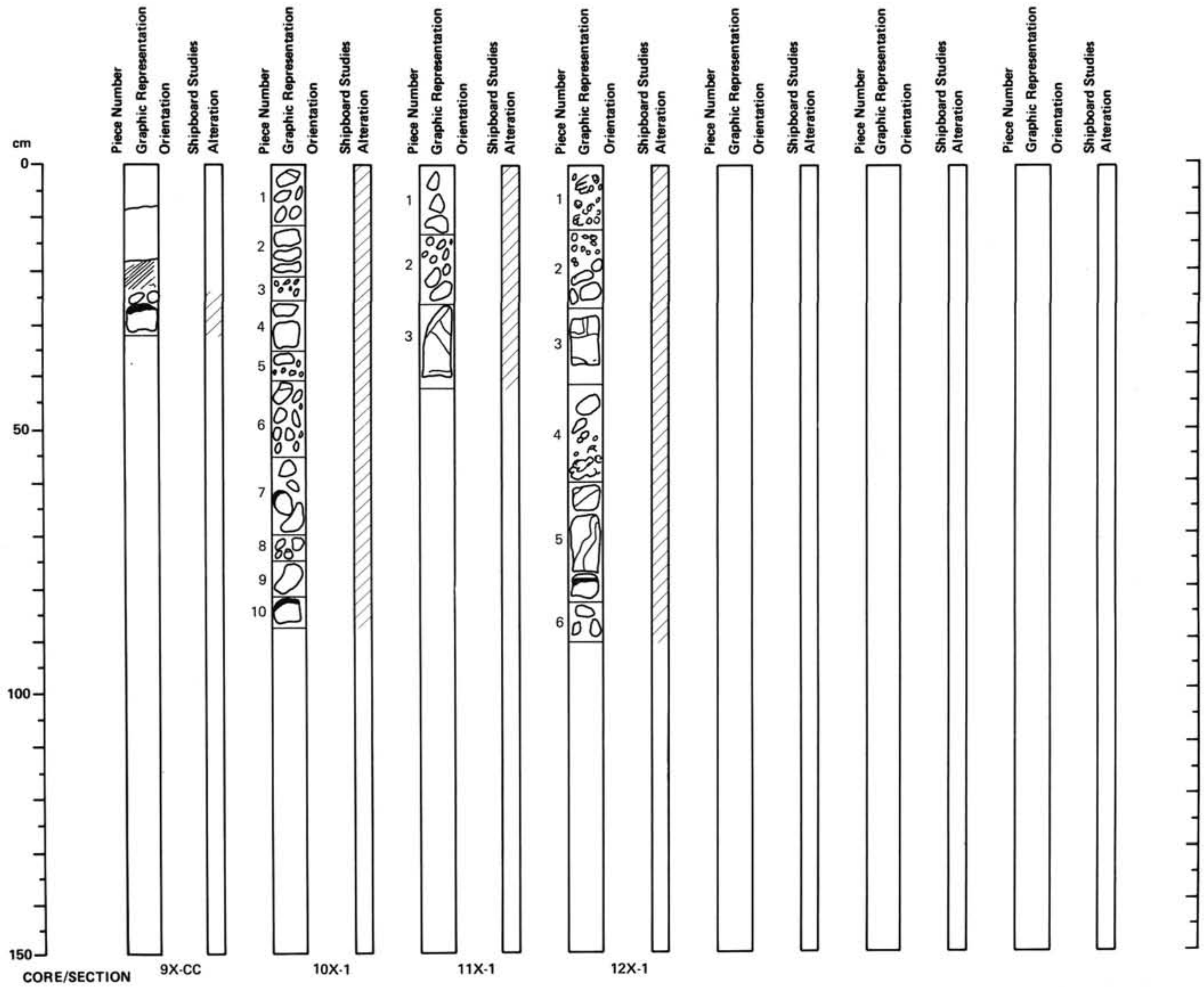

Altered vesicular basalt. Phenocrysts of Ca-plagioclase in a groundmass of olivine, plagioclase and alteration products. Chilled margins common. 107-655A-10X-1, Piece 9 is a micrite (with planktonic forams and nannofossils) in contact with altered basalt. Interval 107-655A-12X-1, 0-60 cm consists of fragments of altered basalt and dark mud. Occasional carbonate veins and crusts.

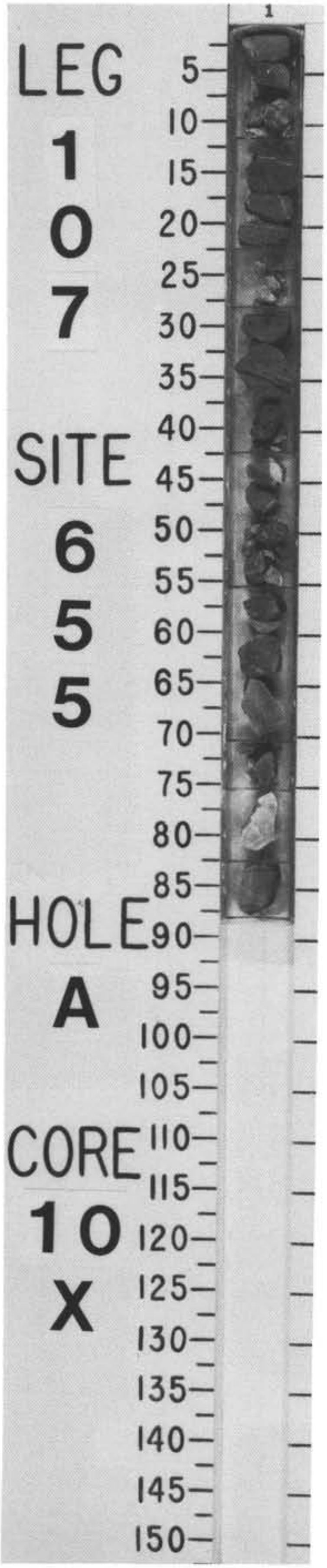
LEG
107
SITE
655
HOLE
A
CORE
10
X

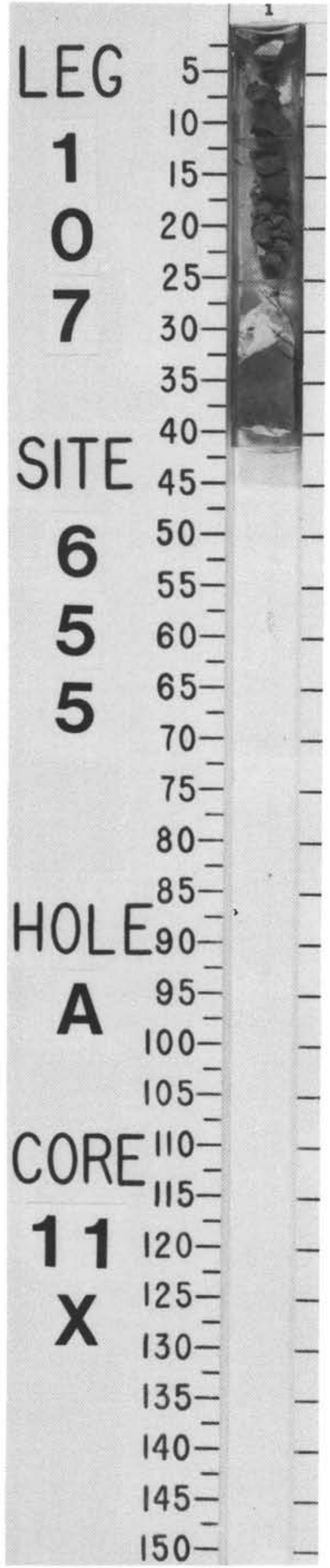
LEG
107
SITE
655
HOLE
A
CORE
11
X

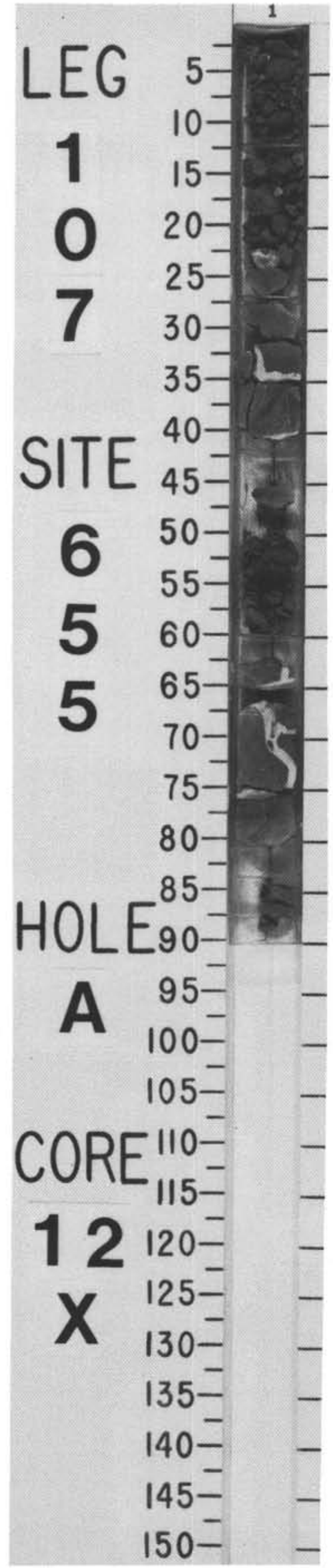
LEG
107
SITE
655
HOLE
A
CORE
12
X

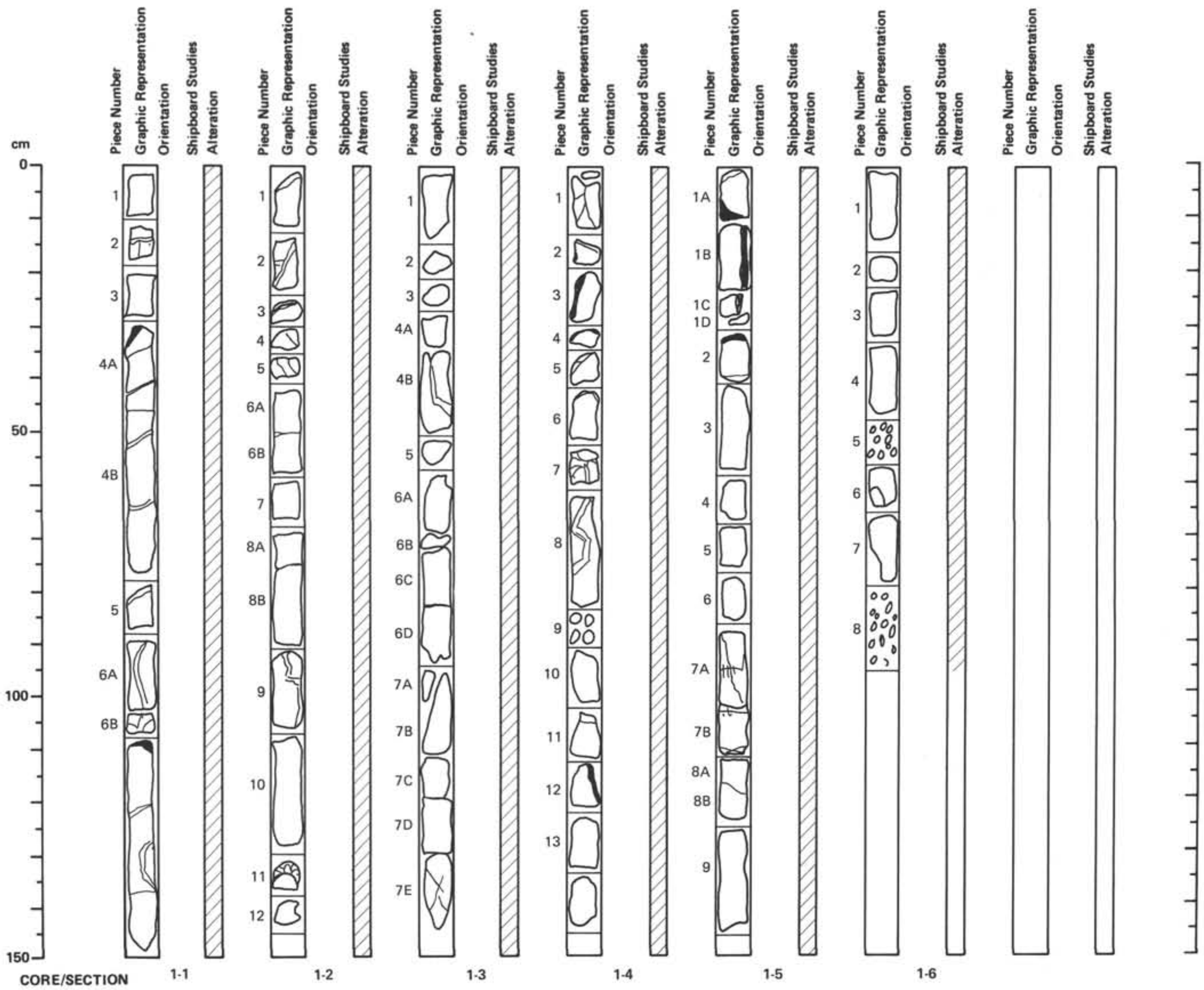

Altered vesicular aphantic basalt. Glomeroporphyritic texture. Clusters of Ca-plagioclase phenocrysts are set in a matrix of scattered skeletal plagioclase, olivine, rare clinopyroxene, and alteration products. Vesicles are fequently lined with carbonates. Chilled glass margins common. Occasional carbonate veins and crusts.

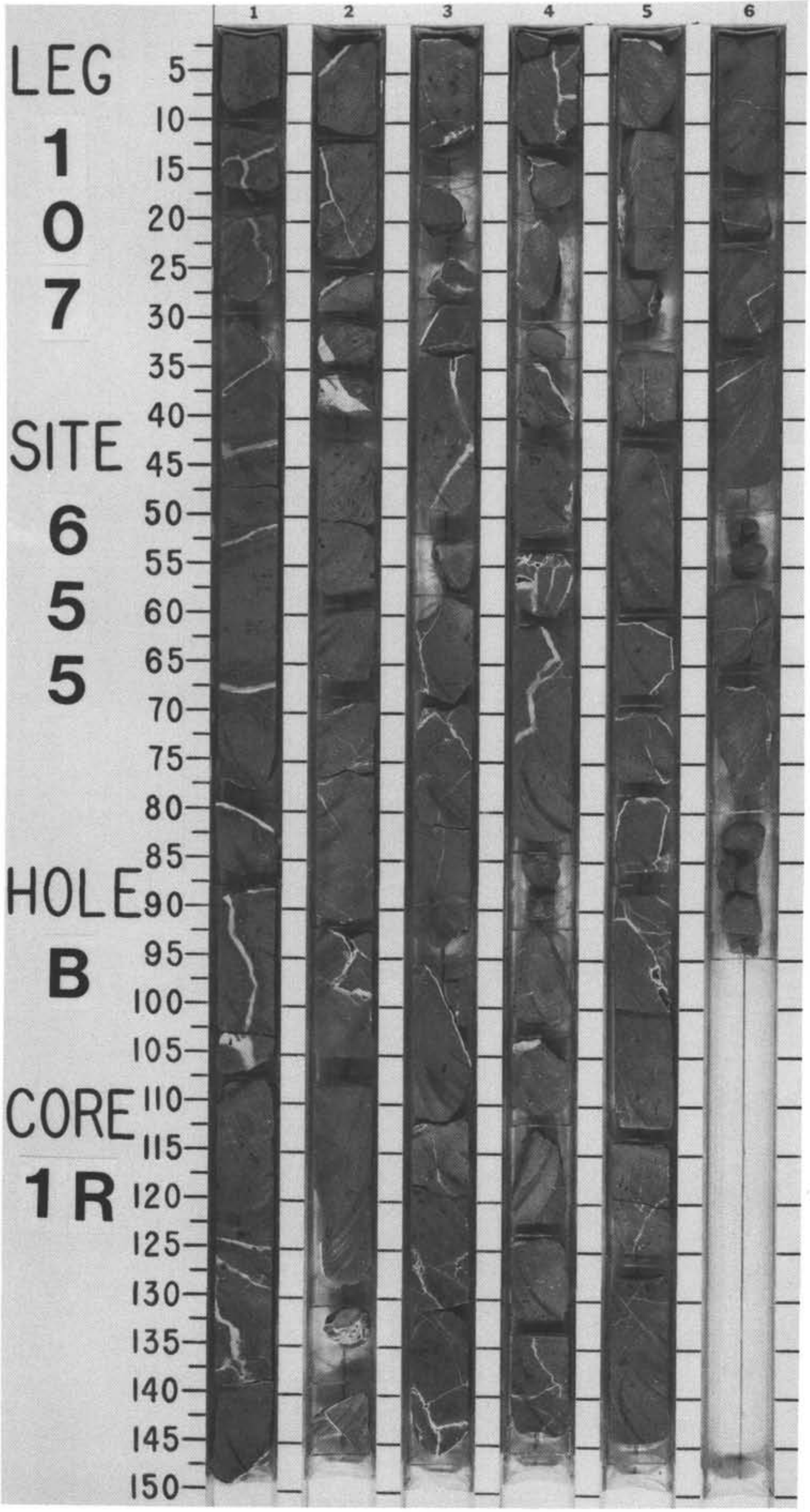
LEG
1
0
7
SITE
6
5
5
HOLE
B
CORE
1R
1
2
3
4
5
6
5
10
15
20
25
30
35
40
45
50
55
60
65
70
75
80
85
90
95
100
105
110
115
120
125
130
135
140
145
150

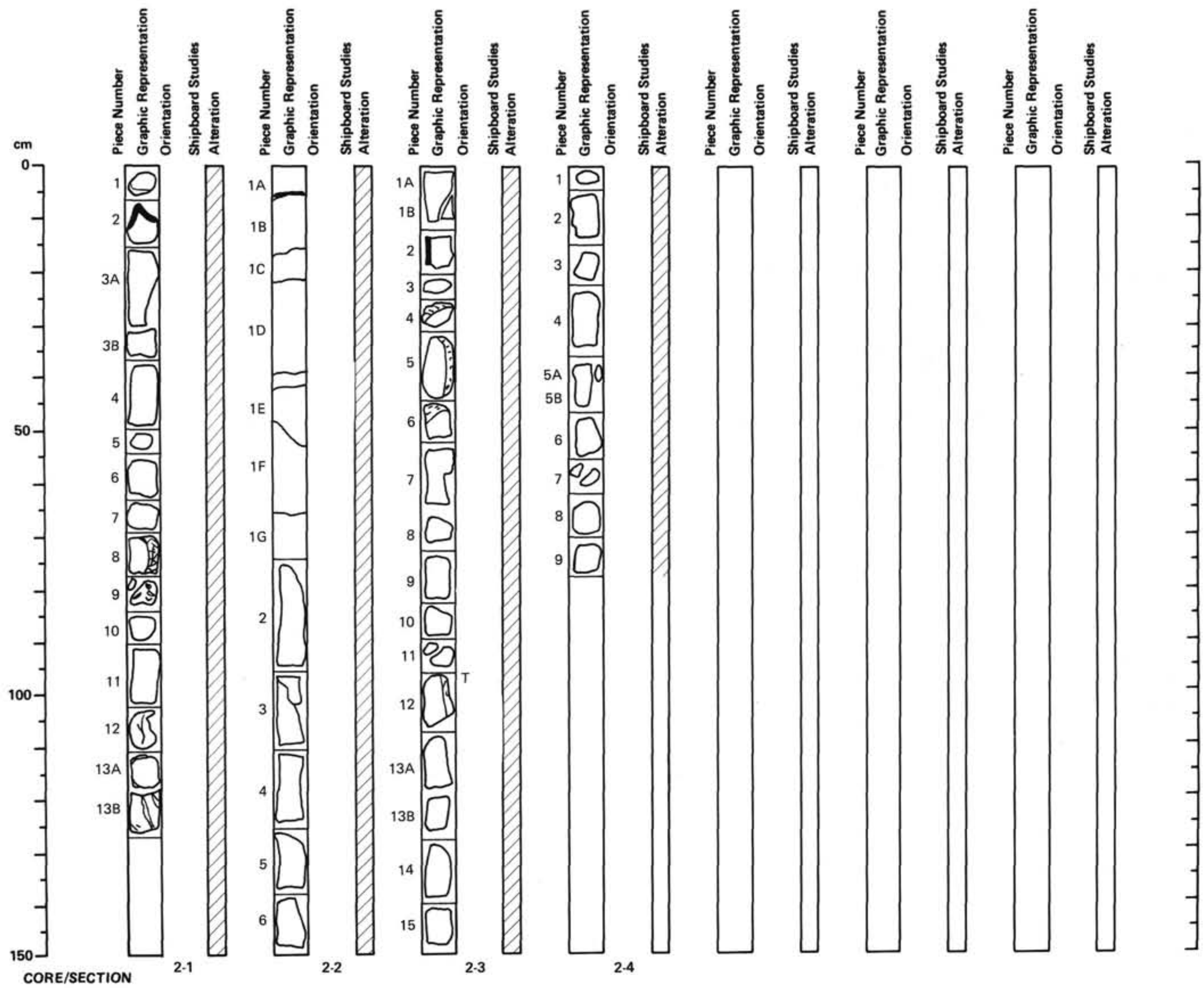

Altered vesicular aphantic basalt. Glomeroporphyritic texture. Clusters of Ca-plagioclase phenocrysts are set in a matrix of scattered skeletal plagioclase, olivine, rare clinopyroxene, and alteration products. Vesicles are fequently lined with carbonates. Chilled glass margins common. Occasional carbonate-filled veins.

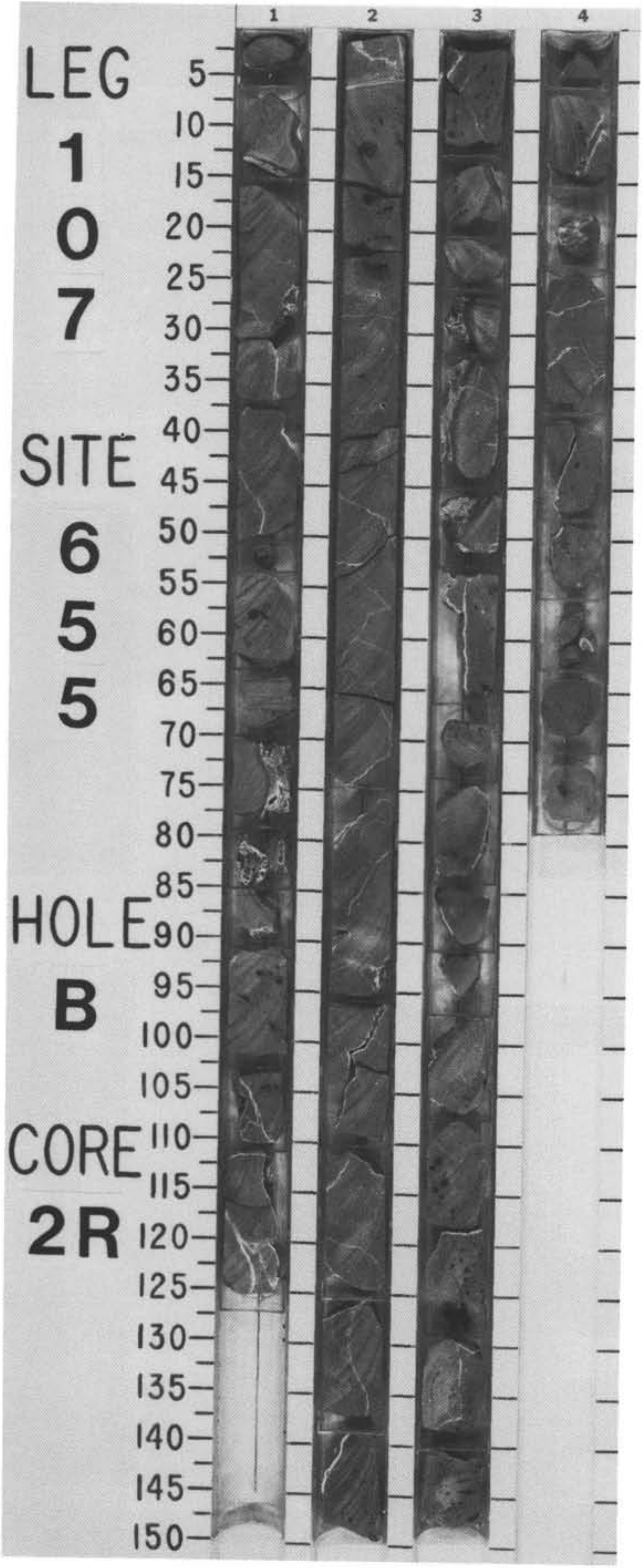
LEG
107
SITE
655
HOLE
B
CORE
2R
1
2
3
4
5
10
15
20
25
30
35
40
45
50
55
60
65
70
75
80
85
90
95
100
105
110
115
120
125
130
135
140
145
150

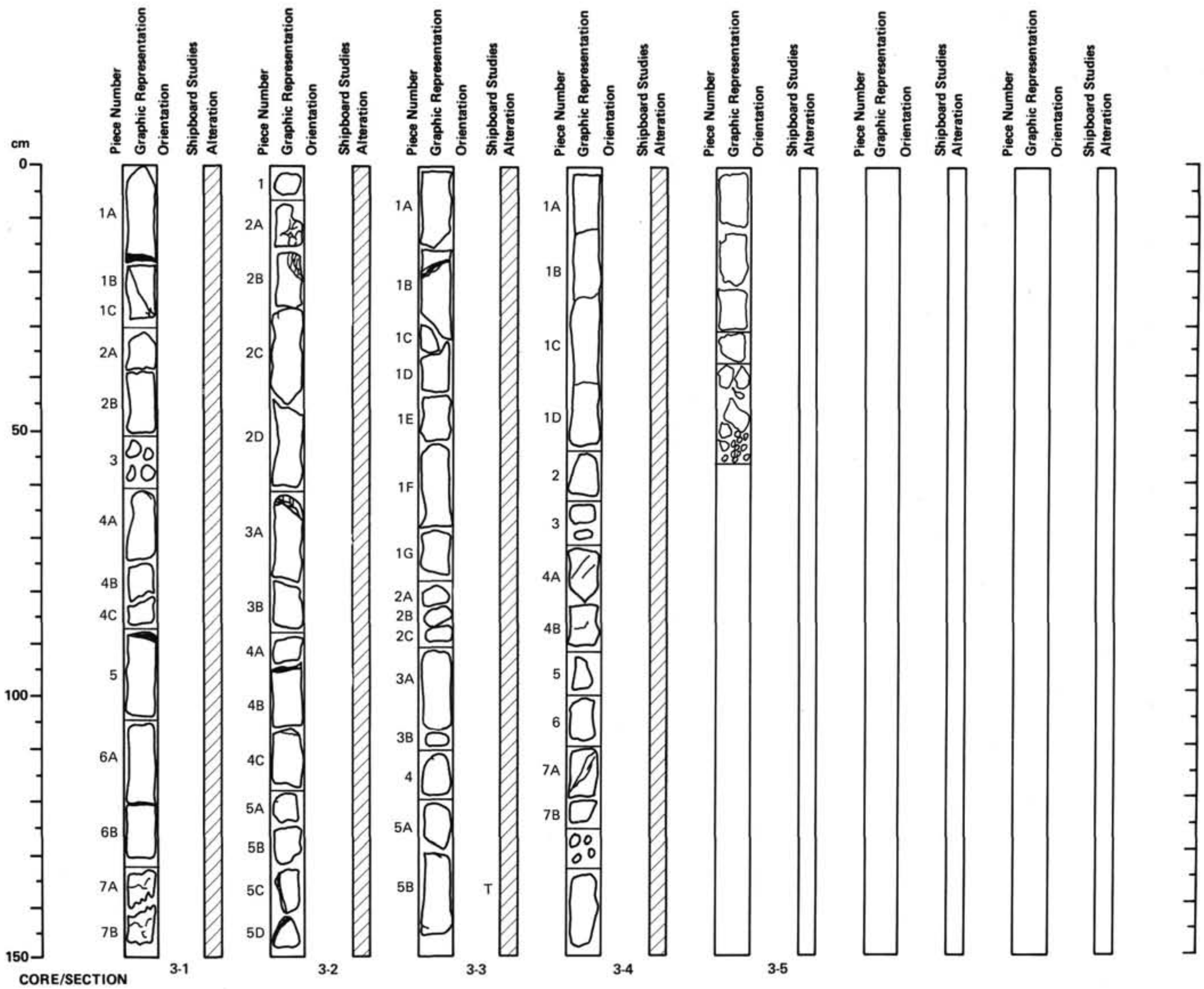

Same as Core 1.

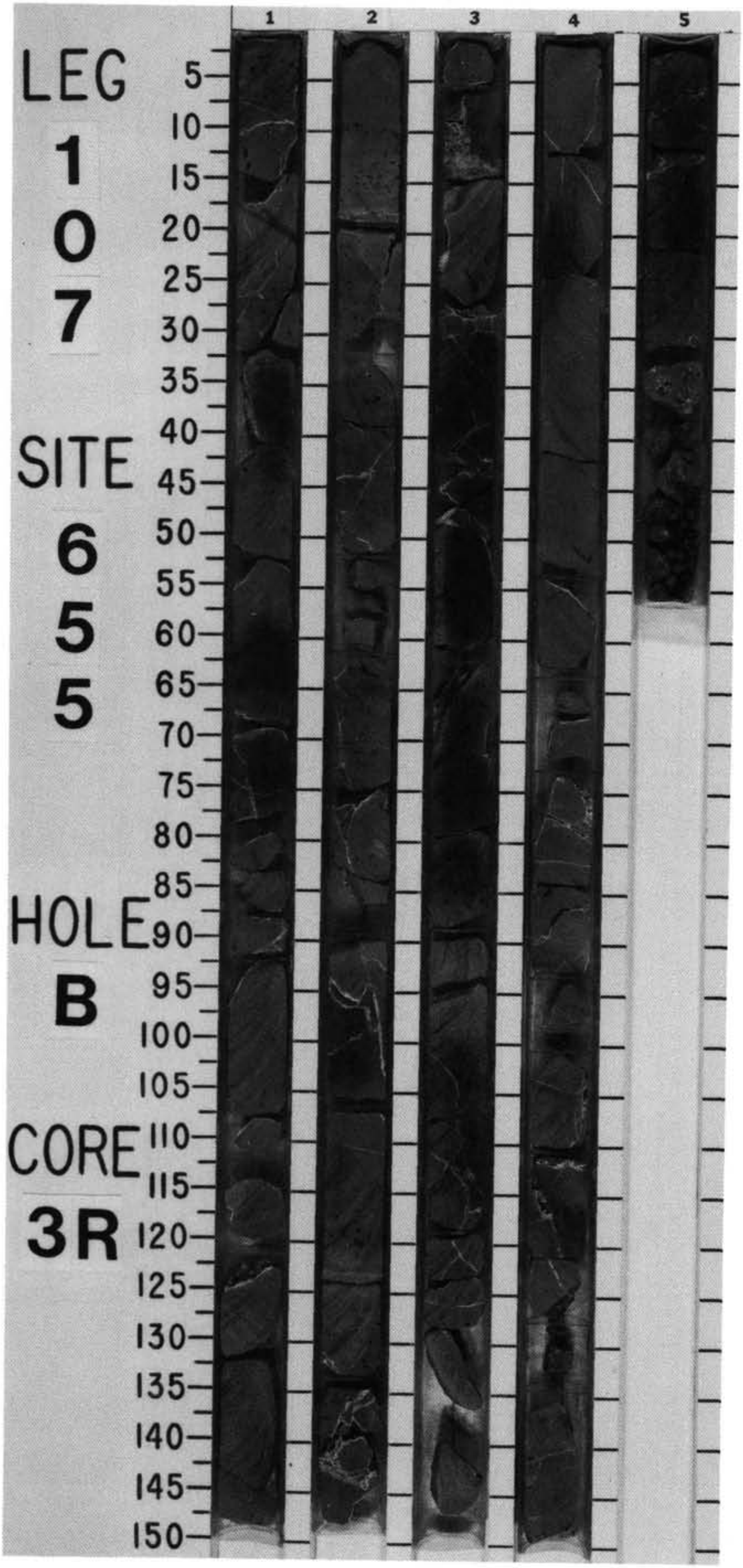
LEG
107
SITE
655
HOLE
B
CORE
3R
1
2
3
4
5

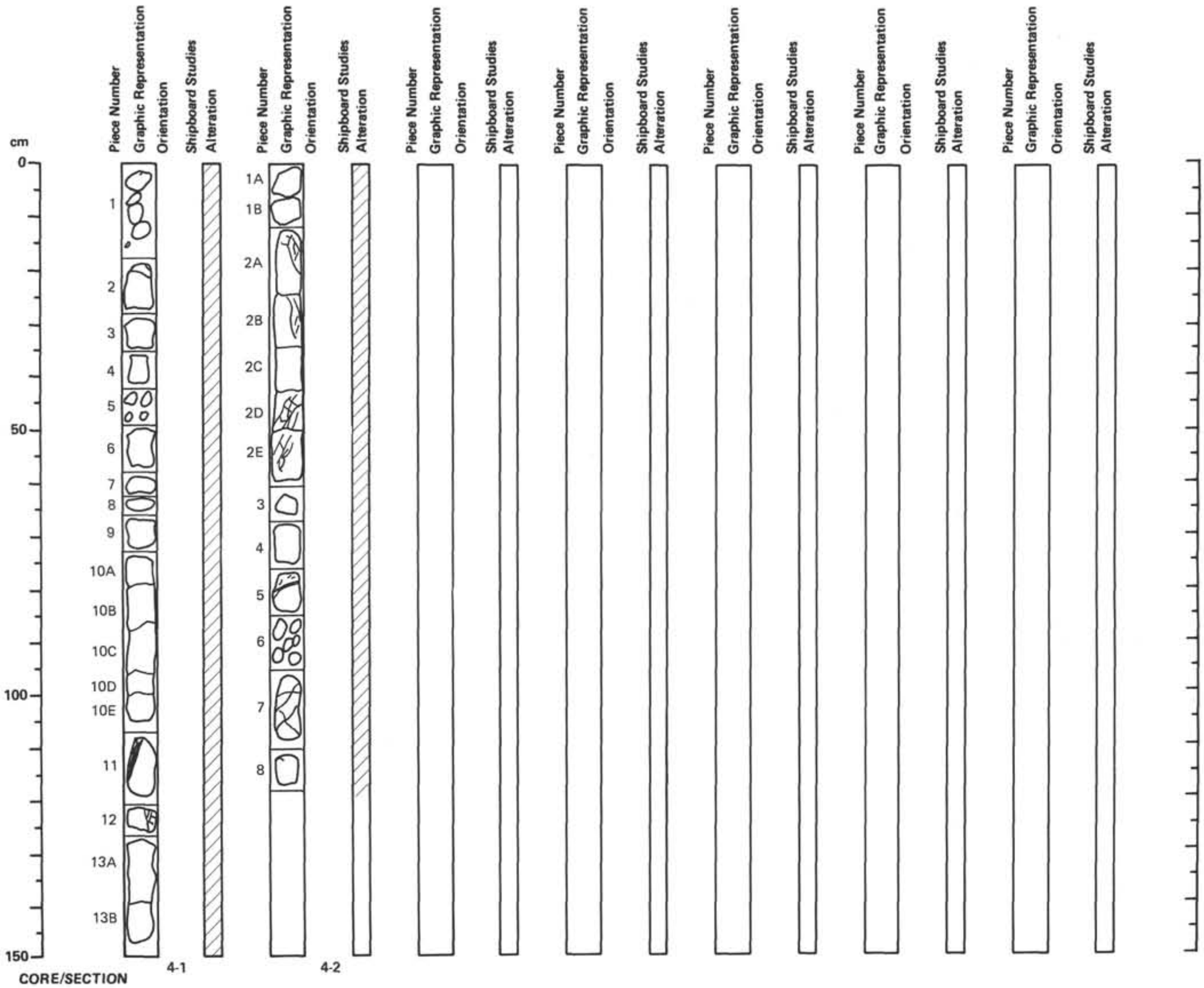

Same as Core 1. 107-655B-4R-2, Pieces 2d and 2e are brecciated, carbonate cemented basalt.

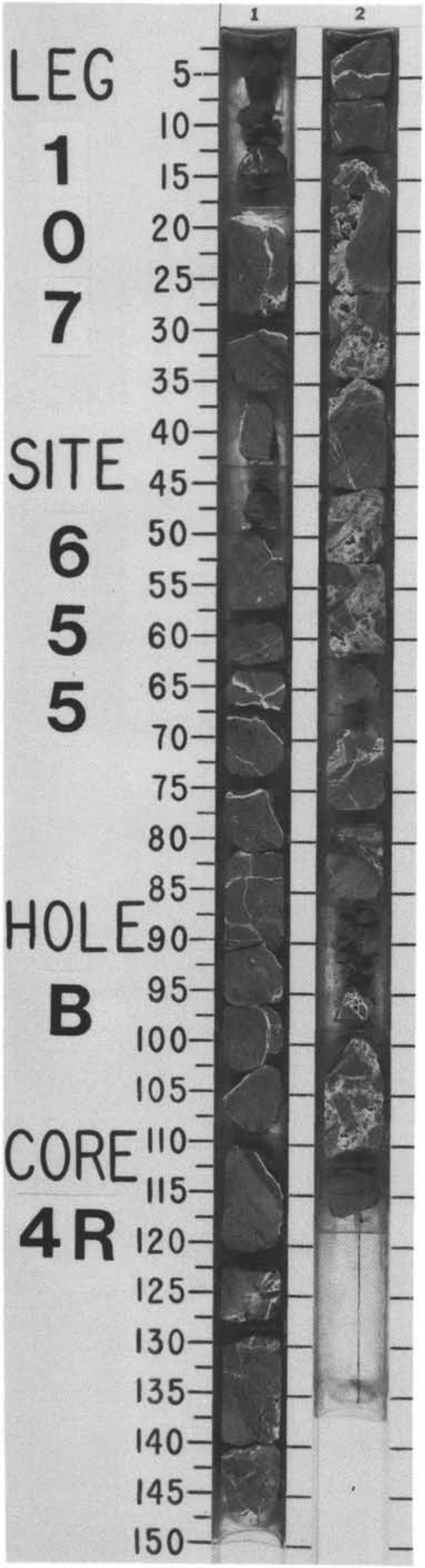
LEG 1 0 7
SITE 6 5 5
HOLE B
CORE 4R
1
2
5
10
15
20
25
30
35
40
45
50
55
60
65
70
75
80
85
90
95
100
105
110
115
120
125
130
135
140
145
150

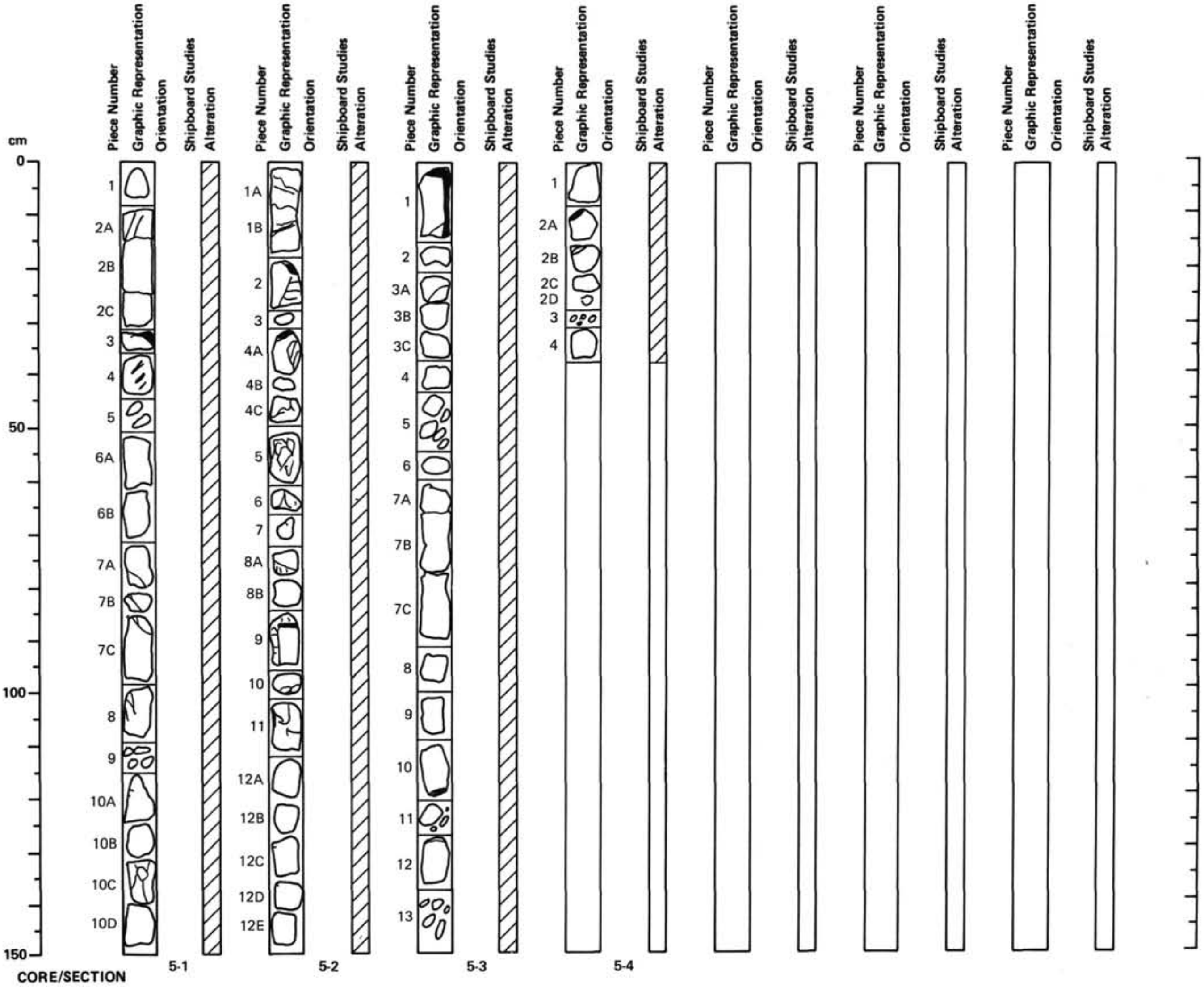

Same as Core 1. 107-655B-5R-1, Piece 4 is limestone with inclusions of altered basaltic glass. 107-655B-5R-2, Pieces 5, 12a, 12b, 12c, 12d, and 12e are brecciated basalt cemented by carbonate. 107-655B-5R-2, Pieces 10 and 11 are limestone with inclusions of basalt.

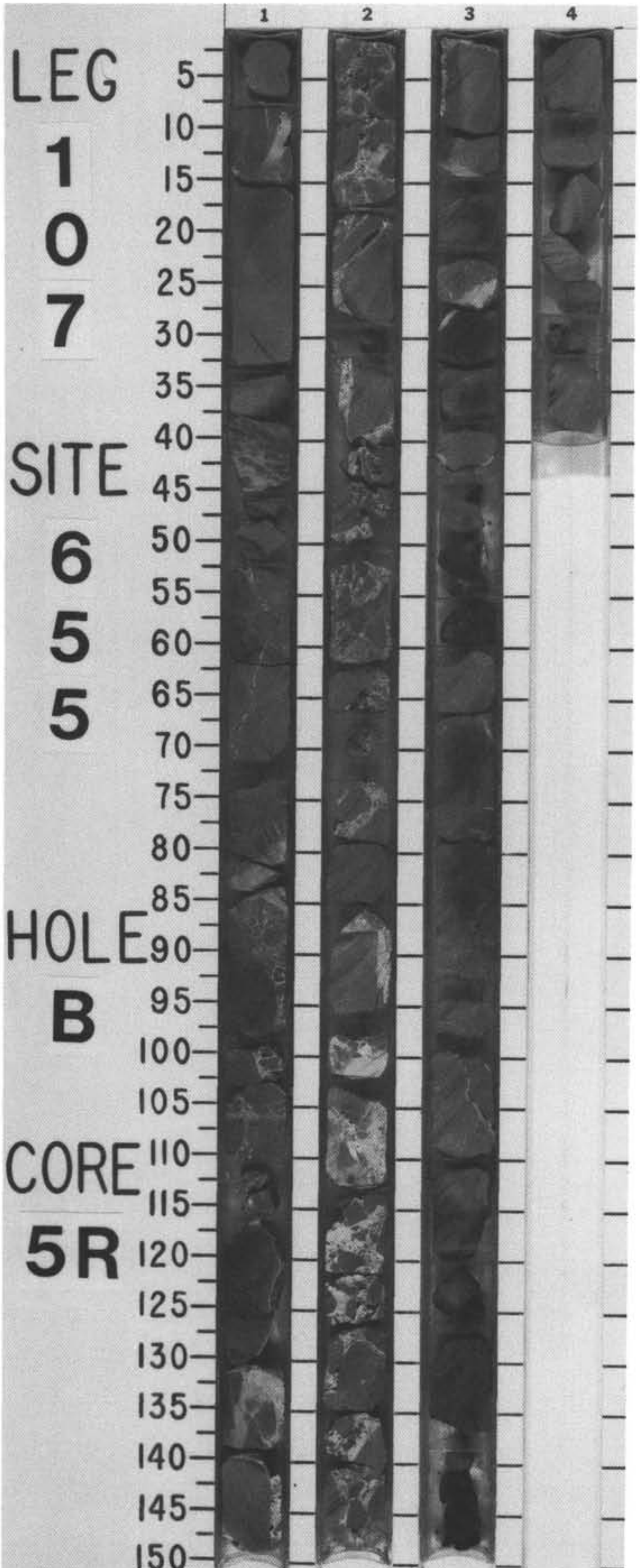
LEG
1
0
7
SITE
6
5
5
HOLE
B
CORE
5R
1
2
3
4
5
10
15
20
25
30
35
40
45
50
55
60
65
70
75
80
85
90
95
100
105
110
115
120
125
130
135
140
145
150

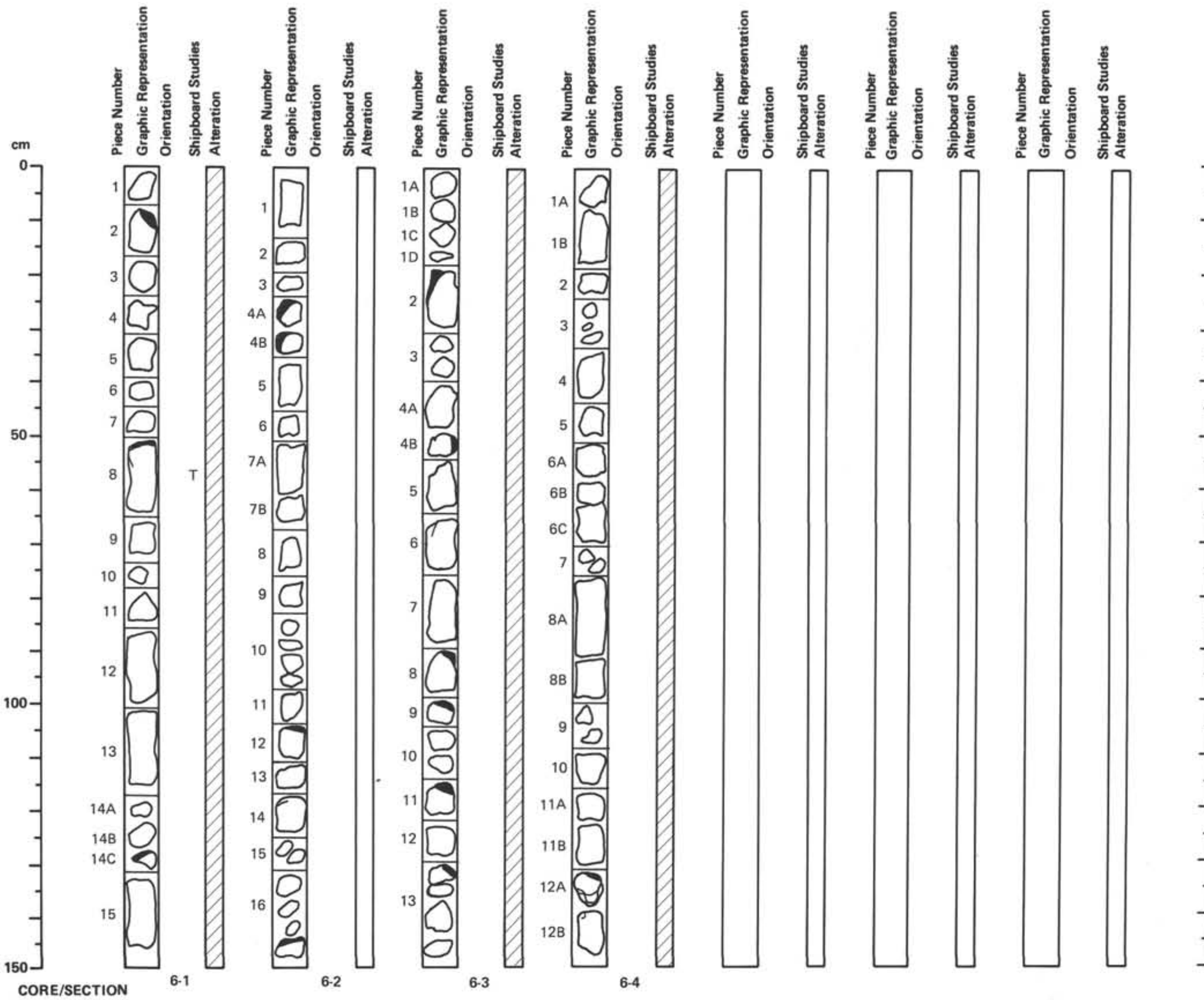

Same as Core 1. Carbonate veins rarely present.

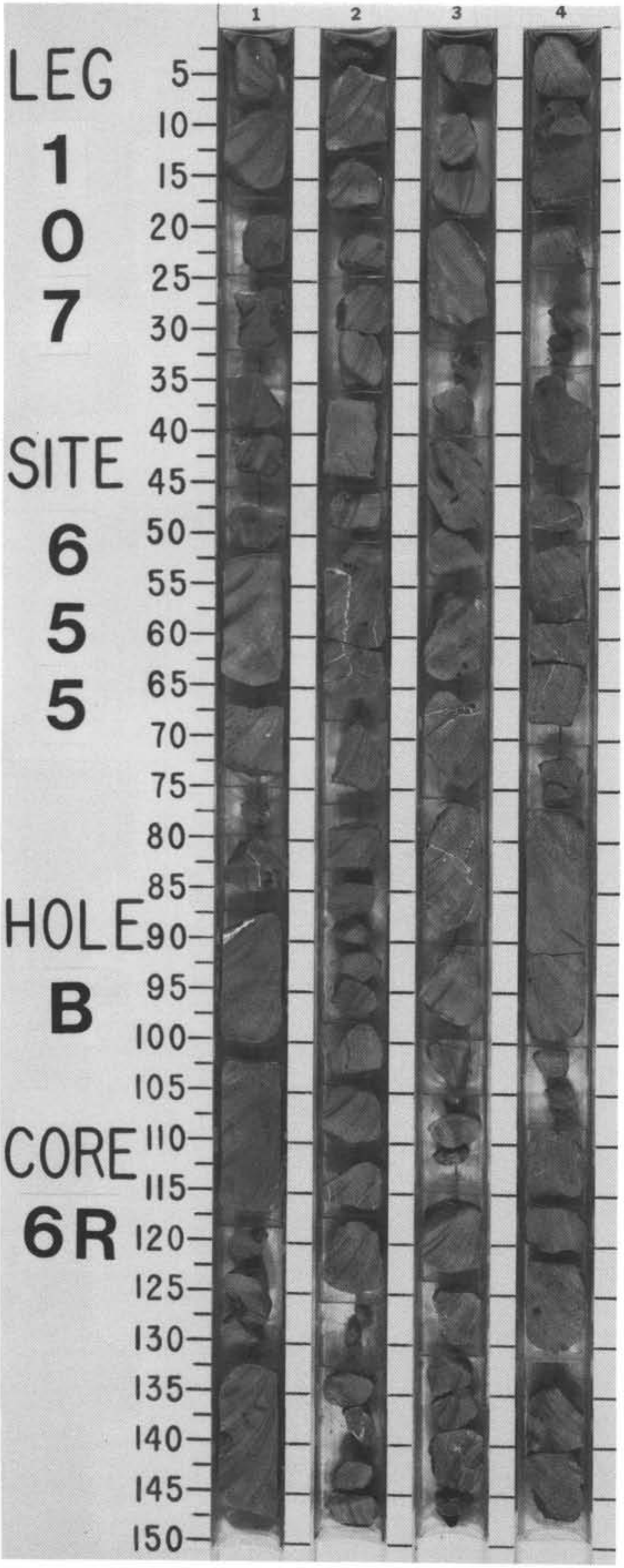
LEG
107
SITE
655
HOLE
B
CORE
6R
1
2
3
4

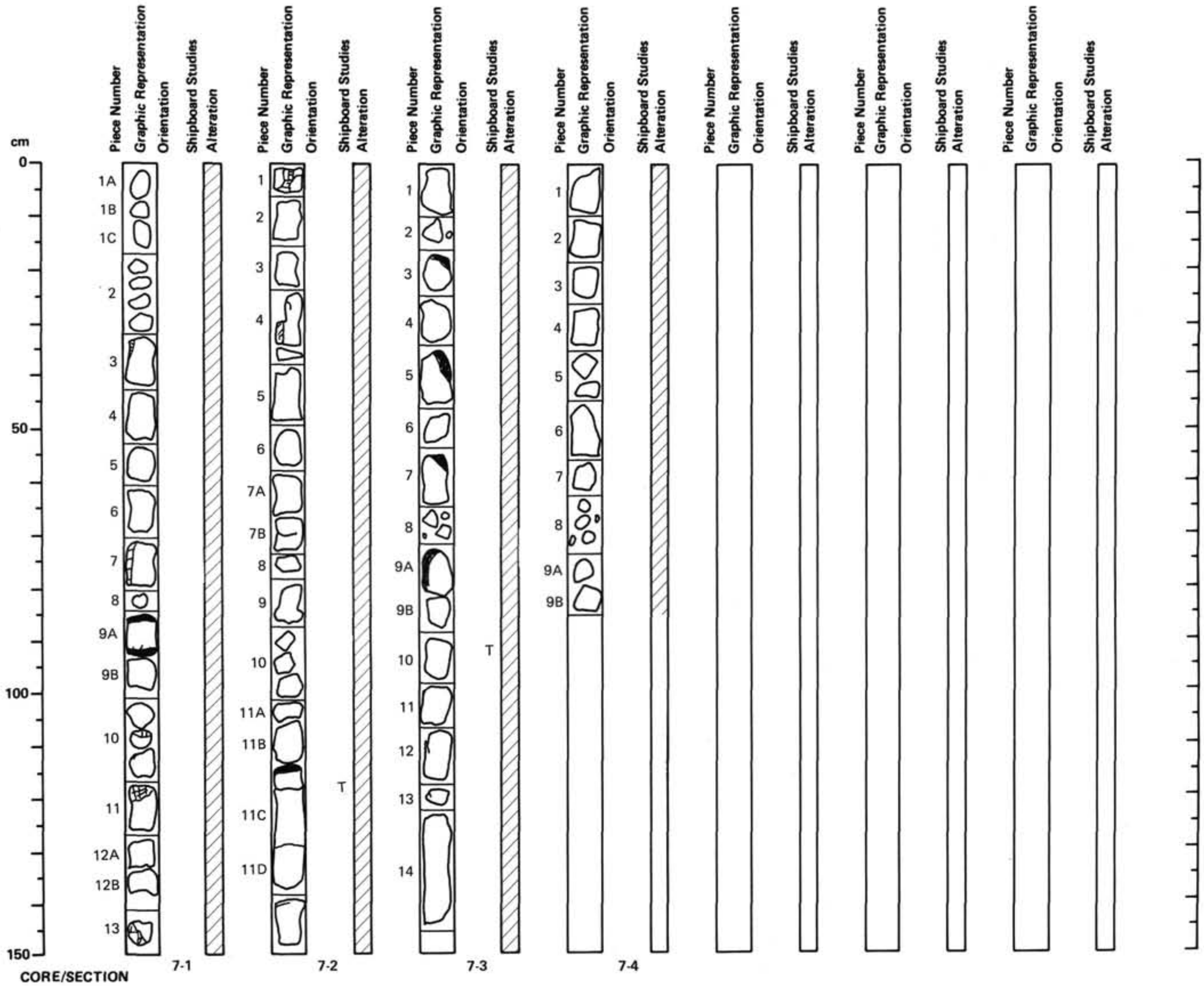

Same as Core 1. 107-655B-7R-1, Piece 11, and 107-655B-7R-2, Piece 1, are carbonate cemented basaltic breccia.

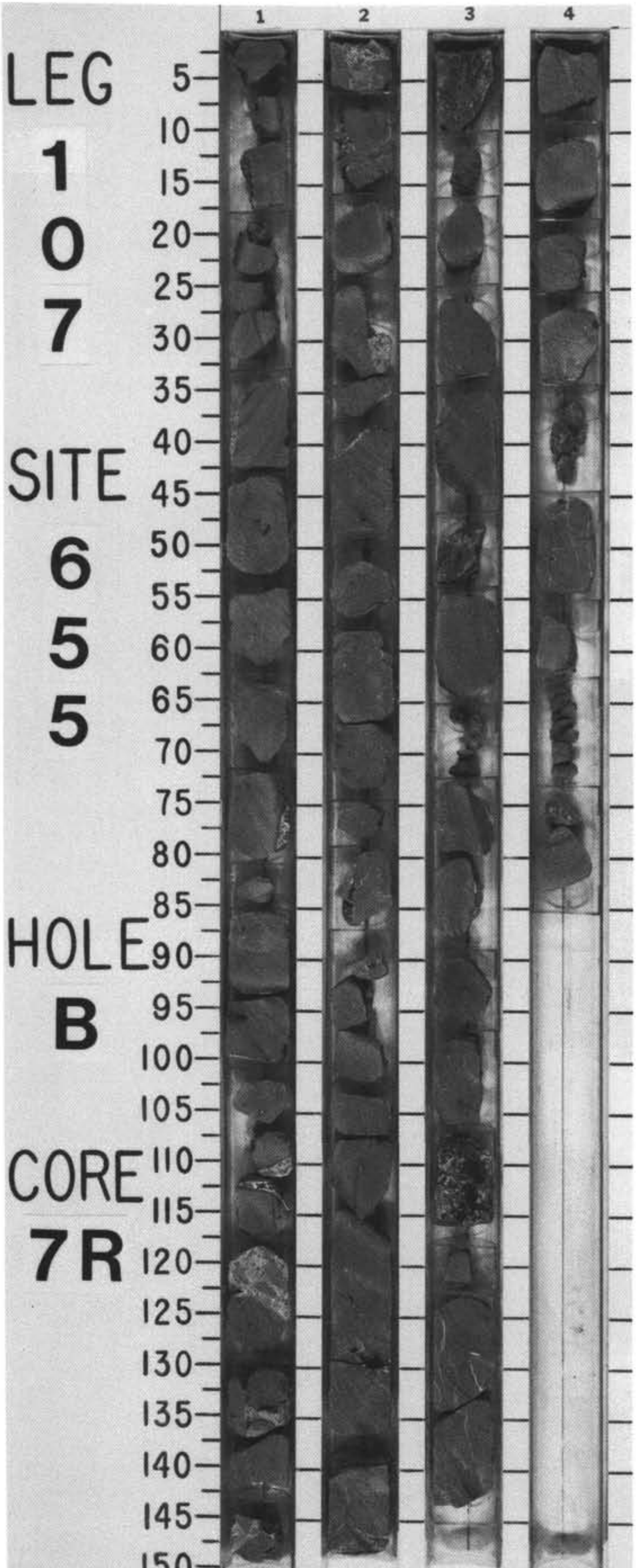
LEG
107
SITE
655
HOLE
B
CORE
7R
1
2
3
4
5
10
15
20
25
30
35
40
45
50
55
60
65
70
75
80
85
90
95
100
105
110
115
120
125
130
135
140
145
150

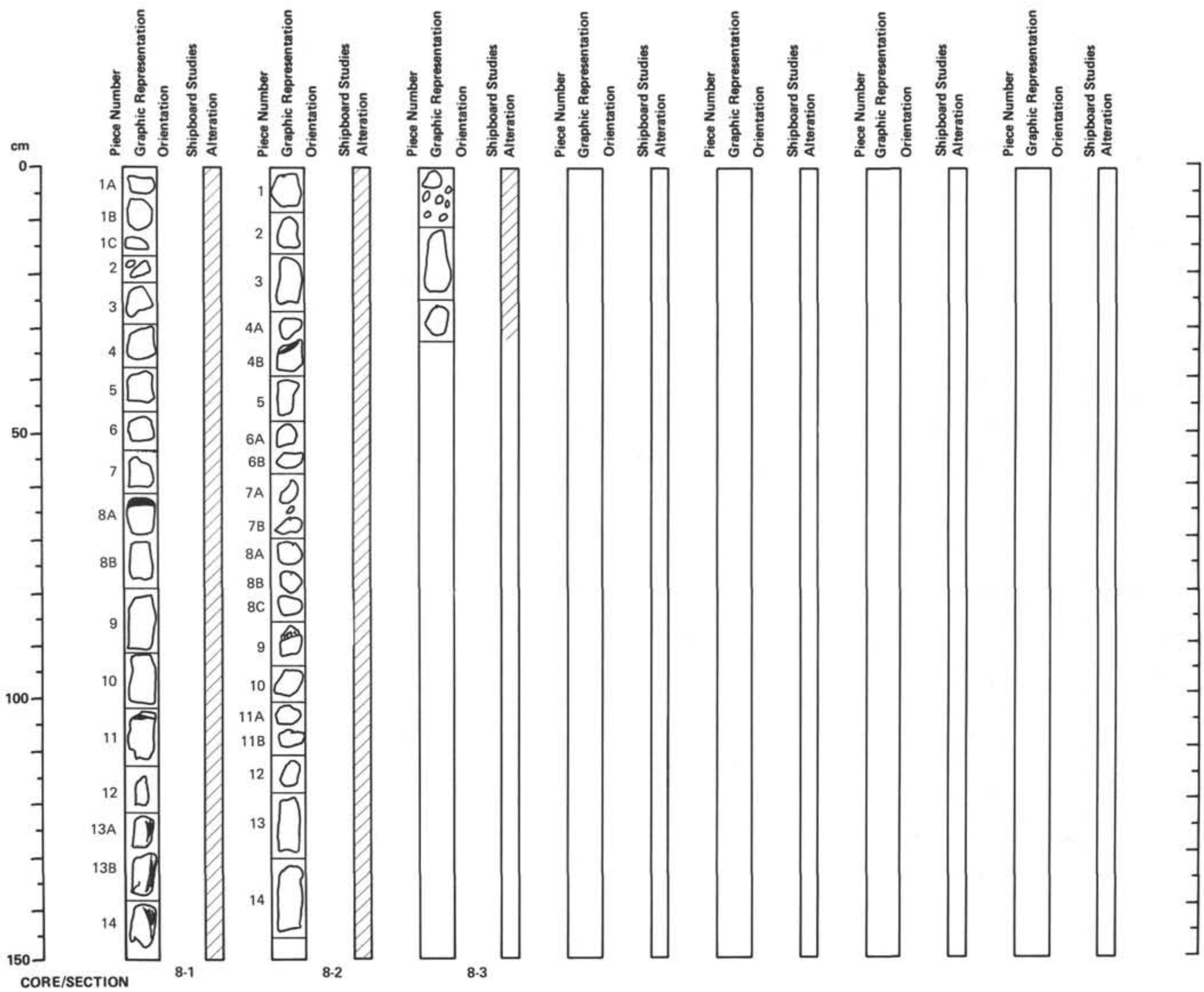

Same as Core 1.

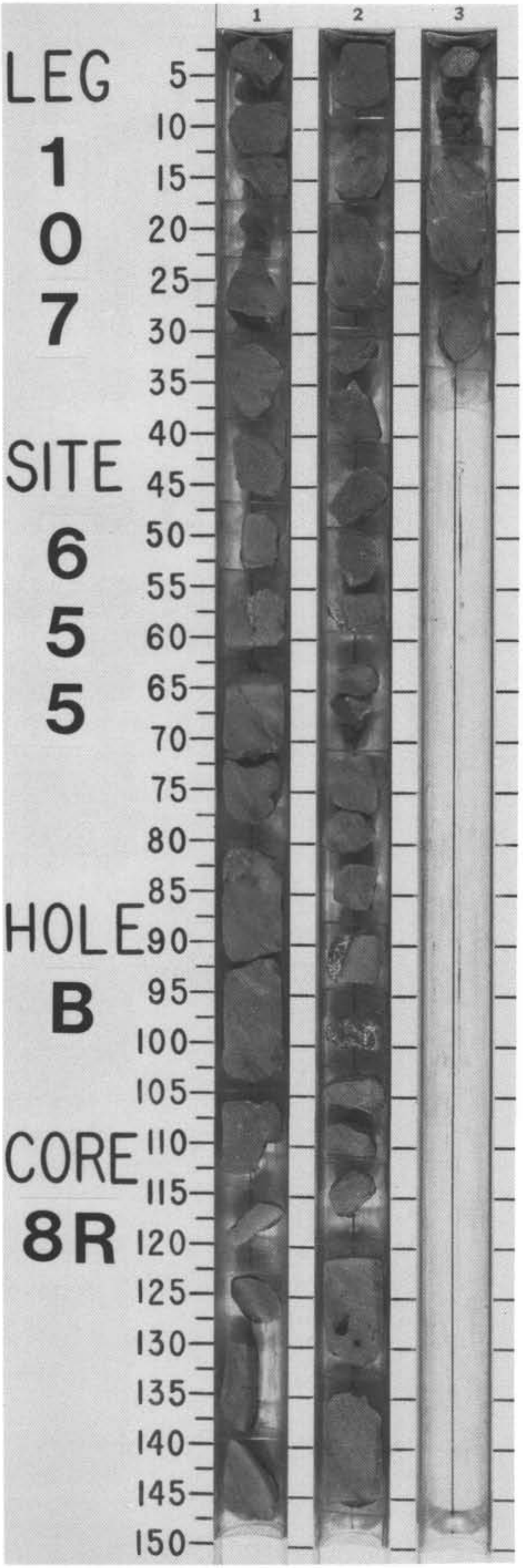
LEG
1
0
7
SITE
6
5
5
HOLE
B
CORE
8R
1
2
3
5
10
15
20
25
30
35
40
45
50
55
60
65
70
75
80
85
90
95
100
105
110
115
120
125
130
135
140
145
150

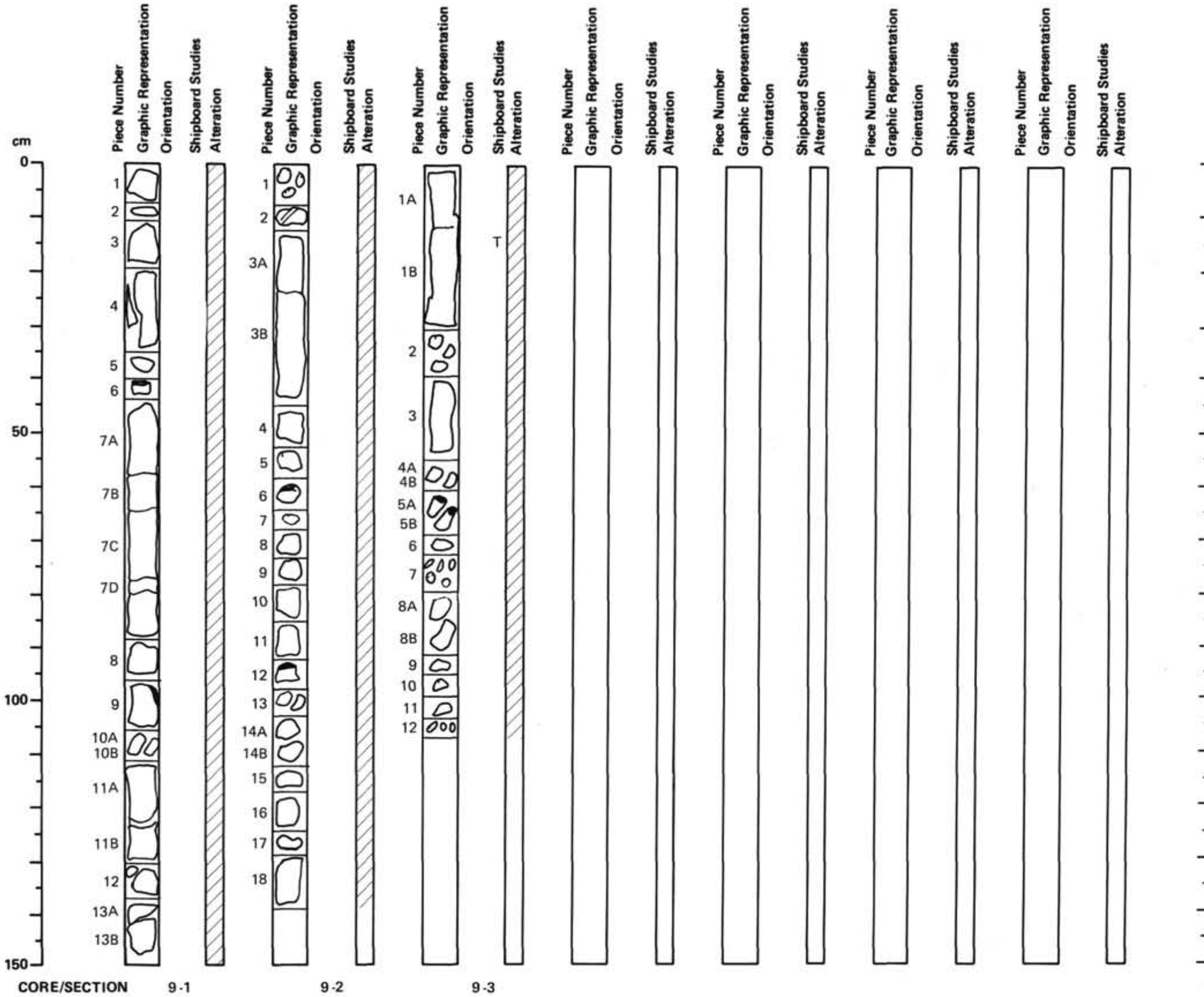

Same as Core 1. 107-655B-9R-3, Piece 1 has phenocrysts of Ca-plagioclase and euhedral olivine.


LEG
1
0
7
SITE
6
5
5
HOLE
B
CORE
9R
1
2
3
5
10
15
20
25
30
35
40
45
50
55
60
65
70
75
80
85
90
95
100
105
110
115
120
125
130
135
140
145
150

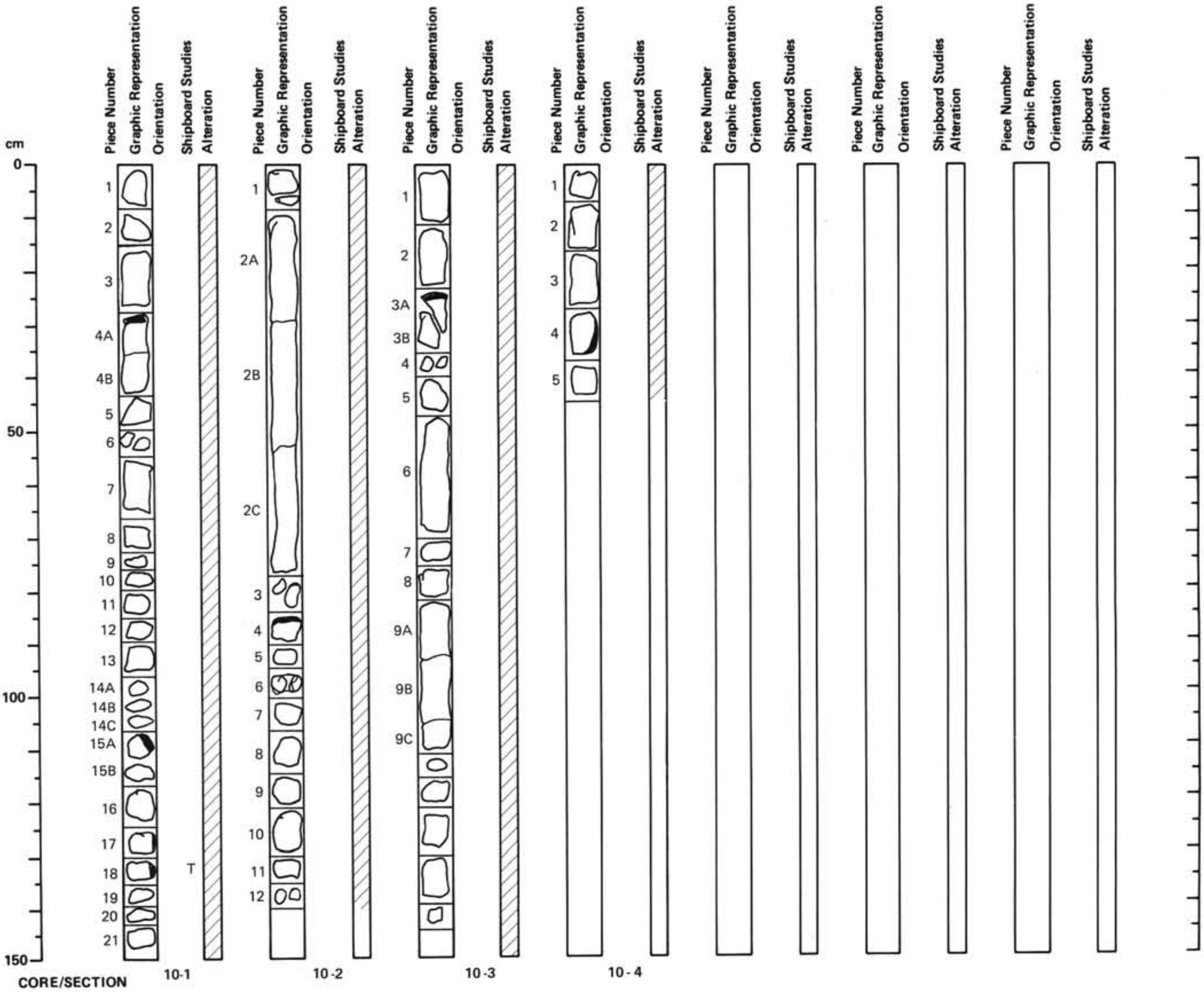

Same as Core 1.

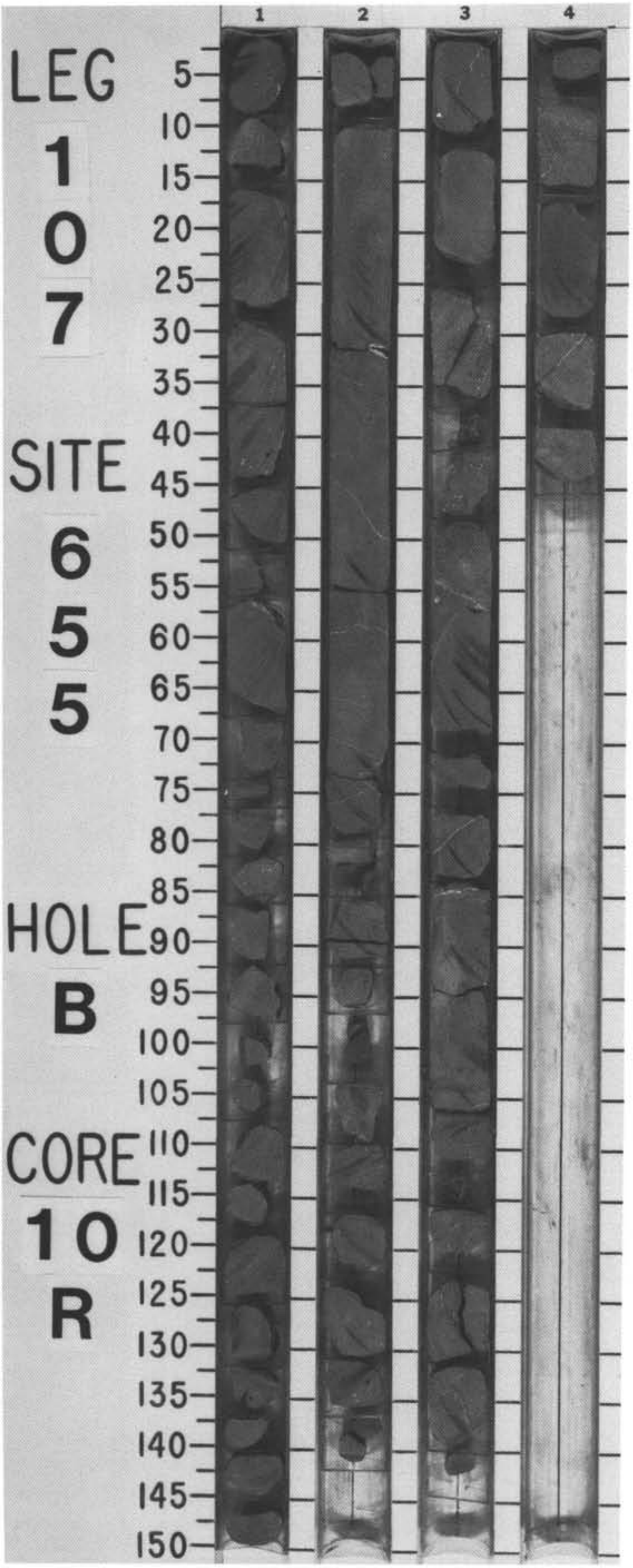
LEG
107
SITE
655
HOLE
B
CORE
10
R
1
2
3
4
5
10
15
20
25
30
35
40
45
50
55
60
65
70
75
80
85
90
95
100
105
110
115
120
125
130
135
140
145
150

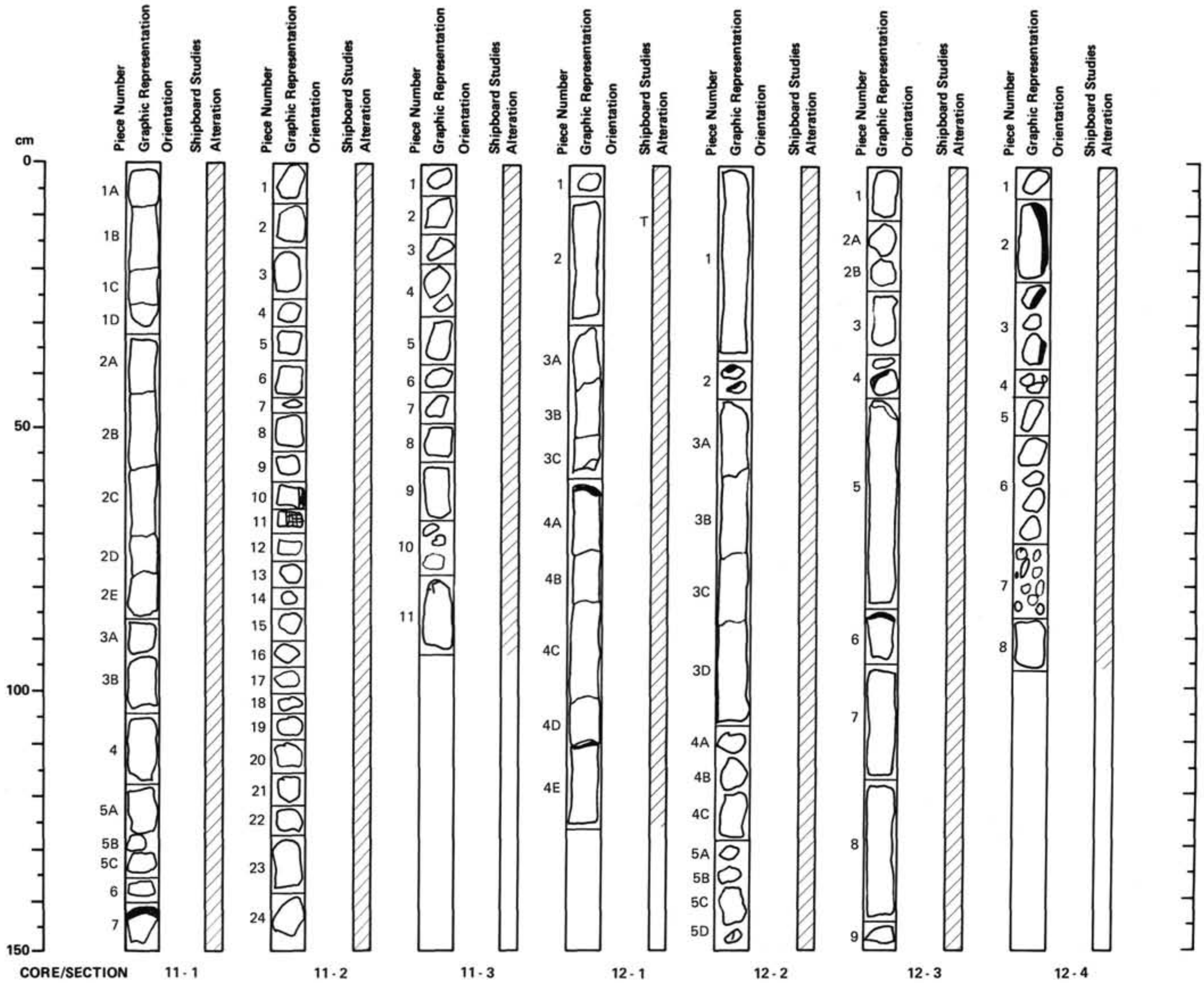

Same as Core 1. Glomerocrysts of Ca-plagioclase and euhedral olivine in 107-655B-12R-1, Piece 2.

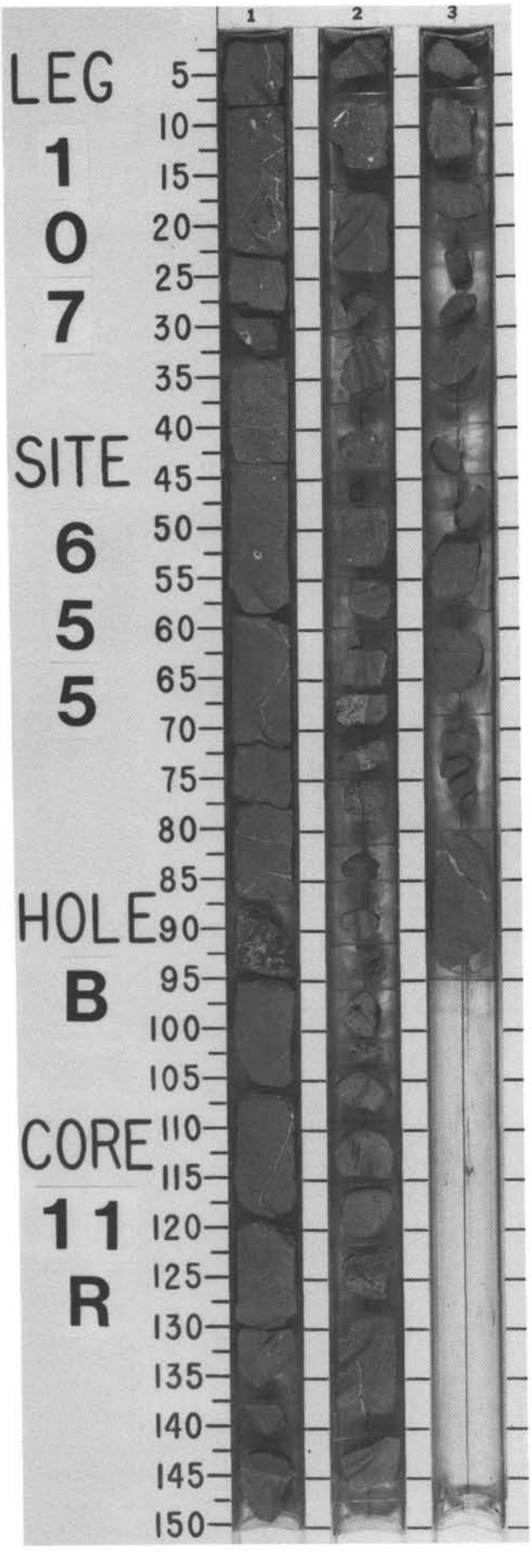
LEG
107
SITE
655
HOLE
B
CORE
11
R

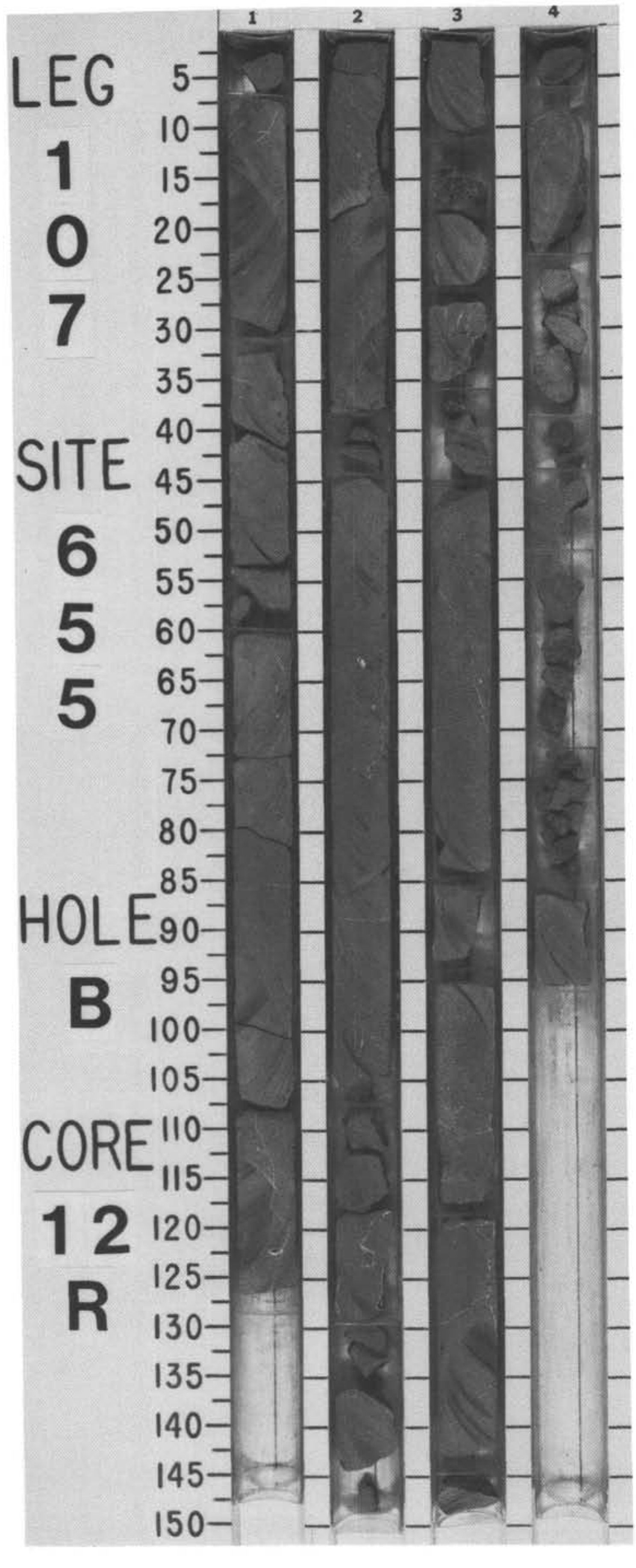
LEG
107
SITE
655
HOLE
B
CORE
12
R